Let me tell you the secret that has led me to my goal. My strength lies solely in my tenacity.

Louis Pasteur

Don't let school get in the way of your education.

Mark Twain

University of Alberta

Organic Films for the Immobilization of Modified Proteins for Biosensor Applications

By

Andrew David Edward Smith

A thesis submitted to the Faculty of Graduate Studies and Research in partial fulfillment of the requirements for the degree of Master of Science

Department of Chemistry

Edmonton, Alberta, Canada

Fall 2008

Library and Archives Canada

Published Heritage Branch

395 Wellington Street
Ottawa ON K1A 0N4
Canada

Bibliothèque et Archives Canada

Direction du Patrimoine de l'édition

395, rue Wellington
Ottawa ON K1A 0N4
Canada

Your file Votre référence
ISBN: 978-0-494-47416-7
Our file Notre référence
ISBN: 978-0-494-47416-7

NOTICE:
The author has granted a non-exclusive license allowing Library and Archives Canada to reproduce, publish, archive, preserve, conserve, communicate to the public by telecommunication or on the Internet, loan, distribute and sell theses worldwide, for commercial or non-commercial purposes, in microform, paper, electronic and/or any other formats.

The author retains copyright ownership and moral rights in this thesis. Neither the thesis nor substantial extracts from it may be printed or otherwise reproduced without the author's permission.

AVIS:
L'auteur a accordé une licence non exclusive permettant à la Bibliothèque et Archives Canada de reproduire, publier, archiver, sauvegarder, conserver, transmettre au public par télécommunication ou par l'Internet, prêter, distribuer et vendre des thèses partout dans le monde, à des fins commerciales ou autres, sur support microforme, papier, électronique et/ou autres formats.

L'auteur conserve la propriété du droit d'auteur et des droits moraux qui protège cette thèse. Ni la thèse ni des extraits substantiels de celle-ci ne doivent être imprimés ou autrement reproduits sans son autorisation.

In compliance with the Canadian Privacy Act some supporting forms may have been removed from this thesis.

While these forms may be included in the document page count, their removal does not represent any loss of content from the thesis.

Conformément à la loi canadienne sur la protection de la vie privée, quelques formulaires secondaires ont été enlevés de cette thèse.

Bien que ces formulaires aient inclus dans la pagination, il n'y aura aucun contenu manquant.

Canada

Dedicated to my family

David Duncan Smith, Kathy Diane (O'Donnell) Smith,

and Struan William Ira Smith

Abstract

The effective immobilization of proteins to surfaces is a key step in the design of many bioassays and sensing devices. The modification of the protein capture agent with a tag provides a pathway for immobilization with controlled orientation. In this work, surface plasmon resonance imaging (SPRi) was used to measure the binding of four hexahistidine-tagged (His_6) proteins, with molecular masses of 48 to 480 kDa, to alkyl thiol monolayers of nitrilotriacetic acid (NTA) via coordination with Ni^{2+}. Protein attachment to a pure NTA monolayer was found to be primarily controlled by the ability of the proteins to pack on the surface. NTA and -OH terminated monolayers proved effective in reducing non-specific adsorption by the larger proteins. Lower molecular weight proteins tended to non-specifically adsorb to a greater extent because less of their surface area is exposed to the OH groups.

An alternative surface chemistry to that of alkyl thiol monolayers was also explored in the form of electrografted aryl films derived from diazonium salts. Para-benzoic acid aryl layers were generated on gold from the diazonium salt by sweeping across a reductive potential at five different scanning rates. Peak currents obtained from cyclic voltammetry increased with voltammetric scanning rates (ν) in a manner consistent with a quasi-reversible, diffusion-limited process. Incomplete film formation at higher values of ν was evident from observable current on the second cycles.

Further characterization was carried out with infrared reflectance absorbance spectroscopy (IRRAS). Changes in the wavenumber and absorbance of the carbonyl stretch with varying voltammetric sweep rates suggests ν to partially control the aryl film's structure. The binding of His_6-tagged cAMP receptor protein (CRP) to these aryl layers was measured using SPRi following EDC/NHS coupling to produce NTA terminal groups on the surface. Binding curves in nickel-loaded buffer confirmed the IRRAS results, showing ν to determine the extent of CRP attachment. Control experiments demonstrated attachment to the NTA-aryl layers occurring both non-specifically and via NTA-Ni^{2+}-His_6 coordination.

Acknowledgements

Obtaining a graduate degree in the experimental sciences is much like undertaking a marathon. This is clichéd, but very true. The three years have been a long, but ultimately fruitful journey. Like many lengthy endeavors, the pitfalls and rewards may not be what was anticipated and planned for at the beginning. The experience has toughened my mind considerably, coming out of this program.

I owe thanks to many people for successfully completing this master's. Chief among them would be my family, whose unconditional love and support have gotten me through difficult times and have shaped the man I am today. Second, my supervisor, Mark McDermott, provided a great work environment with lots of freedom and a light touch as a boss. For that I am grateful. The other McDermott group members were helpful for bouncing around ideas and supplying some insider information. Special thanks goes out to Rory Chisholm and Chris Grant, who were always willing to entertain new ideas, share their expertise, and simply shoot the breeze. Good luck to both of you in finishing your doctorates and entering the next phase, whatever that may be.

Glen Zhang, from the Wiener research group in Biochemistry here at the University of Alberta, collaborated with our group on this project. All fusion proteins employed in Chapters II and III were produced and purified by Glen.

The shadowmask used in Chapter III was fabricated by the chemistry department's machine shop, specifically Vincent Bizon and Roman Lipiecki. Vincent also aided me in the design and construction of an electrode array, which unfortunately did not pan out in the lab. I can't say enough in the way of good things about this shop and the skill of its staff members.

I would like to express my gratitude to Mount Allison faculty members Stephen Duffy, Glen Briand, Steve Westcott, John Read, Andrew Grant, Hans vanderLeest (Classics), and David Torrance (History). Each of you was a major positive influence during my undergraduate years, and left me with fond memories and a solid foundation, both within and outside of chemistry. This also goes for the many students and other members of the Mount Allison and Sackville communities whom I crossed paths with. You know who you are.

Finally, to the many unnamed others who have been a positive part of my life, thank you all.

Table of Contents

CHAPTER I: INTRODUCTION

General Introduction	1
Microarray Technologies	4
Self-Assembled Monolayers of Thiols	13
Surface Plasmon Resonance Imaging	17
Cyclic Voltammetry	19
Infrared Reflectance Absorption Spectroscopy	21
Aryl Layers Derived from Diazonium Salts	23
Research Objectives	26
References	27

CHAPTER II: PROBING THE BINDING OF HEXAHISTIDINE-TAGGED PROTEINS ON MIXED THIOL MONOLAYERS USING SURFACE PLASMON RESONANCE IMAGING

Introduction	33
Experimental	36
Results and Discussion	43
Conclusions	64
References	65

CHAPTER III: ELECTROCHEMICALLY GRAFTED ARYL LAYERS FOR USE IN SURFACE PLASMON RESONANCE IMAGING

Introduction 68

Experimental 75

Results and Discussion 82

Conclusions 102

References 103

CHAPTER IV: CONCLUSIONS AND FUTURE WORK

General Conclusions 106

Suggestions for Future Work 107

References 109

List of Tables

Table 2.1. Selected properties of His_6-tagged proteins used in this study. 44

Table 2.2. Summary of results obtained from fitting the four parameter logistic equation to His_6-protein binding curves. 48

Table 3.1. Peaks obtained for the SPR chip electrodes at various scanning speeds in 2.0 mM p-benzoic acid. 86

List of Figures

Figure 1.01. Adsorption of a protein to a surface. 3

Figure 1.02. Important interactions between adsorbed proteins. 5

Figure 1.03. General categories of immobilization methods for proteins. 9

Figure 1.04. Coordination of a hexahistidine-tagged protein to a nitrilotriacetic acid (NTA) surface functionality via nickel (II). 12

Figure 1.05. Self-assembly of alkyl thiols on a gold surface. 14

Figure 1.06. Schematic for a surface plasmon resonance instrument. 18

Figure 1.07. Setup for a cyclic voltammetry experiment. 20

Figure 1.08. Electrografting and a possible structure of diazonium derived aryl layers. 25

Figure 2.01. Aluminum shadowmask and layout of a fabricated SPR chip, showing the 3 X 3 pattern of 2.0 mm gold spots. 37

Figure 2.02. Synthesis and generation of the HSC_9NTA capture layers. 39

Figure 2.03. Sample difference image of a chip in a nickel-buffer solution of 2000 nM α-amylase. 41

Figure 2.04. Plot of Δ%R vs solution concentration of α-amylase for a 20 % HSC_9NTA capture surface. 46

Figure 2.05. Plot of Δ%R vs solution concentration of β-galactosidase (β-Gal) attaching to a 100 % HSC_9NTA capture surface. 47

Figure 2.06. Binding curves of cAMP receptor protein (CRP) on the three thiol monolayers employed. 50

Figure 2.07. Binding curves of α-amylase (Amyl) on the three thiol monolayers employed. 51

Figure 2.08. Binding curves of fibrinogen activation protein (F_{AP}) on the three thiol monolayers employed. 52

Figure 2.09. Binding curves of β-galactosidase (β-Gal) on the three thiol monolayers employed. 53

Figure 2.10. The maximum change in the reflectivity at the 100 % HSC_9NTA capture surface plotted as a function of the molecular weights of the proteins employed. 55

Figure 2.11. The maximum change in the reflectivity at the 100 % HSC_9NTA capture surface plotted as a function of the calculated surface areas of the proteins employed. 56

Figure 2.12. Bovine serum albumin (BSA) attaching to 100 %, 50 %, and 20 % HSC_9NTA capture surfaces (in buffer containing nickel). 59

Figure 2.13. Fitted SPR curve of cAMP receptor protein (CRP) attaching to a 100 % HSC_9NTA capture surface, in the absence of nickel. 61

Figure 2.14. Partial regeneration of the 50 % HSC_9NTA capture surface after saturation with cAMP receptor protein (CRP). 62

Figure 2.15. Partial regeneration of the 50 % HSC_9NTA capture surface after saturation with fibroblast activation protein (F_{AP}). 63

Figure 3.01. Radical formation and attachment to a surface for a diazonium salt. 69

Figure 3.02. SPR chips for the electrochemical grafting of arrays of p-benzoic acid aryl layers. 77

Figure 3.03. Electrochemical grafting of the p-benzoic acid diazonium salt, activation with EDC and NHS, and subsequent modification with AB-NTA. 80

Figure 3.04. Cyclic voltammetry of 2.0 mM dBA (100 mM $TBABF_4$) at an SPR chip electrode. The scan rate was 50 mV/sec. 84

Figure 3.05. Cyclic voltammetry of 2.0 mM dBA (100 mM $TBABF_4$) at an SPR chip electrode. The scan rate was 400 mV/sec SPR chip. 85

Figure 3.06. Logarithmic plot of peak currents against the scan rate for the SPR chip electrodes. 88

Figure 3.07. Cyclic voltammetry of 2.0 mM dBA (100 mM $TBABF_4$) at an IR slide. The scan rate was 50 mV/sec. 89

Figure 3.08. IRRAS spectra of the aryl layers grafted at varying scan speeds, stacked upon one another. 91

Figure 3.09. Plot of the carbonyl stretch ($\nu_{C=O}$, 1700 cm^{-1}) vs deposition sweep rate for dBA films. 92

Figure 3.10. Plot of the absorbance of the carbonyl stretch ($\nu_{C=O}$, 1700 cm^{-1}) vs deposition sweep rate for dBA films. 93

Figure 3.11. Possible structure of the electrografted para-substituted diazonium salt. 95

Figure 3.12. Difference image of an SPR chip electrode in the flow cell of the GWC SPRimagerII, in a solution of 2000 nM cAMP receptor protein. 97

Figure 3.13. Stacked binding curves of cAMP receptor protein on NTA-terminated dBA layers deposited at varying scan rates. 98

Figure 3.14. Signal intensities from the SPR binding curves of cAMP receptor protein, at 1000 nM, attaching to NTA-conjugated dBA layers deposited over a range of scan rates. 99

Figure 3.15. Comparison of the signal intensities obtained from the protein binding curves on the four aryl layers grafted at 200 mV/sec. cAMP receptor protein (CRP) on the 200 mV/sec sample, CRP on the unactivated surface (no NTA groups), CRP in the absence of nickel sulfate, and bovine serum albumin (60 kDa, no hexahistidine tag). 101

List of Symbols

α_i	Hydropathy score of species *i*
f_i	Frequency of species *i*
$\Delta\%R$	Percentage change in reflectivity
$\Delta\%R_{min}$	Minimum percentage change in reflectivity
$\Delta\%R_{max}$	Maximum percentage change in reflectivity
$SA_{ellipsoid}$	Surface area of an ellipsoid
EC_{50}	Concentration of adsorbate at half of maximum response
K_d	Dissociation constant
[A]	Concentration of adsorbate *A* in solution
R^2	Squared correlational coefficient
ν	Voltammetric scanning rate *or* infrared wavenumber.
ω	Omega, terminal chemical functionality

List of Abbreviations

AB-NTA	(N-5-amino-1-carboxypentyl)imino-diacetic acid
AFM	Atomic force microscopy
Amyl	α-Amylase
β-Gal	β-Galactosidase
BSA	Bovine serum albumin
C_n	Alkyl chain of *n* units
cAMP	Cyclic adenosine monophosphate
CCD	Charge-coupled detector
CI	Confidence interval
CRP	cAMP receptor protein
CV	Cyclic voltammetry *or* cyclic voltammogram
dBA	Diazonium-derived para-benzoic acid
DCC	N-N'-Dicyclohexylcarbodiimide
DFT	Density functional theory
DI	Deionized
EDC	1-ethyl-3-[3-dimethylaminopropyl]carbodiimide hydrochloride
EDTA	Ethylene diamine tetraacetic acid
ESI	Electrospray ionization
F_{AP}	Fibroblast activation protein, alpha
FT	Fourier transform
FTIR-ATR	Fourier transform infrared attenuated total reflectance

FWHM	Full width at half maximum
GRAVY	Grand average of hydrophobicity
His_6	Hexahistidine-tagged
HOPG	Highly oriented pyrolytic graphite
HPLC	High performance liquid chromatography
IgG	Immunoglobulin G
IRRAS	Infrared reflection absorption spectroscopy
JACS	Journal of the American Chemical Society
NHS	N-hydroxysuccinimide
NTA	Nitrilotriacetic acid
p-(polarized)	Parallel (polarized light)
s-(polarized)	*Senkrecht* [German for *perpendicular*] (polarized light)
SCE	Saturated calomel electrode
SERS	Surface enhanced Raman spectroscopy
SFM	Scanning force microscopy
SPR	Surface plasmon resonance
STM	Scanning tunneling microscopy
TOF-SIMS	Time-of-flight secondary ion mass spectrometry
v/v	Fraction by volumes
XPS	X-ray photoelectron spectroscopy

CHAPTER I

INTRODUCTION

General Introduction

Proteins are large heterogeneous polymers composed of twenty naturally occurring amino acids. The sequence of amino acids, or primary structure, in turn dictates how these amino acids interact with both one another and the surrounding aqueous environment. Because the isolectric points and hydrophobicities vary between the amino acids, a large combination of interactions are possible. These interactions produce both local (secondary) and overall (tertiary) three dimensional structures representing stable free energy minimums.[1] In some cases, complexes (or quaternary structures) of one or more kinds of proteins are formed, with the oxygen-ferrying hemoglobin complex as a classic example. It is the aforementioned highly sequence-specific 3-D structures that lend proteins their great utility as structural components, catalysts, gatekeepers, translators, and many other roles in all living organisms.[2] Proteins have even been dubbed "Nature's Robots" by one author.[3]

An interface is an essentially two-dimensional, high energy boundary between phases. A surface, distinct from an interface, is the two-dimensional face of one phase.[4] "Surface" and "interface" are typically used interchangeably, as will be the case here as well. This thesis explores

the analysis of proteins at the solid-liquid boundary, and "surfaces" mentioned from now on will be assumed to be of this type.[5]

Proteins at Interfaces. Exploring the interactions of biomolecules at surfaces, proteins foremost amongst them, is crucial for several reasons. Besides such major applications as implantable materials and devices that resist biofouling,[6-9] the rise of the field of proteomics (see *Microarray Technologies* below) has spurred the development of both general-purpose and highly-specific biosensors.[10-12]

Figure 1.01 illustrates the general process of protein adsorption to a surface. A range of competing events occur, even when considering only a single protein adsorbing to a pristine surface. Nevertheless, a model such as this is still useful as a starting point in the understanding of proteins at interfaces.

Traditionally, entropic (hydrophobic and hydrophilic) interactions are believed to be the primary factor determining adsorptive behaviour.[13, 14] For example, Cha et al. recently measured a variety of interfacial energetics parameters of ten proteins of 11 kDa to 1000 kDa, found in blood.[14] Intriguingly, advancing contact angle measurements showed little discernible variation in Gibbs' surface excess (which measures the difference in the amount of protein adsorbed at solid-vapor (SV) and solid-liquid (SL) interface) among the proteins when adsorbing to the same surface. Having tested four surfaces spanning a range of hydrophobicities, the authors concluded that the displacement of surface-bound water is the

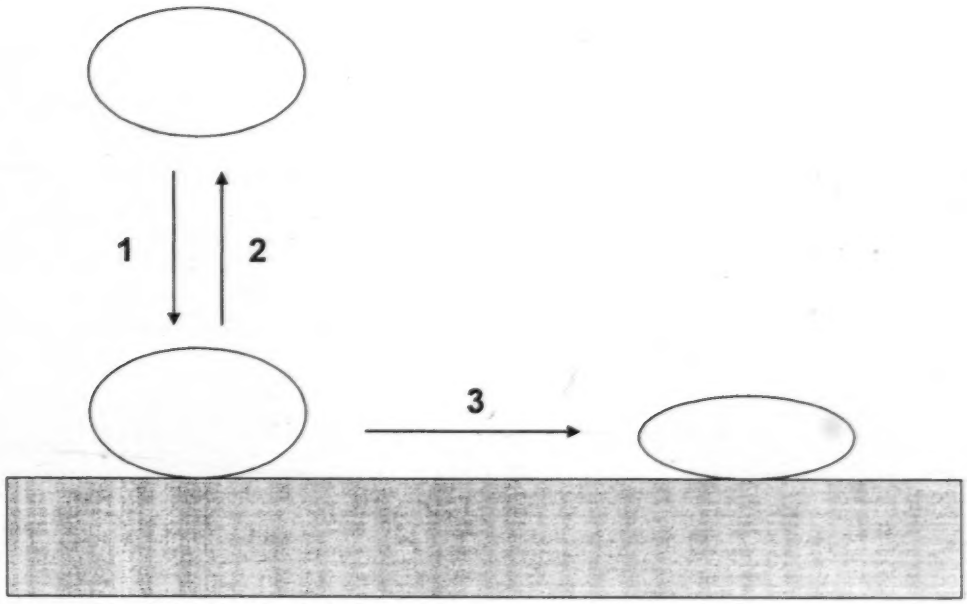

Figure 1.01. Simplified conception of the adsorption of a protein to a surface. 1 = adsorption, 2 = desorption 3 = irreversible denaturation. Note that irreversible adsorption is not the only possible final form an adsorbed protein can take. This illustrations omits many possible intermediate states and events in the interest of clarity.

primary factor controlling the thermodynamics of protein adsorption.

Other researchers emphasize that both electrostatic and entropic interactions are crucial, and will vary in importance depending on the particular protein-surface system.[15-18] Luo and Andrade examined the adsorption of four diverse proteins to (zwitterionic) hydroxyapatite at several pH values, finding the overall charge of the protein and the pH of the solution to control at least the initial stages of the protein adsorption.[16] One of the atypical aspects of the Luo and Andrade study was the use of Hill plots, in place of the standard Langmuir,[17] Freudlich,[19] or similar curves, to fit the adsorption isotherms. The authors extracted two or three Hill coefficients from each of their adsorption isotherms, taking the changing slopes to be a measure of the changing co-operativity of the protein adsorption at different stages (e.g. nearly empty surface, partially filled, almost totally filled). The authors emphasized conformational changes due to a combination of electrostatic protein-surface and protein-protein interactions, although they were unable to separate out one from the other. Several key interactions between two adsorbed model proteins are illustrated in Figure 1.02.

Microarray Technologies

The field of genomics has advanced tremendously following the completion of the Human Genome Project. Now that databases of the complete sequences of multiple keystone species (*E. coli*,[20] yeast,[21] fruit

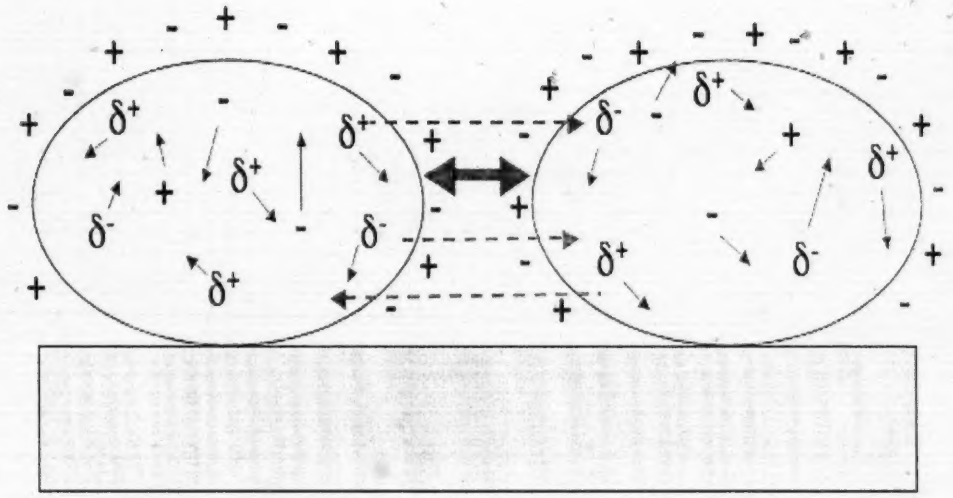

Figure 1.02. Simplified view of some important interactions between adsorbed proteins. *Double-headed blue arrow* = steric and electrostatic repulsion; *green arrows* = attractive combinations of Van der Waals, dipole, and charge interactions; *small red arrows* = spatial fluctuation of "patchy" dipoles and charges. Details of interaction with the surface are omitted.

flies,[22] mice,[23] humans[24, 25]) are available, efforts have shifted to applications of this data in both fundamental studies of the products of gene expression and in medical diagnostics.[26] Only a fraction of the genes in a given cell are expressed, and the control of this expression depends on a multitude of complex and interacting feedback loops involving the presence of messenger and repressor proteins (e.g. the lactose-lac repressor protein-lac operon relationship), concentrations of key molecules and ions within the cell, and other factors.[27] So knowing the sequence of a cell's DNA is only a first step in understanding the cell's behaviour and the intricate web of biochemical cycles within it. The next step, knowing which genes are active and their differing levels of expression, requires a massively parallel experimental technique.

The development of DNA/RNA arrays has allowed the performance of large scale experiments that were formerly impractical, as previous assays did not typically allow for miniaturization or continuous monitoring.[28] In particular, changes in the levels and sequences of messenger RNA (mRNA) can be monitored to determine changes in the presence or absence of expressed genes, their levels, and point mutations in the DNA.[29] This knowledge is important, for example, in the diagnosis of genetic diseases, or in the examination of environmental effects on gene expression in otherwise identical cells.

Despite the importance of DNA and RNA, it is proteins that are the workhorses of every cell, and the ultimate product of the classically

understood DNA ⇒ RNA ⇒ protein pathway. Rapid, high-throughput assays are all the more necessary in the study of proteins, but their implementation faces additional challenges not seen in the development of DNA/RNA microarrays. Whereas DNA and RNA are composed of four nucleotide bases, proteins possess twenty amino acid residues. As a consequence, proteins typically have more elaborate three-dimensional structures than DNA and RNA, which lends them great utility as biochemical tools but also makes them much more fragile than DNA. Finally, there are also post-translational modifications, which involve the alteration of a protein through a variety of means following its translation from RNA at the cell's ribosome. Notable post-translational modifications include the grafting of carbohydrates, but also peptides, lipids, small molecules, and other proteins.[30] These modifications are still poorly understood, expanding an already enormous number of possible proteins into a near infinite range of structural variations.

Attachment methods. Antibodies have long been used as analytical reagents, especially in diagnostic applications such as pregnancy tests.[31] They are favoured for their extreme specificity, whether to proteins, peptides, carbohydrates, or small molecules, and are relatively stable in comparison to most other proteins. Additionally, proteins that have lost their biological activity may still be immunologically active.[32] As such, surface-bound antibodies, adsorbed or covalently bound, are a popular way of immobilizing antigenic proteins to surfaces in a specific manner. They

can also easily be adapted into an array format. Once binding between the immobilized antibody and protein antigen occurs, a variety of techniques can be used for detection and quantitation, either of the antigen itself or an analyte that interacts with the immobilized antigen (such as a substrate if the antigen is an enzyme). Fluorescent and chemilluminescent labels can be conjugated to the species of interest for fluorescence or colorimetric measurements, although other techniques are possible, such as electrochemical measurements.[33] The main disadvantage of antibody-based arrays is the high cost of the antibodies, especially if monoclonal antibodies are employed or if new antibodies must be developed for the antigen of interest.

Antibodies are one class of proteins that are generally immobilized on the surface for bioassays. Another class commonly immobilized for use in biosensors is enzymes. Immobilized enzymes essentially offer the ability to design customized catalytic surfaces that allow for facile separation and purification of a product.[34] Beyond their many uses in industrial syntheses, immobilized enzymes have been employed in diagnostic devices, the most high-profile examples being glucose sensors for diabetics.[35]

The immobilization of proteins to various surfaces can be achieved by a number of means. A cartoon of the three general categories of attachment is shown in Figure 1.03. The easiest among these to perform experimentally would be physisorption, non-covalent interactions such as hydrogen bonding or Van der Waals interactions, resulting in a weak and

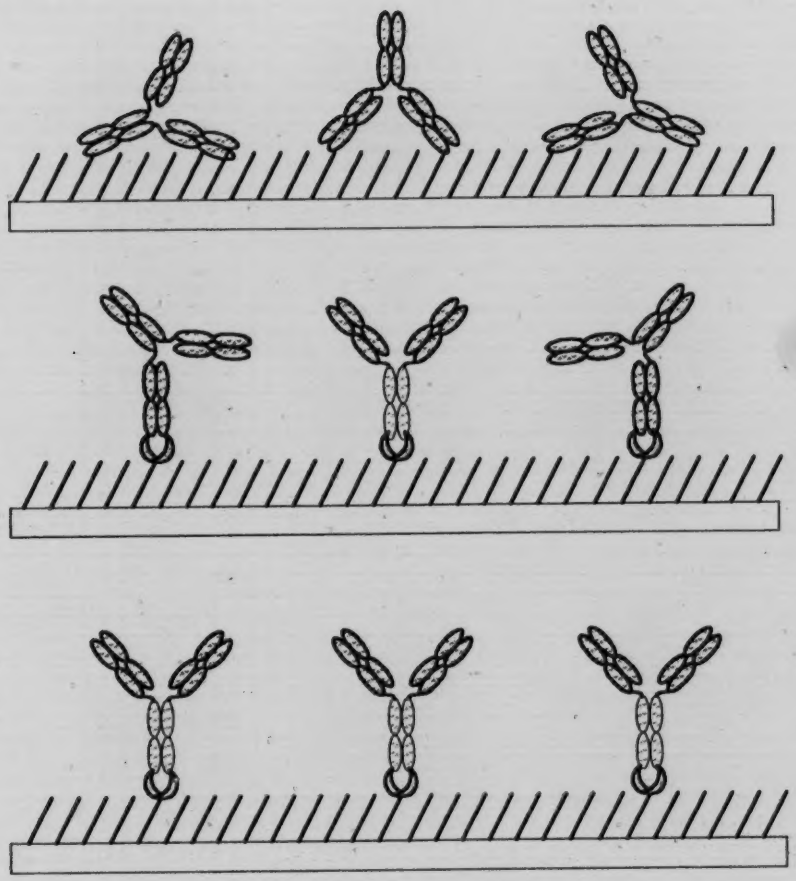

Figure 1.03. General categories of immobilization methods for proteins. From top to bottom: *physisorption*, *unoriented covalent attachment*, and *oriented covalent or coordinate coupling*.

randomly oriented attachment to the surface. Chemical attachment, such as the formation of an amide linkage to the terminus of a protein, is much stronger than physisorption and often easy to perform, but also yields random orientations. Since orientation of an enzyme or antibody away from the surface is necessary for these proteins to retain their native activities and utility in sensors, it is often highly desirable to ensure these species are strongly attached and uniformly oriented, if performance is a consideration. To this end, a number of affinity tags possessing a strong and specific interaction, away from the protein's active binding or catalytic site, have been developed.

Affinity tags. The sequence of the protein of interest, along with a peptide tag, is encoded into the DNA of a target organism, typically *E. coli* or yeast, and overexpressed. This produces a "fusion protein", where the tag is fused to the protein, often on the C- or N-terminus. The fusion protein is purified on a column containing a species that will specifically bind the peptide tag. That species on the column surface can be a protein that recognizes the peptide as a binding partner, such as calmodulin and a fusion protein with calmodulin-binding peptide (CBP) as its tag. Alternatively, the column can incorporate a small molecule that binds to the tag. This may occur directly, as in the case of glutathione S-transferase and glutathione, or through an intermediate such as a coordinated metal centre, seen in the hexahistidine tag/nickel/nitrilotriacetic acid system.[36] In the latter case the metal centre acts as a bridge between the surface

ligands and the tagged protein. This study makes use of the hexahistidine tag, which is discussed in greater detail below.

The His_6-tag. Histidine is the amino acid that features the strongest interaction with immobilized metal resins, coordinating to transition metals via electron donation from its imidazole rings.[37] Although immobilized metal-affinity chromatography has been employed as a protein purification technique since the mid 1970s,[38] it was not until 1988 that a fusion protein, His_6-tagged dihydrofolate reductase, was purified on a nickel ion matrix over nitrilotriacetic acid (NTA).[39] NTA is especially suited for the formation of six-coordinate metal centres, as it forms a quadridentate linkage to the metal, leaving two binding sites open. In the case of its interaction with His_6-tagged proteins, two imidazole groups from the histidines fill the remaining sites. The resulting six-coordinate nickel complex has a specific, reversible interaction of moderate strength (typical dissociation constant of $K_d = 10^{-9}$ to 10^{-6} M).[40, 41] A diagram of NTA coordinating to nickel (II) and a His6-tag is shown below in Figure 1.04.

The His_6-Ni^{2+}-NTA system has been employed in SPR analysis for nearly fifteen years.[42] Since that time, many SPR studies have routinely made use of this system of immobilization, not least because disruption of the coordination allows potential reuse of expensive biochips.[41] Of particular interest with regards to both fundamental studies and potential diagnostic applications are protein-protein interactions.[43, 44] These interactions are crucial in a variety of cellular processes, such as protein

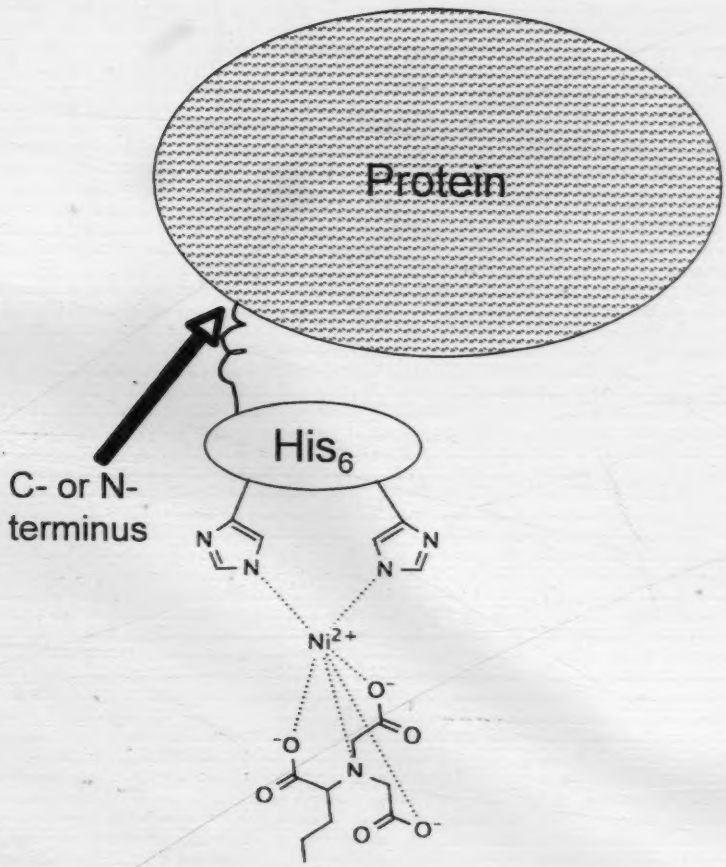

Figure 1.04. Coordination of a hexahistidine-tagged protein to a nitrilotriacetic acid (NTA) surface functionality via nickel (II). Two imidazole groups from the histidines coordinate to the nickel ion. The NTA forms four linkages resulting in a six-coordinate nickel complex.

trafficking and synaptic transmission.[45] SPR imaging has shown itself to be a particularly useful technique in allowing the visualization of these interactions on microarrays.

Self-Assembled Monolayers of Thiols

Self-assembled monolayers (SAMs) are composed of one or more kinds of molecules possessing a functional group or region with a strong affinity for a particular surface. For example, siloxanes are extensively employed for immobilization to silica surfaces.[46] Similarly, thiols (typically alkyl thiols of the form $HS(CH_2)_nR$) currently dominate the modification of gold or silver surfaces.[47]

Alkyl thiol SAMs on gold, as depicted in Figure 1.05, have carved out a large niche in the field of surface chemistry. Fundamental characterization studies began approximately twenty-five years ago.[48] In particular, scanning probe microscopies (SPM),[49, 50] ellipsometry,[51] and infrared reflectance absorbance spectroscopy (IRRAS)[50, 51] have combined to yield a fairly comprehensive portrait on the ordering, mobility, and structural dependence on the assembly conditions.[52, 53] In single component monolayers of this class, the length of the carbon backbone chain seems to be the most important structural parameter. Using IRRAS, ellipsometry, and electron transfer measurements on a series of alkyl thiols [$HS(CH_2)_nCH_3$], Porter et al. showed carbon chains of n = 1 to 5 forming disordered, "liquid" monolayers.[51] Conversely, a transition region of n = 6

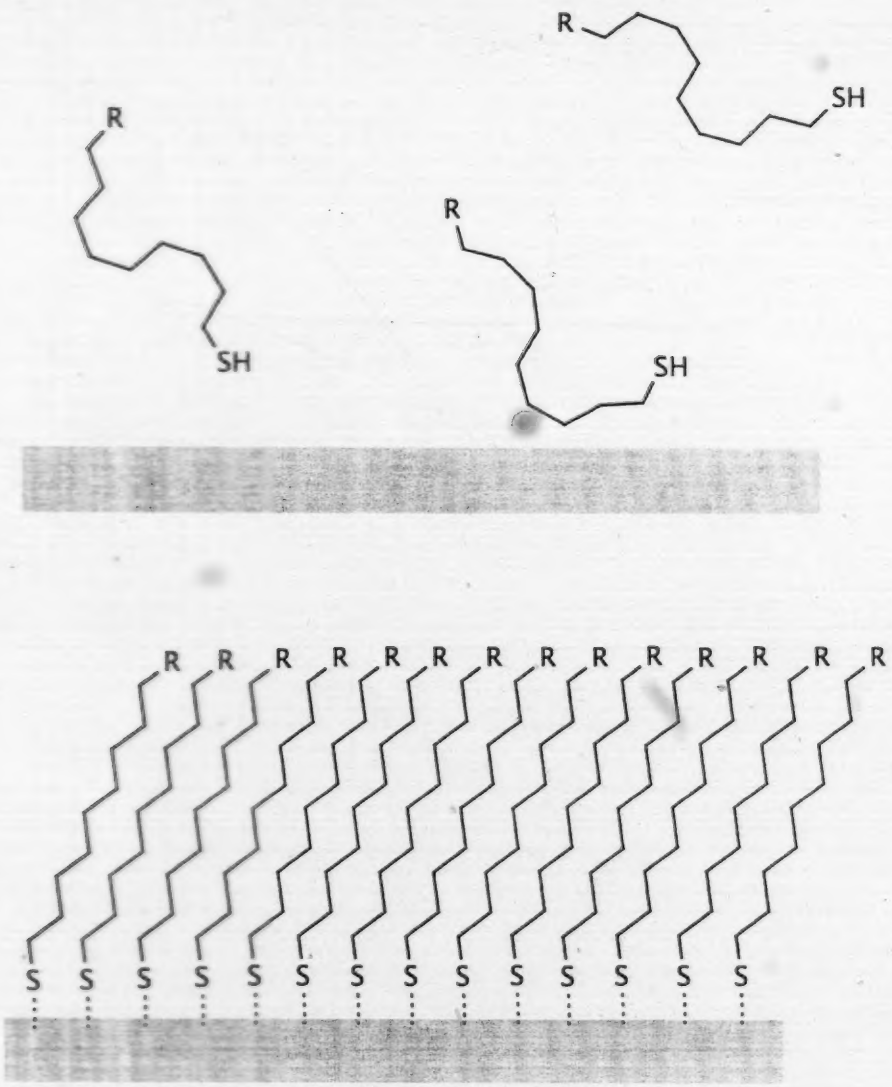

Figure 1.05. Self-assembly of alkyl thiols on a gold surface. Van der Waals interactions between the hydrocarbon backbones of adjacent molecules are thought to be responsible for the crystalline phase ordering of long-chain ($\geq C_{10}$) alkyl thiol monolayers. The hydrocarbon chains are in an all-trans configuration, with an average tilt from the surface normal of 27°. The sulfur's hydrogen is though to leave as H_2 gas following attachment to the gold surface, although the mechanism of this process is unclear at present.

to 9, followed by a crystalline film structure when n ≥ 10, was shown primarily through systematic changes in the methylene and methyl IR peak positions. Van der Waals interactions between adjacent carbon backbones are thought to be the driving force of ordering on the surface and the reason for the SAM's structural dependence on the hydrocarbon chain length. A composite picture of the typical crystalline alkyl thiol film on gold that has emerged from the IRRAS characterization and modeling has the chains all-trans, at 27° normal to the surface (on average).

Although other functionalities may be used to generate SAMs on gold, including sulfides (RSR), disulfides (RSSR), and phosphines (R_3P), SAMs derived from alkyl thiols have been shown to be of superior quality.[52, 54] Recently, the nature of the sulfur-gold interaction has been studied through NMR[55] and X-ray crystallographic[56] experiments.

Mixed alkyl thiol SAMs have also been studied for a number of years, with their mixing behaviour shown to be dependent on disparities in the alkyl chain lengths and interactions of the terminal functional groups. Specifically, mixed alkyl thiols where one of the chain lengths is short (C ≤ 6) or with bulky end groups will phase segregate,[57, 58] while mixtures of similar chain length or where both possess long chain backbones, will typically be homogenous or form very small patches (tens of Angstroms).[49, 59, 60] For alkyl thiols of similar chain lengths, the formation of the SAM is thought to be under thermodynamic control, supported by an unchanging film structure following initial assembly (12 to 24 hours).[52] The composition

of films from alkyl thiols of different chain lengths, on the other hand, do change for several weeks after initial assembly. This suggests the initial SAM is in a metastable, kinetically trapped state, although initial assembly conditions still play a large role.[61]

Following from the above characterization, mixed thiol SAMs have more recently been (and continue to be) extensively employed in the generation of biosensor surfaces, in particular for proteins.[58, 62-66] The composition of these mixed SAMs on the surface can be controlled by varying the molar ratio of the thiols in solution, although the surface must still be characterized since the molar ratio of SAMs on the surface will not necessarily be the same as in solution.[67] This control over the makeup of the mixed SAMs allows the design of surfaces having a specific interaction with an engineered portion of a protein (e.g. $HS(CH_2)_n$—biotin + strepavidin-tagged protein),[68, 69] and minimizing non-specific interactions due to a surrounding protein resistant matrix (e.g. $HS(CH_2)_n$—polyethylene glycol).[62, 65, 70, 71]

One of the chief disadvantages of thiol monolayers is their poor stability under ambient conditions. The thiols are particularly prone to oxidation due to atmospheric exposure and decomposition under ultraviolet light.[47, 53] For this reason electrochemically grafted diazonium-derived aryl layers (see *Aryl Layers Derived from Diazonium Salts* below) are currently being investigated as a potential class of thin films for the generation of sensor surfaces.

Surface Plasmon Resonance Imaging

Surface plasmon resonance (SPR) is a label-free optical sensing technique that has found widespread use in the study of biomolecular interactions.[72, 73] A typical instrumental setup is illustrated in Figure 1.06. In brief, a light source (broadband or laser) passes through a polarization filter to select p-polarized light. This light then passes through an index-matched prism and glass chip prior to hitting a metal surface. Since light has an electric field component, at certain angles of incidence and wavelengths, a portion of the light that is in a plane perpendicular to a metal surface (p-polarized) will couple to the surface's electric field, creating an oscillating evanescent wave or surface plasmon extending from the surface. The intensity of the reflected light to the charge coupled diode (CCD) detector will therefore decrease as coupling to the surface plasmon increases. The surface plasmon resonance will be maximized and the reflected light minimized at a specific angle and wavelength (Figure 1.06).[74]

The surface plasmon results in an evanescent wave that decays exponentially with distance from the surface, becoming greatly diminished at hundreds of nanometres.[75] In practice, it is the space within a few nanometres of the surface that is typically used for sensing purposes. If a mass found in the flow cell solution, such as a protein, attaches to the metal surface, the coupling of the electric fields will be altered due to a

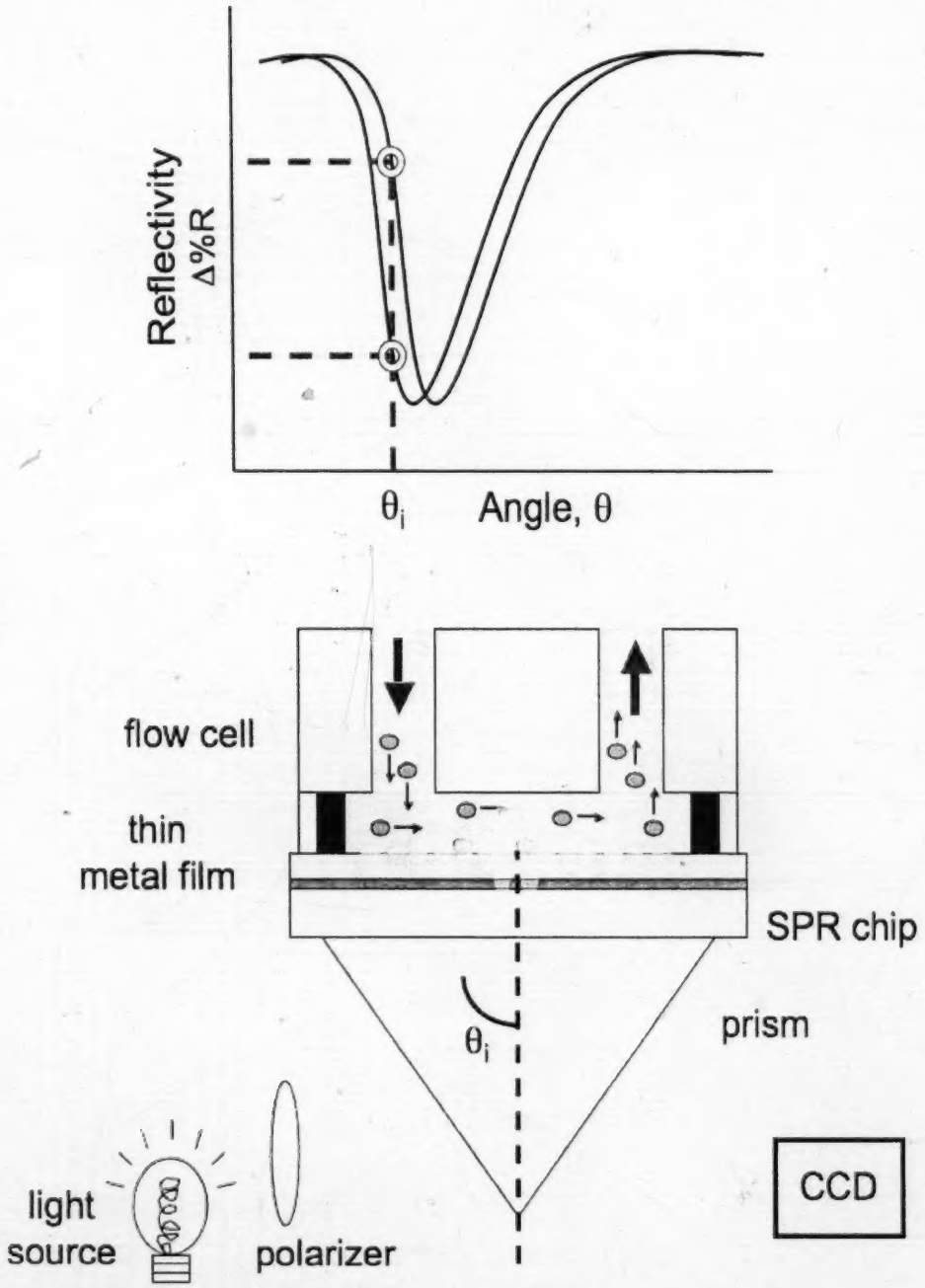

Figure 1.06. Schematic for a surface plasmon resonance instrument. The film of gold and adhesive underlayer (Cr or Ti) is sufficiently thin (< 100 nm) to be optically transparent. The curve above shows a shift in the angle of minimum reflectivity following a binding event at the surface.

change in the refractive index at the surface. The angle at which this coupling is maximal is altered, which is detected via a shift in the angle of the minimum reflectivity. The change in refractive index, and the resulting angle shift, can be correlated to the mass of material on the surface. SPR is thus especially suited to the study of interfacial interactions.

Cyclic Voltammetry

Cyclic voltammetry is an electrochemical technique for the generation and analysis of redox reactions at a surface. A typical experimental setup is shown in Figure 1.07. A conductive surface of known dimensions (the working electrode) is immersed in a solution containing the analyte of interest and a supporting electrolyte to ensure sufficient conductivity. A chemically inert auxiliary electrode, such as platinum metal, completes the circuit. Finally, a solvent matched reference electrode of known half cell potential allows the potential at the working electrode to be measured and controlled.

During an experiment, an applied potential between the working and auxiliary electrodes is varied over a defined range at a constant rate with time. The current over this potential range is measured, with any redox processes occurring at the working electrode's surface appearing as positive and negative peaks. The potentials, widths, and heights of the redox peaks often yield quantitative data such as average surface coverage, thermodynamic properties (half-cell potential $E^{\circ}_{1/2}$, Gibbs free energy,

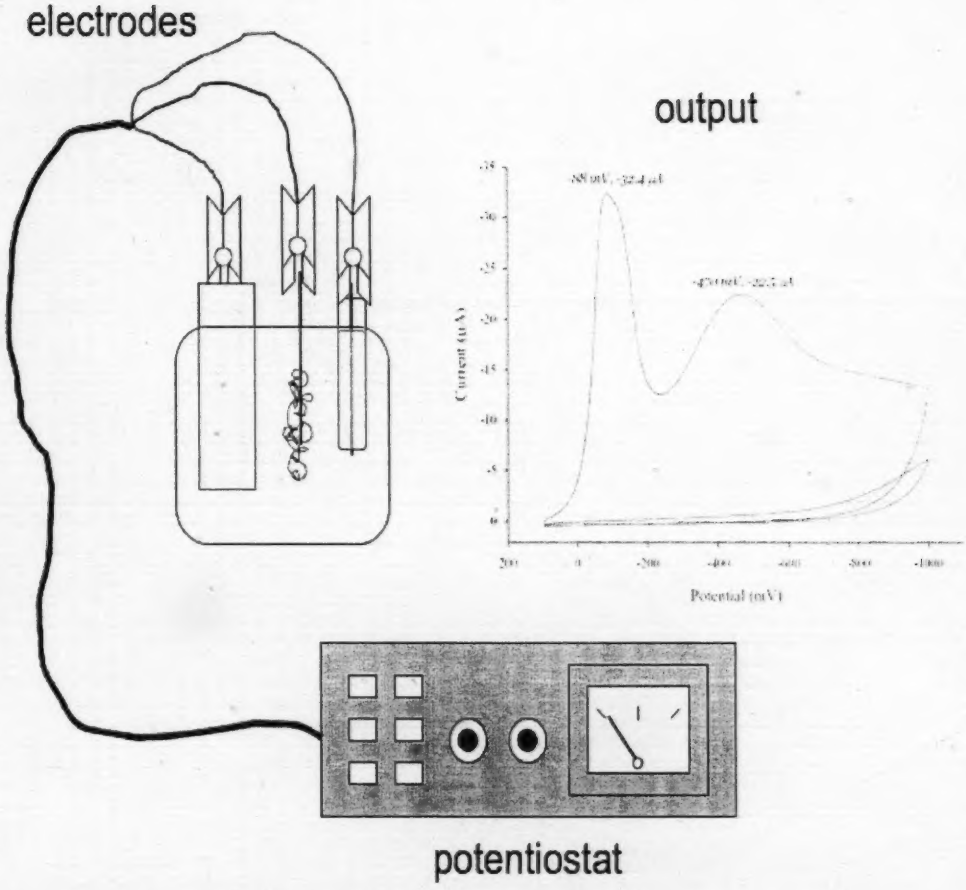

Figure 1.07. Setup for a cyclic voltamettry experiment. Red = working electrode, blue = auxiliary electrode, green = reference electrode. A sample voltammogram in the North American format (inverted axes), showing two reduction peaks.

etc.), and the kinetics of the process (electron transfer rate, diffusion to the surface).[76]

Infrared Reflectance Absorption Spectroscopy (IRRAS)

Fourier-transform IRRAS is an infrared spectroscopic technique for the analysis of surface-bound species. p-Polarized infrared light is shone on the sample surface at a glancing angle, inducing an electric field normal to the surface ($\overrightarrow{E_{z\,INDUCED}}$). This induced electric field couples to the component of the incoming IR light's electric field that is also normal to the surface ($\overrightarrow{E_{z\,IR}}$), enlarging the overall electric field in this direction ($\overrightarrow{E_z}$ = $\overrightarrow{E_{z\,INDUCED}}$ + $\overrightarrow{E_{z\,IR}}$). The perpendicular portion of IR active dipoles of molecules attached to the surface will interact with the enhanced electric field $\overrightarrow{E_z}$, resulting in absorption at the characteristic IR wavelengths of functional groups.[77] Since only the perpendicular portion of IR active dipoles give absorbance, variations in the peak intensities indicate not only the quantity of the surface-bound species, but also their orientations on the surface. IRRAS substrates must have some conductivity in order for an electric field to be induced by incoming p-polarized IR light. For this reason metallic substrates such as gold and silver, having large electric fields, are preferred,[78] although carbon and some other non-metal surfaces can also be used.[79, 80] Changes in peak widths and positions can also give a measure of the ordering of the attached molecules under varying conditions.[51]

IRRAS has found wide application in the field of surface science since it was first described some fifty years ago.[77] Perhaps the most well-known fundamental IRRAS study applied to monolayers was the comparative characterization of a series of alkyl thiols of varied chain lengths on gold by Porter et al. in 1987, previously described in this chapter.[51] Other fundamental studies employing IRRAS include Battaglini et al.'s comparison of the octadecanethiol (ODT) monolayer structure on flat Au (111) and on a stepped Au (755) surface with (111) terraces.[81] IRRAS showed the ODT film on the stepped gold to be *more* crystalline. STM analysis accounted for this by revealing fewer grains compared to the flat Au(111) ODT SAM. IRRAS has also shown hydrogen-bonding to occur on SAMs with terminal carboxylic acid functionalities.[82]

In the context of biosensor applications, IRRAS is typically employed to characterize thin films prior to protein immobilization. In some cases, however, IRRAS is used to quantitatively follow protein attachment via the prominent twin amide bands around 1545 cm^{-1} and 1665 cm^{-1}. For example, Liu et al. were able to quantitatively follow the generation of an amine-terminated film, its coupling to biotin, and the subsequent specific attachment of avidin protein.[83] With the correct instrumental accessories, variants of IRRAS (such as polarization modulation IRRAS, PM-IRRAS) can even follow the modification of a surface and subsequent attachment of a protein *in situ*. This was the case when cytochrome c was attached to an

NTA-terminated SAM on a gold electrode that had been backfilled with a lipid bilayer.[84]

Aryl Layers Derived from Diazonium Salts

Diazonium cations, consisting of an aromatic group with an attached dinitrogen ion [Ph-N≡N]$^+$, are reactive but usually stable intermediates, nowadays typically in the form of borofluorate salts. Long used in organic synthesis,[85, 86] they are produced from an aromatic amine precursor, which is reacted with nitrite in acid. The resulting diazonium cation is strongly activating to nucleophilic substitution, making it a useful synthetic intermediate.

More recently, it has been shown that the aryl radical intermediate resulting from the reduction of diazonium cations can be grafted to an electrode upon application of a reductive potential.[87] It has been frequently noted that the film that is formed on the working electrode requires mechanical abrasion for removal. This has led to speculation that the interaction is covalent, although this has not been unambiguously proven.[88, 89] The proposed mechanism posits the leaving of the dinitrogen as gas and formation of a radical upon application of a reductive potential at the working electrode, followed by the formation of a covalent carbon-surface bond.[87] The thickness of the grafted layer depends on the diazonium used and the conditions employed, including the surface that is being coated with the diazonium.[89-92] Unlike self-assembled monolayers of

thiols, the formation of multilayers is possible and has been directly confirmed with thickness measurements using atomic force microscopy[91, 93] and ellipsometry.[94, 95]

Although most studies producing aryl layers from diazonium salts have been performed on carbon electrodes, electrografting of these salts has also been employed on gold.[92, 96-100] In two instances the aryl layers were used to immobilize proteins and functionalized DNA onto an electrode array.[99, 100] In both cases the biomolecules were coupled to the diazonium presursor molecule's carboxylate group through terminal amines, and subsequently grafted to the electrode surface.

No published articles applying aryl layers for surface plasmon resonance exist at present. However, the above studies show that immobilization and detection of biomolecules onto gold electrode arrays is possible. Diazonium-derived aryl layers may potentially possess a superior shelf-life over the commonly used alkyl thiols on gold, an important consideration in the construction of expensive biosensing assemblies. The conditions of the electrografting process have also been shown to determine the structure of the resulting aryl layers,[93, 97, 101] potentially enabling a degree of control over the biosensor's surface chemistry that is not possible with thiol monolayers.

Recently, it has been proposed that the layers formed may in fact contain some intact azo groups,[102] as a combination of Raman,[103, 104] XPS,[92, 97, 102, 103, 105, 106] and TOF-SIMS[96] evidence may suggest. Figure 1.08 shows a

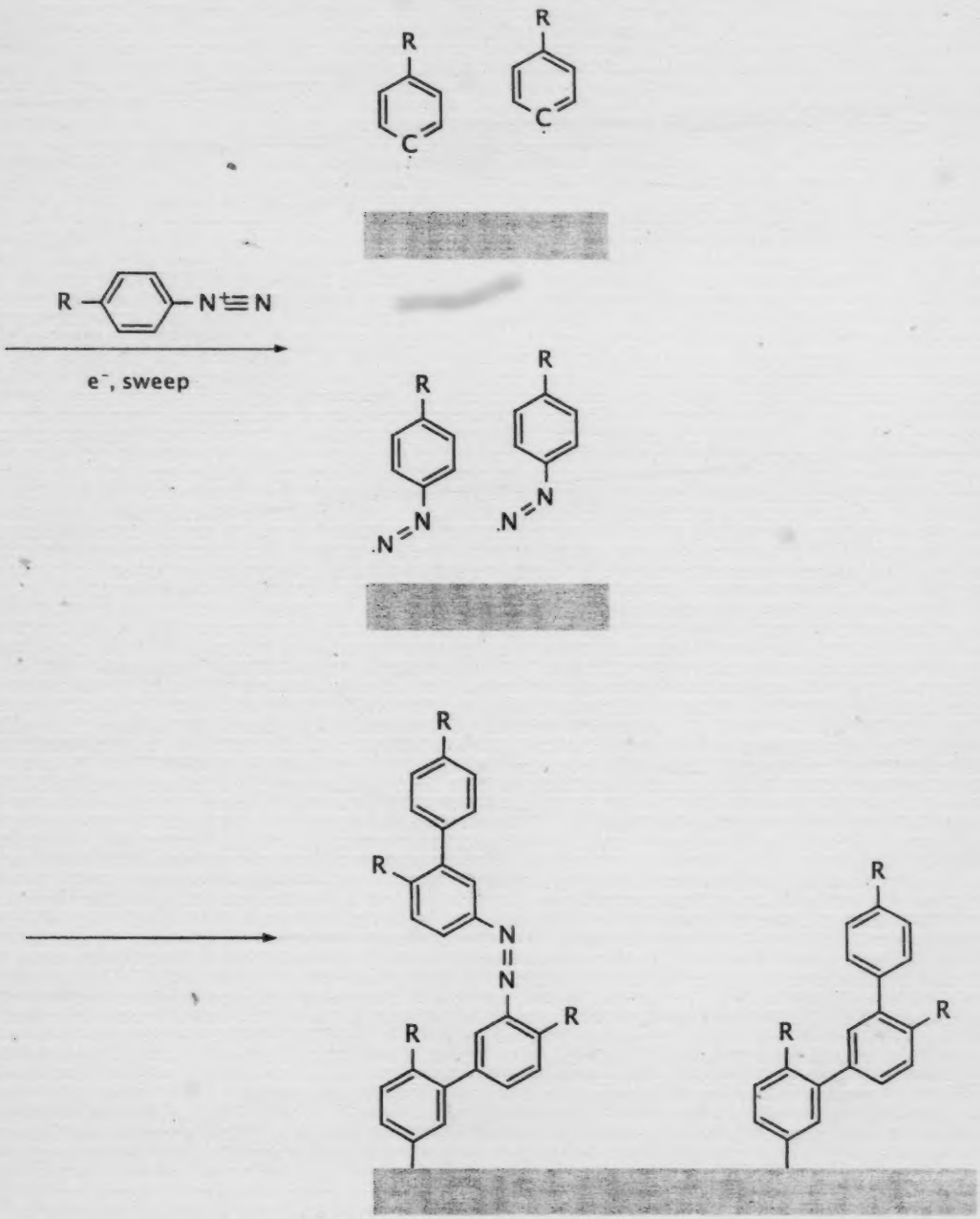

Figure 1.08. Electrografting and a possible structure of diazonium derived aryl layers. At present the mechanism and structure of the electrografted aryl films is unknown.

possible structure of an aryl multilayer. A more detailed description of the structure of the aryl layers is given in the Introduction to Chapter III.

Research Objectives

The overarching goal of this work is to explore factors that affect the immobilization of His_6-proteins to NTA surfaces. Specifically, we are examining the effect of protein size and surface composition. As such, two common classes of surface modification chemistries are pursued.

Chapter II employs self-assembled monolayers of thiols on gold and hexahistidine tagged fusion proteins. The saturation binding of four His_6-proteins, selected for a range in masses of 48 to 480 kDa, are analyzed on three combinations of nitrilotriacetic and hydroxyl terminated thiol monolayers. The goal of this first project is the quantitation of binding to mixed protein binding/protein repulsive thin films, and to understand the role that the size of the protein plays.

Chapter III seeks to use diazonium-derived aryl layers on gold as an alternative to thiol-based monolayers for the generation of novel protein capture surfaces on SPR chips. The advantages of these aryl layers over the thiol SAMs are enhanced storage stability (resistance to oxidation, stronger attachment to the surface) and a potential for greater control of the capture layer's structure. This latter point is explored through the variation of scan rate in the electrografting process using cyclic voltammetry. The

resulting variations in film structure are analyzed via IRRAS and subsequent saturation binding of a His_6-protein on electroaddressed SPR chips.

References

(1) Dill, K. A.; Ozkan, S. B.; Shell, M. S.; Weikl, T. R. *Annu. Rev. Biophys.* **2008**, *37*, 289-316.

(2) Whitford, D. *Proteins: Structure and Function*; John Wiley & Sons: New York, NY, USA, 2005.

(3) Tanford, C.; Reynolds, J. *Nature's Robots: A History of Proteins*; Oxford University Press: New York, NY, USA, 2001.

(4) Erbil, H.; Erbil, Y. *Surface Chemistry of Solid and Liquid Interfaces*; Blackwell Publishing: Oxford, UK, 2006.

(5) McCash, E. M. *Surface Chemistry*; Oxford University Press: Oxford, UK, 2001.

(6) Yakimova, R., et al. *J. Physics D* **2007**, *40*, 6435-6442.

(7) Wisniewski, N.; Reichert, M. *Coll. Surf. B* **2000**, *18*, 197-219.

(8) Adiga, S. P., et al. *JOM* **2008**, *60*, 26-32.

(9) Gademann, K. *Chimia* **2007**, *61*, 373-377.

(10) Smith, J. C.; Lambert, J.-P.; Elisma, F.; Figeys, D. *Anal. Chem.* **2007**, *79*, 4325-4344.

(11) Walker, J. M., Ed. *The Proteomics Protocols Handbook*; Humana Press: Totowa, NJ, 2005.

(12) Zhu, H., et al. *Science* **2001**, *293*, 2101-2105.

(13) Norde, W. *Adv. Colloid. Inter. Sci.* **1986**, *25*, 267-340.

(14) Cha, P.; Krishnan, A.; Fiore, V. F.; Vogler, E. A. *Langmuir* **2008**, *24*, 2553-2563.

(15) Arai, T.; Norde, W. *Coll. Surf.* **1990**, *51*, 1-15.

(16) Luo, Q.; Andrade, J. D. *J. Colloid Interf. Sci.* **1998**, *200*, 104-113.

(17) Glomm, W. R.; Halskau, Ø. J. *J. Phys. Chem. B* **2007**, *111*, 14329-14345.

(18) Norde, W. *Coll. Surf. B* **2008**, *61*, 1-9.

(19) Sharma, S.; Agarwal, G. P. *Anal. Biochem.* **2001**, *288*, 126-140.

(20) Blattner, F. R., et al. *Science* **1997**, *277*, 1453-1462.

(21) Mewes, H. W., et al. *Nature* **1997**, *387*, 7-65.

(22) Adams, M. D., et al. *Science* **2000**, *287*, 2185-2195.

(23) Gibbs, R. A., et al. *Nature* **2004**, *428*, 493-521.

(24) Bentley, D. R. *Med. Research Rev.* **2000**, *20*, 189-196.

(25) Rogers, J. *Symposia on Quant. Biol.* **2003**, *68*, 1-11.

(26) Weston, A. D.; Hood, L. *J. Proteome Res.* **2004**, *3*, 179-196.

(27) Ansari, A. Z. *Nature Chem. Biol.* **2007**, *3*, 2-7.

(28) Sassolas, A.; Leca-Bouvier, B. D.; Blum, L. J. *Chem. Rev.* **2008**, *108*, 109-139.

(29) Sauer, U.; Heinemann, M.; Zamboni, N. *Science* **2007**, *316*, 550-551.

(30) Mann, M.; Jensen, O. N. *Nature Biotech.* **2003**, *21*, 255-261.

(31) Sutton, J. M. *Clinica Chemica Acta* **2004**, *341*, 199-203.

(32) Walsh, G. *Proteins: Biotechnology and Biochemistry*, 2nd ed.; John Wiley & Sons: New York, NY, USA, 2002.

(33) Warsinke, A. *Adv. Biochem. Engin./Biotechnol.* **2008**, *109*, 155-193.

(34) Mesing, R. *Immobilized Enzymes for Industrial Reactors*; Academic Press: Burlington, MA, USA, 1995.

(35) Wang, J. *Electroanalysis* **2001**, *13*, 983-988.

(36) Lichty, J. J.; Malecki, J. L.; Agnew, H. D.; Michelson-Horowitz, D. J.; Tan, S. *Protein Expression and Purification* **2005**, *41*, 98-105.

(37) Terpe, K. *Appl. Microbiol. Biotechnol.* **2003**, *60*, 523-533.

(38) Porath, J.; Carlsson, J.; Olsson, I.; Belfrage, G. *Nature* **1975**, *258*, 598-599.

(39) Hochuli, E.; Bannwarth, W.; Döbeli, H.; Gentz, R.; Stüber, D. *Bio. Tech.* **1988**, *6*, 1321-1325.

(40) Krishnan, B.; Szymanska, A.; Gierasch, L. M. *Chem. Biol. Drug. Des.* **2007**, *69*, 31-40.

(41) Nieba, L., et al. *Anal. Biochem.* **1997**, *252*, 217-228.

(42) Gershon, P. D.; Khilko, S. *J. Immun. Methods* **1995**, *183*, 65-76.

(43) Jung, S. O., et al. *Proteomics* **2005**, *5*, 4427-4431.

(44) Klenkar, G., et al. *Anal. Chem.* **2006**, *78*, 3643-3650.

(45) Fuentes, M., et al. *Journal of Chromatography B* **2007**, *849*, 243-250.

(46) Duchet, J., et al. *Langmuir* **1997**, *13*, 2271-2278.

(47) Love, J. C.; Estroff, L. A.; Kriebel, J. K.; Nuzzo, R. G.; Whitesides, G. M. *Chem. Rev.* **2005**, *105*, 1103-1169.

(48) Nuzzo, R. G.; Allara, D. L. *J. Am. Chem. Soc.* **1983**, *105*, 4481-4483.

(49) Stranick, S. J.; Parikh, A. N.; Tao, Y.-T.; Allara, D. L.; Weiss, P. S. *J. Phys. Chem.* **1994**, *98*, 7636-7646.

(50) Morales-Cruz, A. L.; Tremont, R.; Martínez, R.; Romañach, R.; Cabrera, C. R. *Appl. Surf. Sci.* **2005**, *241*, 371-383.

(51) Porter, M. D.; Bright, T. B.; Allara, D. L.; Chidsey, C. E. D. *J. Am. Chem. Soc.* **1987**, *109*, 3559-3568.

(52) Bain, C. D.; Evall, J.; Whitesides, G. M. *J. Am. Chem. Soc.* **1989**, *111*, 7155-7164.

(53) Sandhyarani, N.; Pradeep, T. *Int. Reviews in Physical Chemistry* **2003**, *22*, 221-262.

(54) Bain, C. D.; Biebuyck, H. A.; Whitesides, G. M. *Langmuir* **1989**, *5*, 723-727.

(55) Hasan, M.; Bethell, D.; Brust, M. *J. Am. Chem. Soc.* **2002**, *124*, 1132-1133.

(56) Jadzinsky, P. D.; Guillermo, C.; Ackerson, C. J.; Busnell, D. A.; Kornberg, R. D. *Science* **2007**, *318*, 430-433.

(57) Moon, J., et al. *Appl. Surf. Sci.* **2007**, *253*, 7554-7558.

(58) Huang, Y.-W.; Gupta, V. K. *J. Chem. Phys.* **2004**, *121*, 2264-2271.

(59) Li, L.; Chen, S.; Jiang, S. *Langmuir* **2003**, *19*, 3266-3271.

(60) Briand, E., et al. *Biosensors and Bioelectronics* **2006**, *22*, 440-448.

(61) Labinis, P. E.; Nuzzo, R. G.; Whitesides, G. M. *J. Phys. Chem.* **1992**, *96*, 5097-5105.

(62) Cheng, F.; Gamble, L. J.; Castner, D. G. *Anal. Chem.* **2008**, *80*, 2564-2573.

(63) Gaus, K.; Hall, E. A. H. *Analytica Chemica Acta* **2002**, *470*, 3-17.

(64) Nye, J. A.; Groves, J. T. *Langmuir* **2008**, ASAP article.

(65) Ostuni, E.; Chapman, R. G.; Holmlin, R. E.; Takamaya, S.; Whitesides, G. M. *Langmuir* **2001**, *17*, 5605-5620.

(66) Wang, Z.-H.; Viana, A. S.; Jin, G.; Abrantes, L. M. *Bioelectrochemistry* **2006**, *69*, 180-186.

(67) Shang, H. Dissertation (Ph.D.), University of Alberta, Edmonton, 2008.

(68) Mann, C. J.; Stephens, S. K.; Burke, J. F. In *Protein Microarray Technology*; Khambhampati, D., Ed.; Wiley-VCH Verlag GmbH & Co.: Weinham, Germany, 2004, pp 153-194.

(69) Jung, L. S., et al. *Sens. Actuators B* **1999**.

(70) Lee, J. K.; Kim, Y.-G.; Chi, Y. S.; Yun, W. S.; Choi, I. S. *J. Phys. Chem. B* **2004**, *108*, 7665-7673.

(71) Feldman, K.; Hähner, G.; Spencer, N. D.; Harder, P.; Grunze, M. *J. Am. Chem. Soc.* **1999**, *121*, 10134-10141.

(72) Homola, J.; Piliarik, M.; Kvasnička, P. *Proceedings of SPIE* **2007**, *6619*, 1-6.

(73) Rich, R. L.; Myska, D. G. *J. Mol. Recognit.* **2007**, *20*, 300-366.

(74) Kanda, V. K. Dissertation (Ph.D.), University of Alberta, Edmonton, 2004.

(75) Homola, J. *Chem. Rev.* **2008**, *108*, 462-493.

(76) Bard, A. J.; Faulkner, L. R. *Electrochemical Methods: Fundamentals and Applications*, 2nd ed.; John Wiley & Sons: New York, USA, 2000.

(77) Francis, S. A.; Ellison, A. H. *J. Opt. Soc. Am.* **1959**, *49*, 131-138.

(78) Trenary, M. *Annu. Rev. Phys. Chem.* **2000**, *51*, 381-403.

(79) Boyd, D. A.; Hess, F. M.; Hess, G. B. *Surf. Sci.* **2002**, *519*, 125-138.

(80) Chen, X.; Ruan, C.; Kong, J.; Deng, J. *Anal. Chim. Acta* **2000**, *412*, 89-98.

(81) Battaglini, N.; Repain, V.; Lang, P.; Horowitz, G.; Rousset, S. *Langmuir* **2008**, *24*, 2042-2050.

(82) Tielens, F.; Costa, D.; Humblot, V.; Pradier, C.-M. *J. Phys. Chem. C* **2008**, *112*, 182-190.

(83) Liu, Z.; Amiridis, M. D. *Surface Science* **2005**, *596*, 117-125.

(84) Ataka, K., et al. *J. Am. Chem. Soc.* **2004**, *126*, 16199-16206.

(85) Hantzsch, A. *Berichte der Deutschen Chemischen Gesellschaft* **1897**, *30*, 2334.

(86) Hantzsch, A. *Berichte der Deutschen Chemischen Gesellschaft* **1900**, *33*, 505-522.

(87) Pinson, J.; Podvorica, F. *Chem. Soc. Rev.* **2005**, *34*, 429-439.

(88) Boukerma, K.; Chehimi, M. M.; Pinson, J.; Blomfield, C. *Langmuir* **2003**, *19*, 6333-6335.

(89) Combellas, C.; Kanoufi, F.; Pinson, J.; Podvorica, F. I. *Langmuir* **2005**, *21*, 280-286.

(90) Allongue, P., et al. *J. Am. Chem. Soc.* **1997**, *119*, 201-207.

(91) Kariuki, J. K.; McDermott, M. T. *Langmuir* **2001**, *17*, 5947-5951.

(92) Laforgue, A.; Addou, T.; Bélanger, D. *Langmuir* **2005**, *21*, 6855-6865.

(93) Kariuki, J. K.; McDermott, M. T. *Langmuir* **1999**, *15*, 6534-6540.

(94) Harper, J. C.; Polsky, R.; Wheeler, D. R.; Brozik, S. M. *Langmuir* **2008**, *24*, 2206-2211.

(95) Shabani, A.; Mak, A. W. H.; Gerges, I.; Cuccia, L. A.; Lawrence, M. F. *Talanta* **2006**, *70*, 615-623.

(96) Doppelt, P.; Hallais, G.; Pinson, J.; Podvorica, F.; Verneyre, S. *Chem. Mater.* **2007**, *19*, 4570-4575.

(97) Lyskawa, J.; Bélanger, D. *Chem. Mater.* **2006**, *18*, 4755-4763.

(98) Jiang, D.-e.; Sumpter, B. G.; Dai, S. *J. Am. Chem. Soc.* **2006**, *128*, 6030-6031.

(99) Corgier, B. P.; Li, F.; Blum, L. J.; Marquette, C. A. *Langmuir* **2007**, *23*, 8619-8623.

(100) Harper, J. C.; Polsky, R.; Wheeler, D. R.; Dirk, S. M.; Brozik, S. M. *Langmuir* **2007**, *23*, 8285-8287.

(101) Brooksby, P. A.; Downard, A. J. *Langmuir* **2004**, *20*, 5038-5045.

(102) Saby, C.; Ortiz, B.; Champagne, G. Y.; Bélanger, D. *Langmuir* **1997**, *13*, 6805-6813.

(103) Nowak, A. M.; McCreery, R. L. *Anal. Chem.* **2004**, *76*, 1089-1097.

(104) Chisholm, R. *unpublished work*; University of Alberta: Edmonton, 2008.

(105) Liu, Y.-C.; McCreery, R. L. *J. Am. Chem. Soc.* **1995**, *117*, 11254-11259.

(106) Toupin, M.; Bélanger, D. *Langmuir* **2008**, *24*, 1910-1917.

CHAPTER II

PROBING THE BINDING OF HEXAHISTIDINE-TAGGED PROTEINS ON MIXED THIOL MONOLAYERS USING SURFACE PLASMON RESONANCE IMAGING

Introduction

Following from past and continuing research into the fundamentals of the interfacial behaviour of biomolecules, notably proteins, studies into the applications of such knowledge towards functional diagnostic technologies have gained momentum. Because of the great promise held in the field of proteomics with regards to medical diagnostics, there has been a general push on to integrate bioanalytical techniques of instrumental analysis with the microarray technology developed from the more mature field of genomics. Notable among the bioanalytical techniques that are now being applied to microarray formats are surface plasmon resonance (SPR)[1], immuno- and enzymatic assays,[2, 3] mass spectrometry,[4] and fluorescence,[5] often in various combinations.[6]

Surface plasmon resonance is perhaps the most extensively employed instrumental technique in the laboratory setting for the examination of protein binding and adsorption to surfaces. The instrument's relative ease of use, the quantitative information obtained without the requirement of analyte labelling, and the commercial availability of various ready-to-use sensor chips are the major advantages of SPR for interfacial biomolecular analysis. The poor limit of detection (LOD) relative to many other techniques (typical LOD for protein binding or adsorption of between 0.1 nM

to 10 nM on a fixed angle instrument[7]) and the undiscriminating nature of the detection with regards to events at the surface are the technique's chief disadvantages.

Both the non-specific and specific attachment of proteins onto bare gold and single component monolayers has long been studied.[8-15] Complementary work has also been performed on the fundamental structural characteristics of both single component[16, 17] and mixed monolayers.[18-20] Simultaneously, in the field of molecular biology, genetic or pre-expression modifications to proteins, combined with metal affinity chromatography, has become a mature technique for the production and recovery of a wide variety of proteins from engineered microbes. Specifically, the terminal hexahistidine tag (His_6-tag), coordinated via a metal ion such as nickel or copper to carboxylic acid end groups of a substrate-bound molecule on the column, has become particularly popular. From these parallel developments, the use of mixed thiol monolayers and His_6-tagged proteins have converged as a popular system to study the specific binding of proteins at surfaces, as well as a potential biosensor assembly.[3, 21-24]

Despite the proliferating biosensor studies of proteins, the quality of the data and its interpretation is often disappointing.[1] Looking only at data interpretation, it is frequently assumed that proteins are not interacting with one another at the surface and that the Langmuir equation can be applied to binding curves, a suspect proposition at best when looking at

surfaces covered with a high density of proteins. This approach also ignores irreversible binding and conformational rearrangements. Although we currently do not understand how the kinetics,[25] entropy and enthalpy,[26] hydrophobicity and hydrophillicity,[27] electrostatics of both the proteins and the surface,[28, 29] and Van der Waals interactions[30] converge to give experimental adsorptive behaviour for proteins, we do have some understanding of these important factors on their own or in partial combinations.

The focus of the current study is the use of SPR imaging on low-density protein arrays to examine the immobilization of His_6-tagged proteins on several mixed thiol monolayers, and to discern the effects of protein size and monolayer composition. Using methodology previously developed in our research group,[31] we have employed high mixing ratios (50/50 and 20/80 % molarity) to generate NTA terminated C_9 alkyl thiols embedded in a protein resistant C_{11} ω-thioalcohol. Binding curves on the two mixed monolayers, as well as on a pure NTA terminated monolayer, were obtained for four His_6-tagged proteins: cAMP receptor protein [CRP, 48 kDa], α-amylase [Amyl, 60 kDa], fibroblast activation protein, alpha [F_{AP}, 120 kDa], and β-galactosidase [β-Gal, 480 kDa]. Control and surface regeneration experiments were also performed to assess the degree of non-specific binding to the surfaces.

Experimental

Reagents and Materials. N-[5-(3'-maleimidopropylamido)-1-carboxypentyl]iminodiacetic acid disodium salt (maleimido-C_3-NTA, Dojindo Laboratories), 1,9-nonanedithiol (Aldrich), 11-mercapto-1-undecanol ($HSC_{11}OH$, Sigma), and tridecafluoro-1,1,2,2-tetrahydrooctyl)-1-dimethylchlorosilane (United Chemical Technologies) were used as received. All hexahistidine-tagged (His_6, at C-termini) proteins were obtained via fusion expression from E. coli and were dissolved in a buffer of 50 mM Tris HCl, 100 mM KCl, and 40 mM $NiSO_4 \cdot 6H_2O$ at pH 7.80 unless otherwise noted.

Fabrication of Surface Plasmon Resonance (SPR) Sensor Chips. A sheet of 1.0 mm thick SF-10 glass (Schott Glass) was diced into 1.8 cm X 1.8 cm squares. The squares were cleaned via immersion in boiling Pirhana (3:1 H_2SO_4:H_2O_2) for thirty minutes, thoroughly rinsed with 18.2 MΩ deionized (DI) water, and dried under a stream of argon. The cleaned squares were placed into a homemade aluminum shadowmask with a series of 3 X 3 square patterns, each consisting of 2.0 mm diameter circular holes with 1.0 mm spacings between them. The shadowmask and fabricated chip are illustrated in Figure 2.01. The assembly was loaded into a thermal evaporator (Torr International Inc.) and the evaporator's chamber was pumped down to 4.0×10^{-6} Torr prior to the sequential deposition of 1.0 nm of chromium (adhesive layer, 99.999 % purity relative to other rare earth metals, Electronic Space Products International) and 45.0 nm of gold (99.99

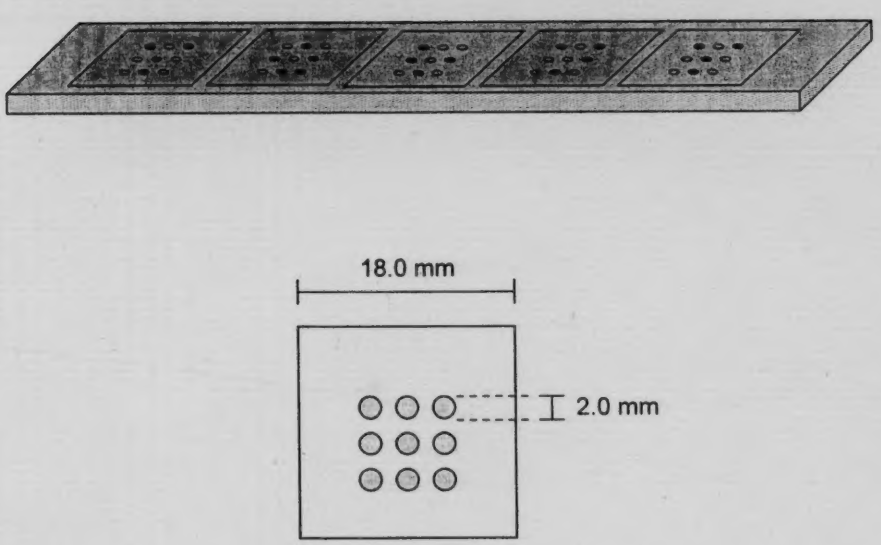

Figure 2.01. Aluminum shadowmask and layout of a fabricated SPR chip, showing the 3 X 3 pattern of 2.0 mm gold spots.

% purity relative to other rare earth metals, Electronic Space Products International). Following deposition, the SPR chips were placed into a dessicator under vacuum containing small open vials of the fluorinated silane and left overnight to react with the exposed glass surfaces. The fluorinated SPR chips were then stored under vacuum prior to the surface attachment of HSC_9NTA and $HSC_{11}OH$.

Synthesis and Surface Attachment of HSC_9NTA. 1,9-nonanedithiol (75 mM in water) and maleimido-C_3-NTA (25 mM in water) were combined and reacted overnight at room temperature and pH 7.90, as shown in figure 2.02. Several hours after combination, the pH was checked again and readjusted to 7.90. The HSC_9NTA product was separated and purified as a white powder using a water-methanol gradient and 0.1 % formic acid at room temperature on a reverse-phase HPLC column. The product eluted at 50/50 (v/v) water/methanol and was confirmed by electrospray ionization mass spectrometry (ESI-MS). The solid HSC_9NTA was dissolved in 50/50 water/ethanol (v/v) to 1.0 mM fractions.

For the generation of the monolayer capture surfaces, the fluorinated SPR chip was ozone-cleaned for ten minutes and subsequently rinsed with 18.2 MΩ DI water to remove oxidized organic films. Hydrophobicity on the uncoated fluorinated glass areas was maintained and seen in a visual inspection of its high contact angle with DI water. Meanwhile, the gold spots had a very low contact angle with DI water, implying a clean surface. The HSC_9NTA or mixed $HSC_9NTA/HSC_{11}OH$ (50/50

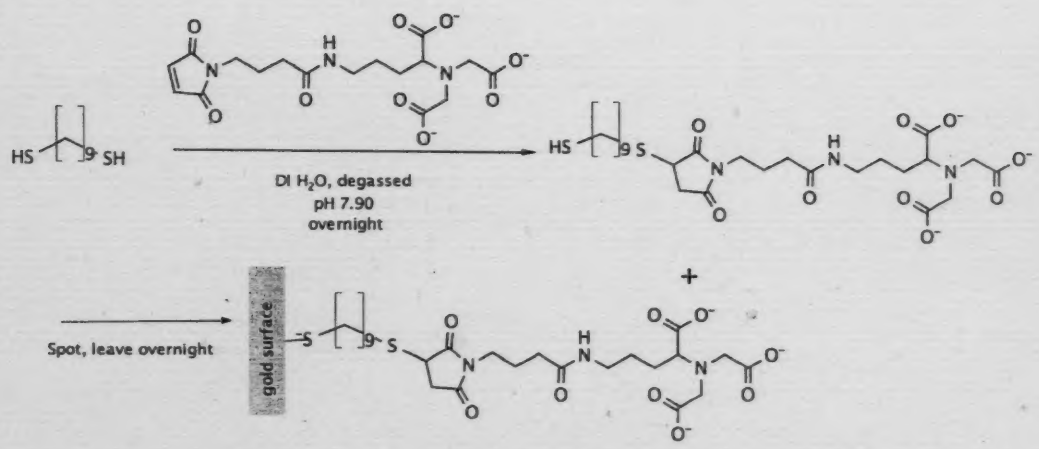

Figure 2.02. Synthesis and generation of the HSC_9NTA capture layers. The product was purified by reverse-phase chromatography and eluted at 50/50 (v/v) water/methanol, at room temperature.

or 20/80 molar fractions) solutions were then deposited using a micropipette over eight spots, with one remaining corner spot covered with a 1.0 mM $HSC_{11}OH$ solution (in 50/50 water/ethanol (v/v)) as a negative control. An SPR difference image of such a chip is shown in Figure 2.03. The spotted SPR chip was left overnight in a small Petri dish containing a wet Kimwipe, sealed with Parafilm, and covered from light.

Surface Plasmon Resonance Imaging of Fusion Protein Attachments.

Following the surface attachment of the thiols to the gold spots, the droplets of solution were vacuumed off using a Pasteur pipet, thoroughly rinsed with 18.2 MΩ DI water, and dried under a stream of argon. The chip was immediately placed into a prism flow cell assembly of a GWC SPRimagerII instrument running Digital Optics V^{++} 4.0 imaging software and had the Tris-KCl-nickel buffer run through the cell for two minutes. The angle of incidence was adjusted to obtain an average signal of two-thirds of the minimum (on the steeper side of the angle-signal curve) from the gold spots under p-polarized light. All measurements were taken at this fixed angle unless otherwise noted. Reference images were then obtained under both s- and p-polarized light. All gold spots were selected as regions of interest with the software, and the intensity of the reflected light passing through the prism was measured with respect to the protein concentration using a CCD camera measuring at 813 nm. The flow cell settled to 22.2 °C ± 0.5 °C after warming up and being shut off during the ten minute long equilibration steps.

Figure 2.03. **(A)** Sample difference image of a chip in a nickel-buffer solution of 2000 nM α-amylase. Eight of the spots were coated with the 50/50 $HSC_9NTA/HSC_{11}OH$ solution, while the spot at the top right was coated with the $HSC_{11}OH$ solution. The white line is a cross-section of the signal taken from top to bottom, **(B)** plotted from left to right below.

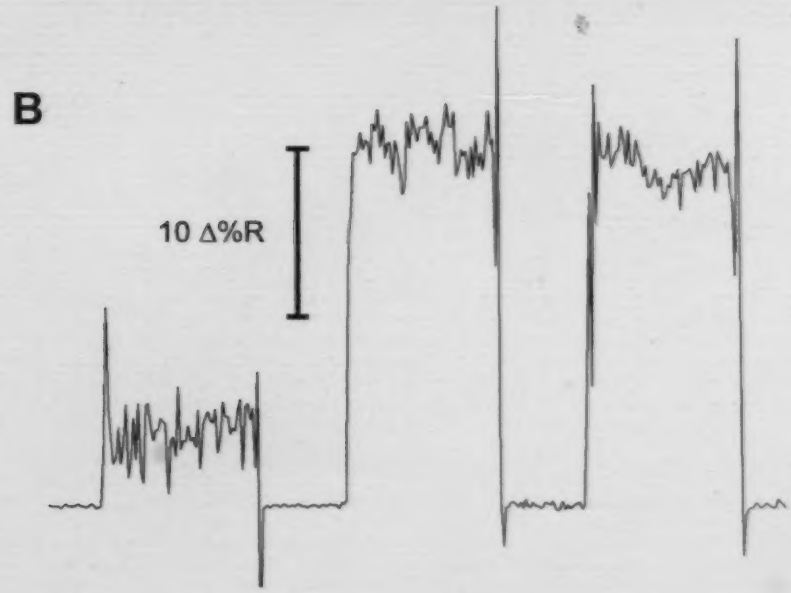

A series of solutions of a hexahistidine-tagged protein in the $NiSO_4$-Tris-KCl buffer (cAMP receptor protein [CRP, 48 kDa], α-amylase [Amyl, 60 kDa], fibroblast activation protein, alpha [F_{AP}, 120 kDa], or β-galactosidase [β-Gal, 480 kDa]), ranging in concentration from 1.0 nM to 2000 nM (unless otherwise noted), were flowed over the chip's surface for two minutes and subsequently allowed to equilibrate for ten minutes. Buffer was then flowed through for two minutes to remove any free floating and loosely bound protein before measuring the reflected light intensity.

Binding curves. For all protein-SAM combinations, dissociation constants (K_d = EC_{50}) were obtained from a four-parameter logistic equation:

$$\Delta\%R = \Delta\%R_{\min} + \left(\frac{\Delta\%R_{\max} - \Delta\%R_{\min}}{1 + 10^{(\log[A] - \log EC_{50}) \bullet hillslope}} \right) \qquad (2.1)$$

where Δ%R is the percent change in the measured reflectivity, $\Delta\%R_{min}$ and $\Delta\%R_{max}$ are the measured minimum and maximum reflectivities with respect to the buffer reference image using p-polarized light, [A] is the concentration of protein in solution, EC_{50} is the concentration of protein in solution when Δ%R is halfway between $\Delta\%R_{min}$ and $\Delta\%R_{max}$, and hillslope describes the shape and direction of the curve. All raw signal (pixel) values were converted to Δ%R using the following formula:

$$\Delta\%R = \frac{(0.85)(I_p)}{I_s} \bullet 100\% \qquad (2.2)$$

with I_p as the raw signal intensity under p-polarized light at a given solution protein concentration, and I_s as the raw signal value under s-polarized light prior to protein attachment. The (0.85) is a conversion factor for the intensities of I_p and I_s.

Results and Discussion

At present, quantitative experimental studies comparing the attachment of proteins of disparate properties onto mixed monolayers are sparse. While several fundamental studies of protein attachment onto both single-component monolayers[32] and unmodified surfaces[15, 28] have been undertaken, these protein-surface systems are typically of limited use in biosensing. Building on previous work in our group that has examined the biosensing applications of hexahistidine-tagged proteins onto mixed NTA thiol and thioalcohol monolayers,[31] we have set out to examine how the size of the His_6-protein, as well as the composition of the mixed NTA monolayer, affects its attachment to the surface.

Table 2.1 shows relevant properties of the His_6-proteins used in this study, allowing for electrostatic (charge at pH 8.0) and steric (dimensions) interactions to be evaluated with regards to the experimental data. Charges at pH 8.0 were calculated from the primary amino acid sequence of a given protein, using the online software ProtParam.[33] Dimensions were manually obtained from the proteins' X-ray crystal structures using Jmol Viewer.[34-37]

	CRP	Amyl	F_{AP}	β-Gal
MW (kDa)	48	60	120	480
Dimensions (Å)	56.5 * 67.3 * 51.8[34]	75.1 * 42.4 * 55.3[35]	126.3 * 73.5 * 63.3[36]	172.9 * 132.8 * 83.2[37]
pI	8.44	6.51	6.17	5.19
Charge at pH 8.0	+1.0	-7.6	-22.1	-184.4
# of structural units	dimer	monomer	dimer	tetramer
# of His_6 tags	2	1	2	4

Table 2.1. Selected properties of His_6-tagged proteins used in this study. Below, clockwise from top left: X-ray crystal structures of cAMP receptor protein (CRP), α-amylase (Amyl), fibroblast activation protein, alpha (F_{AP}), and β-galactosidase (β-Gal).

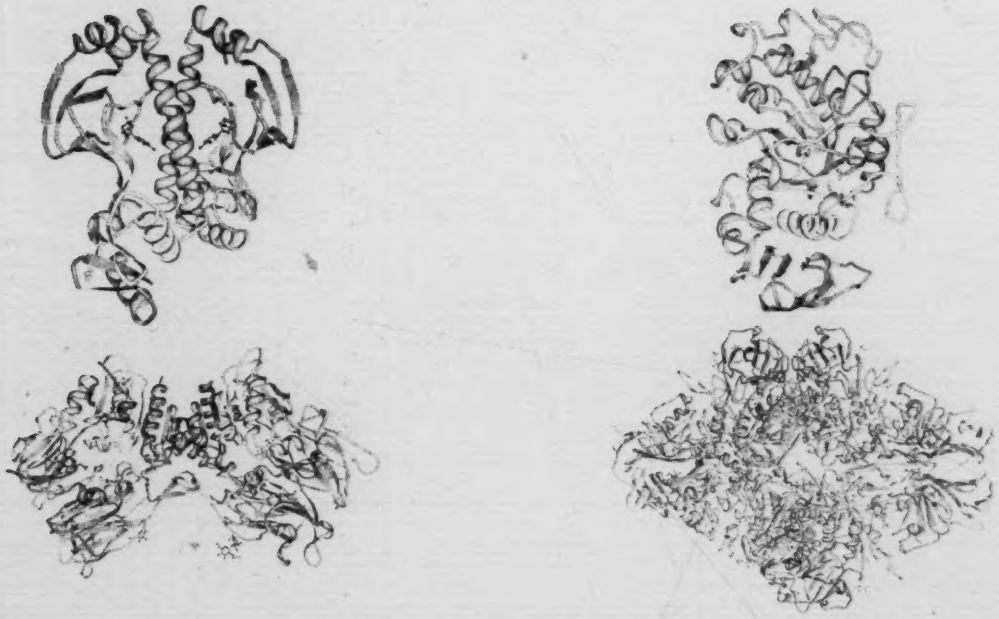

Figures 2.04 and 2.05 show sample fits to the binding curves of α-amylase on 20 % HSC_9NTA and β-galactosidase on 100 % HSC_9NTA surfaces. The remaining binding curves are summarized in Table 2.2. The data points represent the mean value from eight spots while the error bars represent the standard deviation about the mean using 95 % confidence intervals (except BSA, CRP on 100 NTA, and CRP on 50 NTA; all used three spots). The dissociation constants (K_d's) obtained for α-amylase, F_{AP}, and β-Gal appear to scale inversely with the number of His_6 tags possessed by each. This follows a trend expected from co-perativity due to the tags, although not quantitatively. The latter point is likely due to non-specific adsorption as an additional contributing factor to protein attachment.

One of the limitations of fixed-angle SPR imaging is that Δ%R is linear with refractive index (n) change, and thus surface coverage, only over a limited range. According to calculations and quantitative SPR microscopy measurements performed by Shumaker-Parry and Campbell,[38] deviation of the signal from linearity begins to occur around Δ%R = 10. However, this deviation is slight (5 – 10 %) up until about Δ%R = 30. At Δ%R = 40, the deviation grows to ~20 %. Although the latter error is sizeable, no measured change in reflected intensity in this study exceeds Δ%R = 40, while the maximum measured reflectivity change in the majority of binding curves shown below does not exceed Δ%R = 30, as can be seen in Figures 2.06 to 2.09. The binding curves are therefore judged to be acceptable as measurements of the quantity of bound protein.

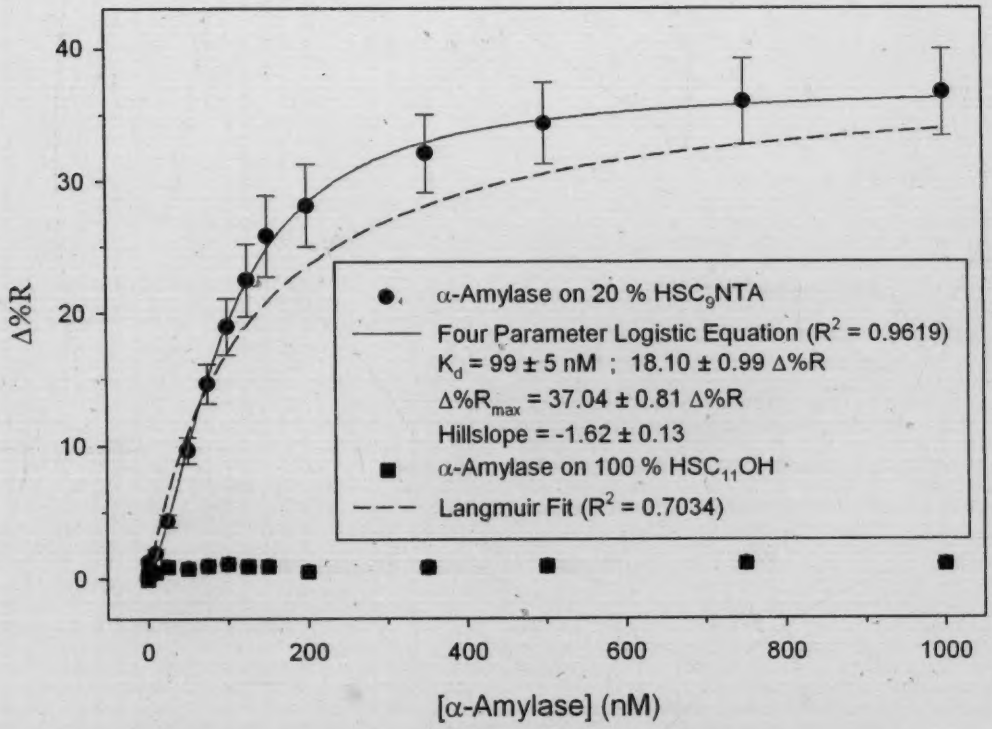

Figure 2.04. Plot of Δ%R vs solution concentration of α-amylase for a 20 % HSC_9NTA capture surface. The points are the mean value of eight spots and the error bars represent the standard deviation of 95 %. The line through the data is the four-parameter logistical fit to the data. Fitting parameters are listed in the inset. The Langmuir fit is shown for comparison.

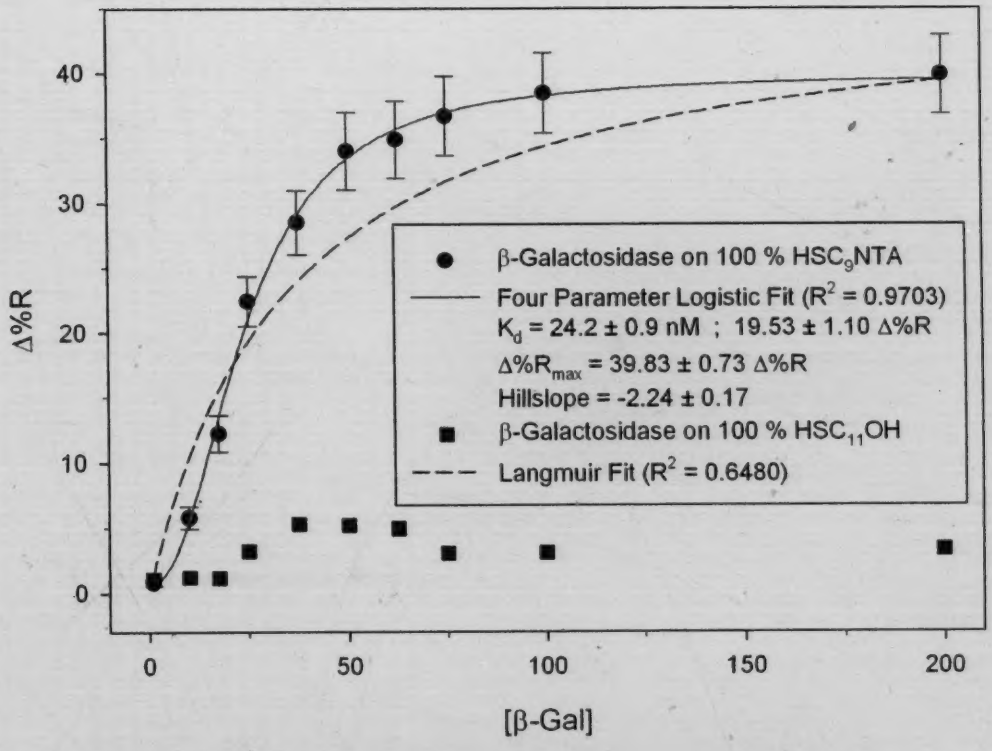

Figure 2.05. Plot of Δ%R vs solution concentration of β-galactosidase (β-Gal) attaching to a 100 % HSC_9NTA capture surface. The points are the mean value of eight spots and the error bars represent the standard deviation of 95 %. The line through the data is the four-parameter logistical fit to the data. Fitting parameters are listed in the inset. The Langmuir fit is shown for comparison.

Protein	Surface	R^2	K_d (nM)	$\Delta\%R_{max}$	Hillslope
CRP	100 NTA	0.9899	136 ± 5	17.70 ± 0.42	-2.10 ± 0.16
CRP	50 NTA	0.9891	79 ± 5	24.77 ± 0.51	-2.18 ± 0.21
CRP	20 NTA	0.9792	88.4 ± 2.6	32.70 ± 0.51	-3.08 ± 0.25
α-Amyl	100 NTA	0.9889	65.0 ± 1.5	23.85 ± 0.22	-2.06 ± 0.09
α-Amyl	50 NTA	0.9571	849 ± 280	30.54 ± 3.96	-0.80 ± 0.09
α-Amyl	20 NTA	0.9619	99 ± 5	37.04 ± 0.81	-1.62 ± 0.13
F_{AP}	100 NTA	0.9735	53.2 ± 1.8	28.12 ± 0.39	-1.84 ± 0.10
F_{AP}	50 NTA	0.9815	558 ± 92	44.49 ± 3.19	-0.90 ± 0.04
F_{AP}	20 NTA	N/A	N/A	N/A	N/A
β-Gal	100 NTA	0.9703	24.2 ± 0.9	39.83 ± 0.73	-2.24 ± 0.17
β-Gal	50 NTA	0.9555	266 ± 39	48.42 ± 3.07	-1.01 ± 0.07
β-Gal	20 NTA	N/A	N/A	N/A	N/A
$CRP_{no\ Ni2+}$	100 NTA	0.9932	328 ± 7	42.27 ± 0.42	-2.23 ± 0.09
BSA	100 NTA	0.9978	181 ± 5	26.13 ± 0.32	-1.96 ± 0.10

Table 2.2. Summary of results obtained from fitting the four parameter logistic equation to binding curves obtained for the above protein-surface combinations. The mean uncertainties are calculated from eight spots, using 95 % confidence intervals (except BSA, CRP on 100 NTA, and CRP on 50 NTA; all used three spots). F_{AP} and β-Gal on 20 % HSC_9NTA could not be fitted to this logistic equation.

Figures 2.06 to 2.09 correspond to the four hexahistidine-tagged proteins employed on the three monolayers examined. The four His_6-proteins (CRP, 48 kDa; Amyl, 60 kDa; F_{AP}, 120 kDa; and β-Gal, 480 kDa) were selected in order to examine the effect of protein size on three types of monolayers containing different ratios of protein binding to protein resistant components. In this case, the protein binding component, a nitrilotriacetic acid functionalized alkyl thiol (HSC_9NTA), is capable of both specific coordination at the C-terminal His_6-tag, as well non-specific interactions. The protein resistant component, an ω-functionalized alkylthiol ($HSC_{11}OH$), is mixed with the HSC_9NTA in molar ratios of 50:50 and 20:80 (80 % $HSC_{11}OH$), which will be referred to from now on as the 50 % and 20 % NTA surfaces. The third monolayer is simply undiluted HSC_9NTA (the 100 % NTA surface).

Quantitative trends on the 100 % NTA surface. In order to probe interactions at the surface, and possible relations to key structural parameters of the proteins employed, attachment to a single component monolayer was examined. Such a monolayer presents a uniform surface to the attaching proteins, and therefore simplifies consideration of possible protein-surface interactions, allowing experimental observations to be more readily compared to the proteins' structural properties. Upon closer inspection, the binding curves for the 100 % NTA surfaces present clear trends, dependent on the sizes of the proteins. Two properties

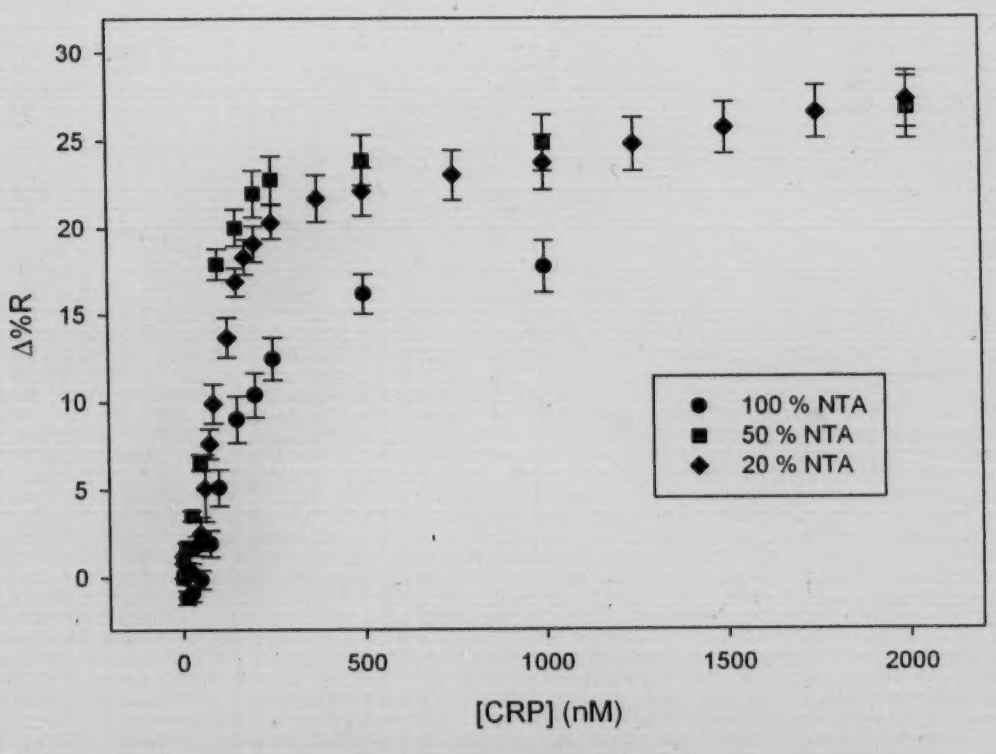

Figure 2.06. Binding curves of cAMP receptor protein (CRP) on the three thiol monolayers employed. The points are the mean value of three spots and the error bars represent the standard deviation of 95 %.

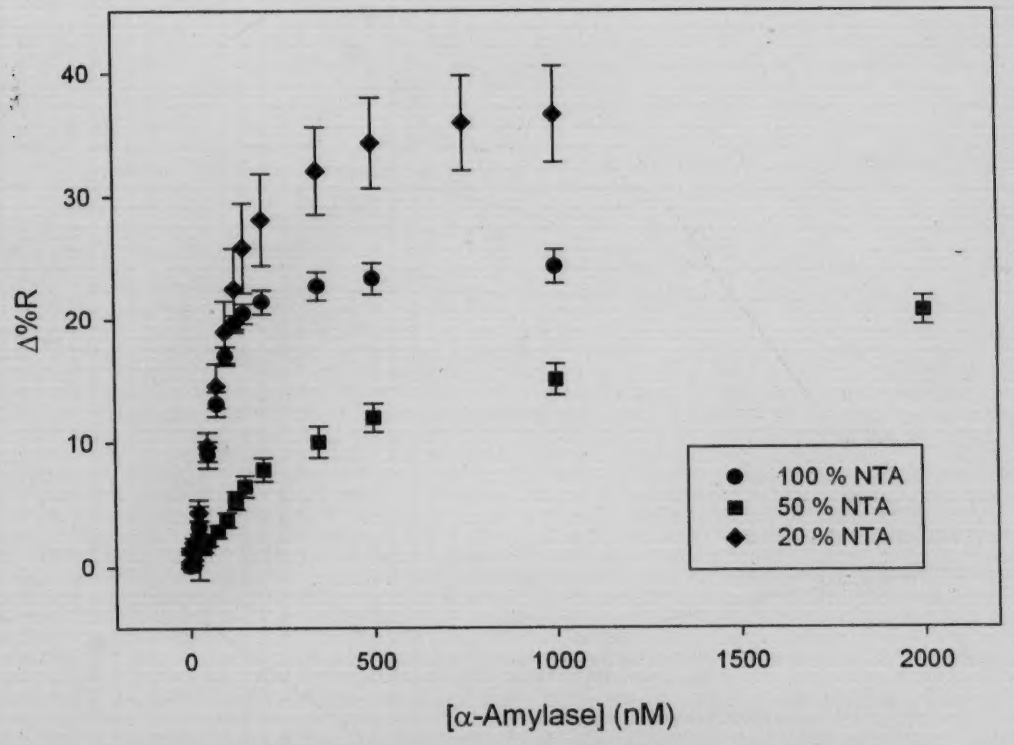

Figure 2.07. Binding curves of α-amylase (Amyl) on the three thiol monolayers employed. The points are the mean value of eight spots and the error bars represent the standard deviation of 95 %.

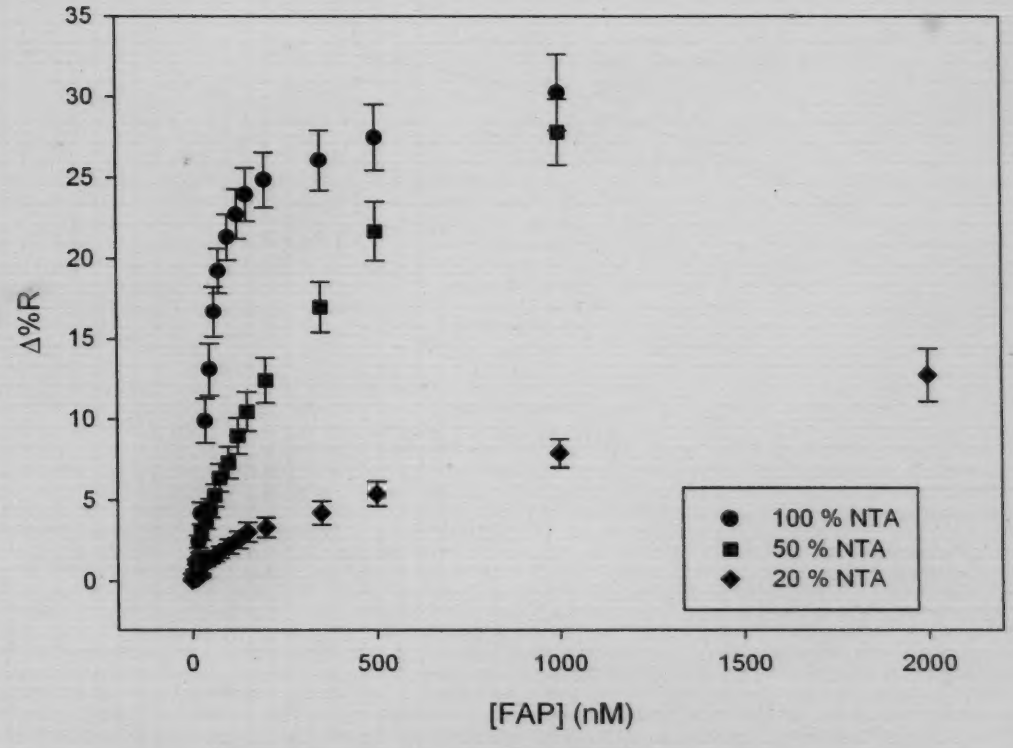

Figure 2.08. Binding curves of fibrinogen activation protein (F_{AP}) on the three thiol monolayers employed. The points are the mean value of eight spots and the error bars represent the standard deviation of 95 %.

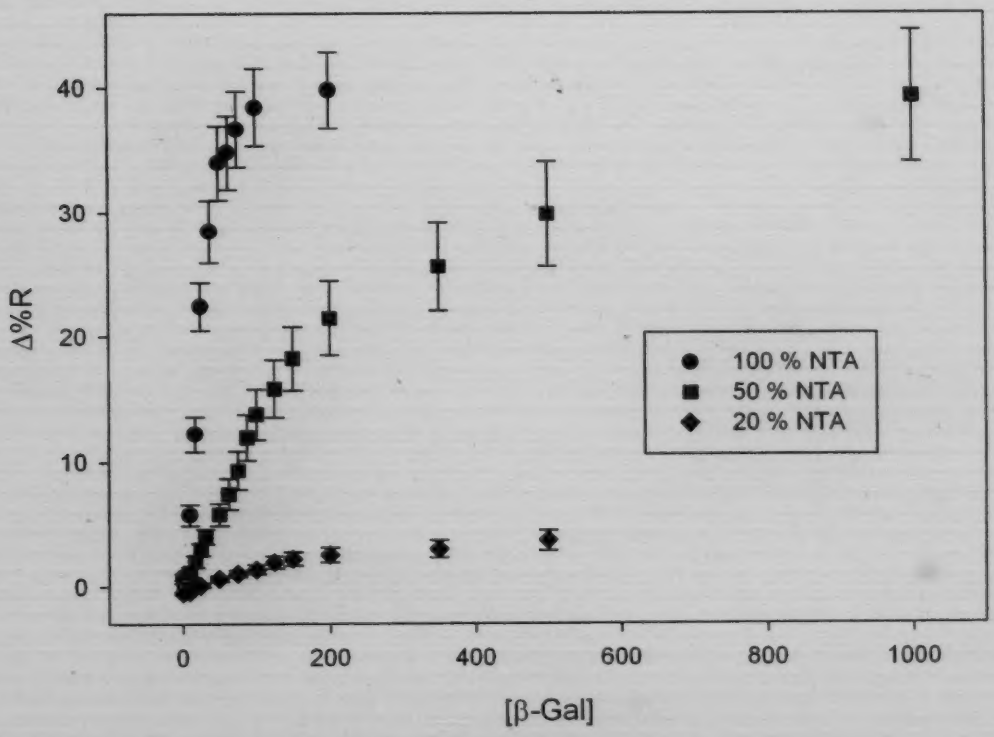

Figure 2.09. Binding curves of β-galactosidase (β-Gal) on the three thiol monolayers employed. The points are the mean value of eight spots and the error bars represent the standard deviation of 95 %.

representing protein size, molecular weight and exposed surface area, are plotted in Figures 2.10 and 2.11, respectively, against the maximum signal intensity ($\Delta\%R_{max}$).

To obtain the exposed surface areas of the proteins, a computational method developed by Mark Gernstein was employed.[39] A probe size of 1.4 Angstroms was used, and all atoms and heteroatoms of the protein were included, with the exception of water.

Against the proteins' molecular weights, $\Delta\%R_{max}$ appears to increase as the masses are increased, shown in Figure 2.10. When the maximum signal is compared to the calculated surfaces areas, a roughly monotonic increase is seen in Figure 2.11. This disparity between the proteins masses and their available surface areas suggests that the packing of the proteins is a limiting factor to protein attachment. Namely, large proteins cannot be packed as efficiently as smaller proteins. The larger proteins will, however, form a thicker layer on the 100 % NTA surface, generating a larger signal in spite of their packing.

Qualitative trends on the 20 % and 50 % NTA surfaces. An unusual feature found in the overlaid binding curves of the smaller CRP and α-amylase (Figures 2.06 and 2.07) is the higher signal intensities observed on both the 20 % and 50 % NTA surfaces for the CRP, and on the 20 % NTA surface for the α-amylase relative to the 100 % NTA surface. It would be expected, given that the pure -OH terminated monolayer shows little

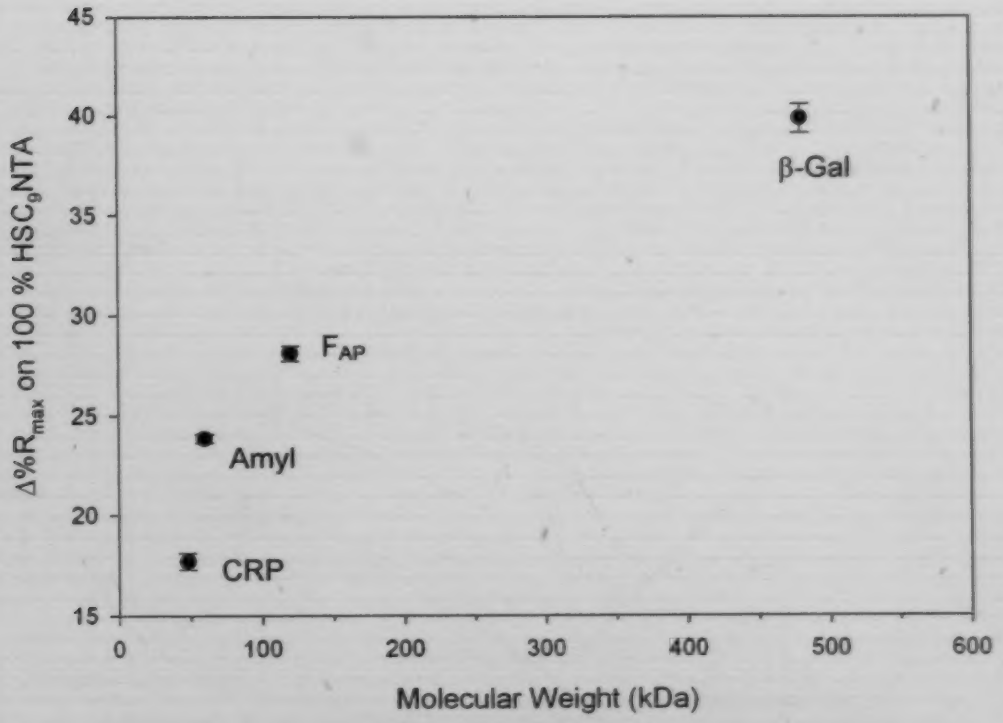

Figure 2.10. The maximum change in the reflectivity at the 100 % HSC_9NTA capture surface plotted as a function of the molecular weights of the proteins employed. The points are the mean value of eight spots (except for CRP, using three spots) and the error bars represent the standard deviation of 95 %.

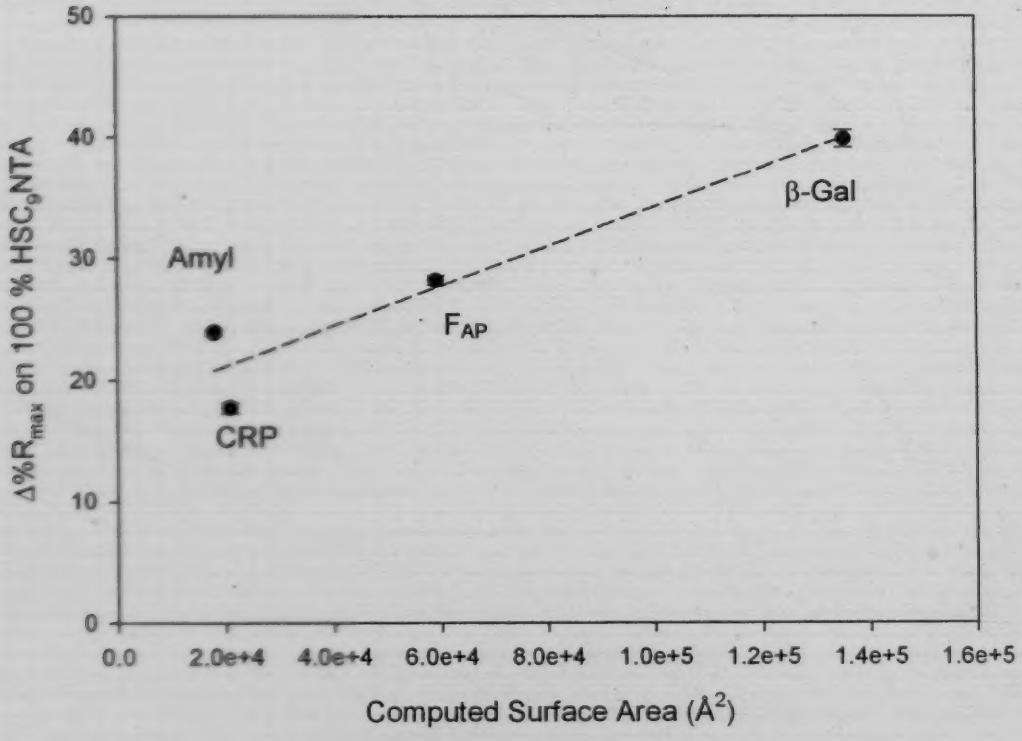

Figure 2.11. The maximum change in the reflectivity at the 100 % HSC_9NTA capture surface plotted as a function of the calculated surface areas of the proteins employed. The points are the mean value of eight spots (except for CRP, using three spots) and the error bars represent the standard deviation of 95 %.

protein binding at low to moderate protein concentrations (typically 1 nM to 500 nM), that the 20 % and 50 % NTA surfaces should show reduced signal intensity. Indeed, this is borne out for the larger F_{AP} and β-Gal proteins in Figures 2.08 and 2.09. The larger F_{AP} and β-Gal have greater portions of their surface areas exposed to the -OH groups on the surface. An especially dramatic drop in the signal intensity (Δ%R) is evident for β-Gal on the mixed monolayers, consistent with it being the largest protein (480 kDa versus F_{AP}'s 120 kDa). This suggests that either the binding of F_{AP} and β-Gal on the 100 % and 50 % NTA surfaces is dominated by non-specific adsorption, which "out-competes" specific binding via coordination of the C-terminal His_6-tag, or that the repulsive -OH groups substantially reduce the specific binding via NTA-Ni^{2+}-His_6 coordination. A combination of these two scenarios is also possible.

As for the larger signals generated by CRP and α-amylase on the mixed layers, a mix of specific and non-specific binding would also account for this. Specific-binding will be more competitive relative to non-specific binding for the smaller proteins, since the C-terminal His_6-tag will have fewer potential non-specific binding sites on the protein competing with it for access to the surface NTA groups. As well, fewer non-specific binding sites on CRP and α-amylase may also reduce the frequency of irreversible adsorption, allowing more frequent desorption of weakly bound proteins and potential reattachment via NTA-Ni^{2+}-His_6 coordination, although this last point is somewhat speculative.

Extending this argument to α-amylase in particular (Figure 2.07), it appears a reduction in non-specific adsorption occurs on the 50 % NTA surface, but without an appreciable increase in specific binding at the NTA sites. α-Amylase may be too large, as the "medium-sized" protein, for the His_6-tag to overcome the combination of repulsive and attractive non-specific interactions at this particular surface. For α-amylase on the 20 % NTA surface, on the other hand, non-specific adsorption should be further reduced, "steering" the His_6-tag to the NTA site(s), and changing the way α-amylase packs on the surface. By this, we mean that the increased density of -OH terminal groups may very well change the orientation and/or conformation of the protein around the His_6-tag to minimize the interactions of the surrounding protein surface with the higher density protein resistant $HSC_{11}OH$ film component.

Control experiments. To confirm the role of the -OH terminated layers in the dramatic reduction of adsorption seen above with F_{AP} and β-Gal on the 20 % and 50 % NTA surfaces, the binding of bovine serum albumin (BSA), a well-studied protein, was examined on the three thiol monolayers. Figure 2.12 below clearly shows the same sizeable reduction in the maximum signal intensity as the NTA groups are diluted with the $HSC_{11}OH$. Since the BSA used did *not* have a hexahistidine tag, only non-specific adsorption is possible. This confirms the importance of the protein's size in the determination of the mode of attachment to the monolayer surfaces.

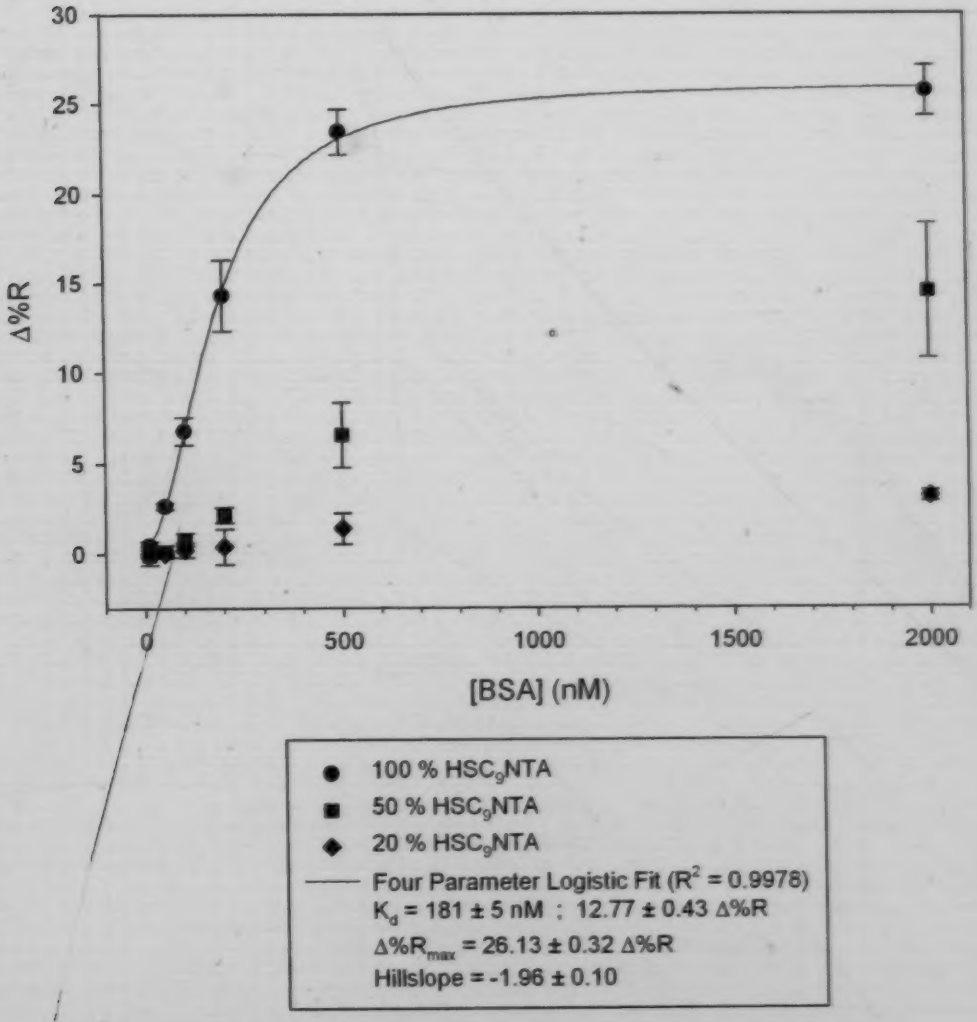

Figure 2.12. Bovine serum albumin (BSA) attaching to 100 %, 50 %, and 20 % HSC_9NTA capture surfaces (in buffer containing nickel). The BSA does not have a terminal hexahistidine tag. The points are the mean value of three spots and the error bars represent the standard deviation of 95 %.

Namely, that the attachment of the larger proteins at the 100 % and 50 % NTA surfaces is dominated by non-specific adsorption.

The extent of non-specific adsorption with the smaller proteins CRP and α-amylase is still somewhat ambiguous. To determine the importance of the C-terminal His_6-tag, or possible lack of importance, the binding of CRP on the 100 % NTA surface in the absence of nickel ions was examined, and is shown below in Figure 2.13. At an intensity of 42, $\Delta\%R_{max}$ without the presence of nickel is significantly higher than a $\Delta\%R_{max}$ of 18, with nickel (Figure 2.06, 100 % NTA curve). The fusion tag clearly does have an effect on the attachment of CRP, even on the 100 % NTA surface. The roughly doubled signal upon removal of nickel would indicate that substantially more CRP is present on the surface, packed more efficiently now that the orientation at the interface is no longer constrained by the location of the His_6-tag.

Regeneration of the surfaces. Considering that His_6 tagged proteins are typically eluted from affinity columns with competing complexation agents for Ni^{2+}, it is possible to regenerate NTA interfaces following applications in a similar manner. Two separate regeneration experiments were performed, the first using 2000 nM CRP on the 50 % HSC_9NTA capture surface, the second using 2000 nM F_{AP} on the same surface type. Both are depicted in Figures 2.14 and 2.15. As with the binding isotherms, the protein solutions were flowed over the chip for two minutes and were

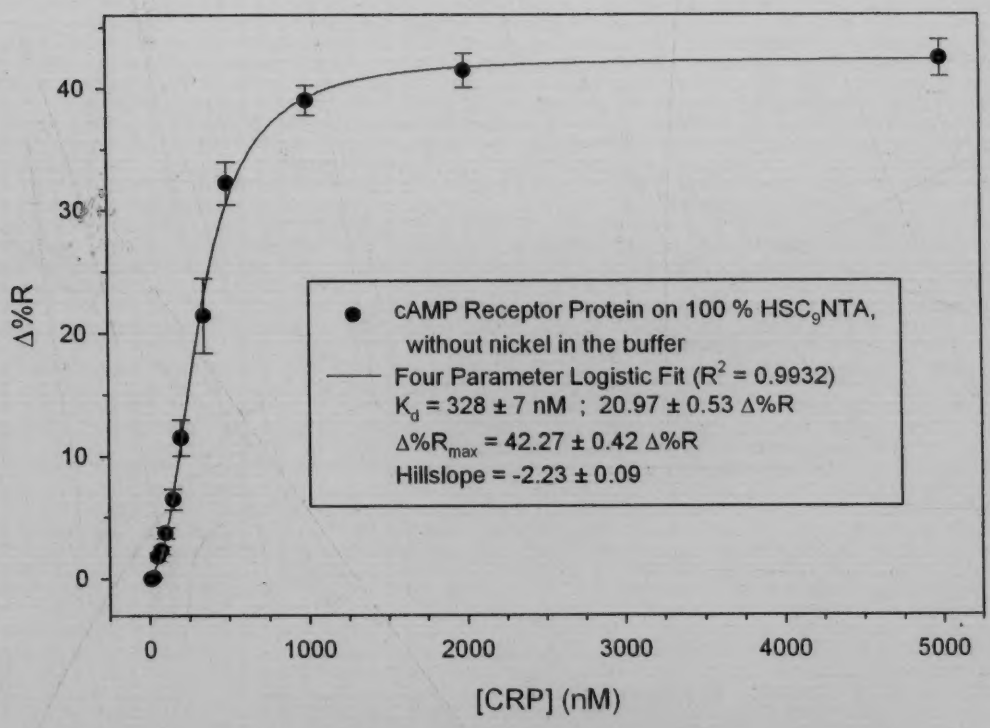

Figure 2.13. Fitted SPR curve of cAMP receptor protein (CRP) attaching to a 100 % HSC_9NTA capture surface, in the absence of nickel. The points are the mean value of eight spots and the error bars represent the standard deviation of 95 %.

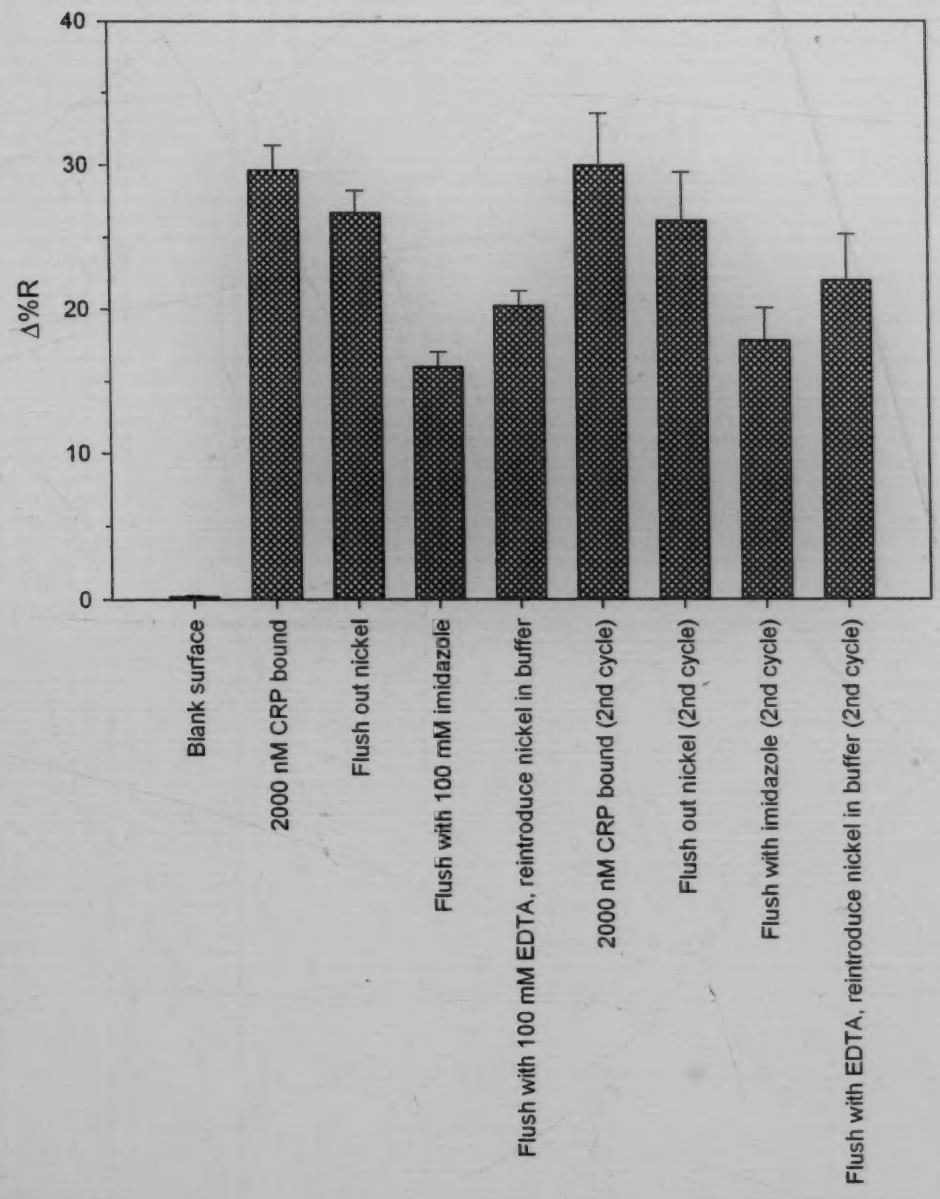

Figure 2.14. Partial regeneration of the 50 % HSC_9NTA capture surface after saturation with cAMP receptor protein (CRP). The points are the mean value of eight spots and the error bars represent the standard deviation of 95 %.

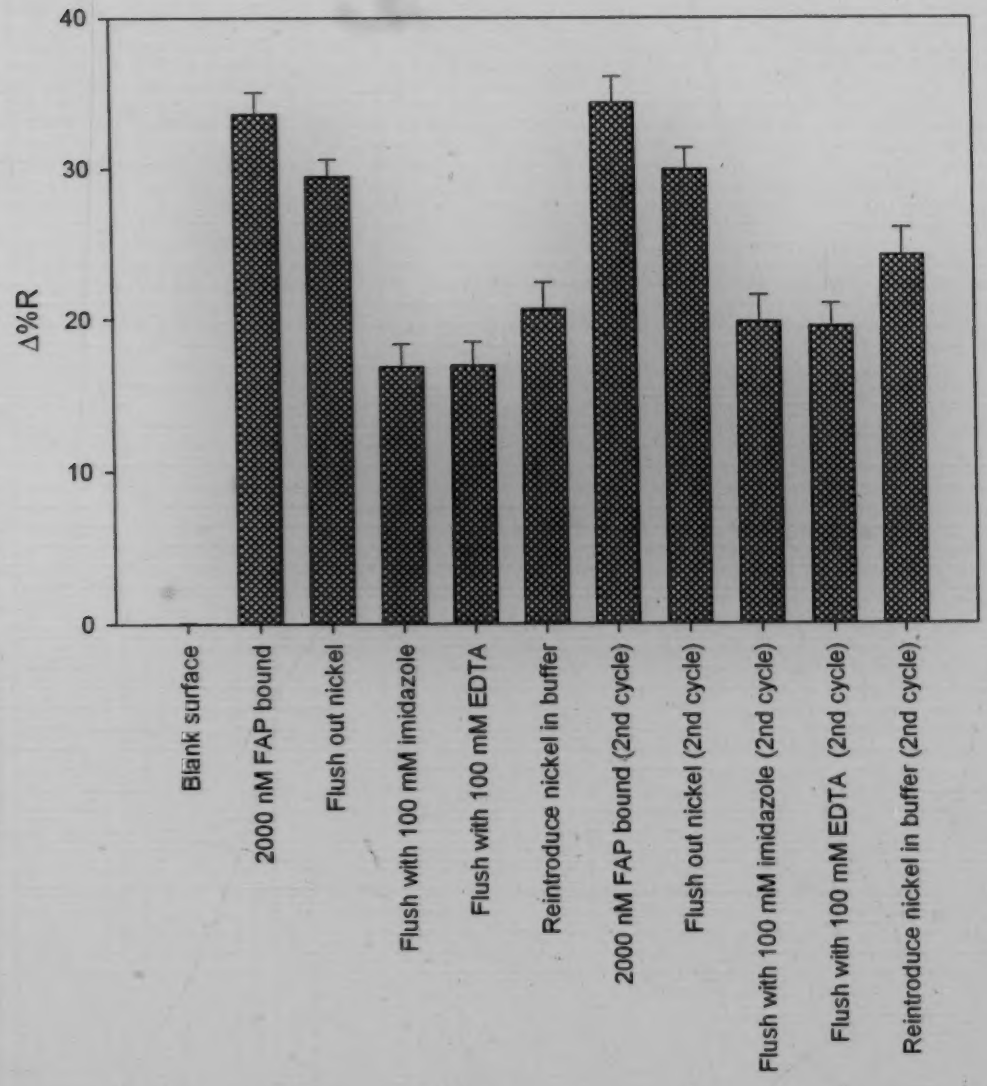

Figure 2.15. Partial regeneration of the 50 % HSC_9NTA capture surface after saturation with fibroblast activation protein (F_{AP}). The points are the mean value of eight spots and the error bars represent the standard deviation of 95 %.

allowed to equilibrate for ten minutes prior to flowing buffer over the chip for two minutes, first with nickel, and then without nickel. 100 mM imidazole and 100 mM EDTA were sequentially flowed over the chip, with rinsings of nickeless buffer in between. EDTA and imidazole partially regenerated the 50 % NTA capture surface saturated with either CRP or the larger F_{AP}, supporting the control experiments that showed a mixture of coordination via the hexahistidine tag and irreversible non-specific adsorption. This indicates that the 50 % NTA surface was insufficient to halt non-specific binding even for the smallest protein, CRP. Interestingly, it would appear that the second regeneration cycle is slightly less efficient than the first, which is more noticeable with the F_{AP}. This could be accounted for by a small increase in the fraction of non-specifically and irreversibly bound protein following the first cycle of regeneration and subsequent second exposure to the protein solution.

Conclusion

Surface plasmon resonance imaging was successfully employed in the analysis of protein binding on mixed thiol monolayers using the NTA-Ni^{2+}-His_6 capture system. It was found that a higher proportion of protein resistant $HSC_{11}OH$ (80 vs. 50 % molar) is required to effectively limit non-specific adsorption in the four-proteins studied. Additionally, binding curves on the 100 % NTA capture surface showed higher signals with larger proteins. However, with increasing molecular weight the maximum signal

rose proportionally less, suggesting less efficient packing of the larger proteins on this monolayer.

The control and regeneration experiments together show protein size to have a dramatic effect on the composition of the surface required to minimize non-specific adsorption. The OH groups largely failed in preventing non-sepecific adsorption by CRP and Amyl. They were effective, however, in greatly limiting non-specific adsorption of F_{AP}, β-Gal, and BSA.

References

(1) Rich, R. L.; Myska, D. G. *J. Mol. Recognit.* **2007**, *20*, 300-366.

(2) Ramachandran, N.; Larson, D. N.; Stark, P. R. H.; Hainsworth, E.; LaBaer, J. *FEBS Journal* **2005**, *272*, 5412-5425.

(3) Zhu, H., et al. *Science* **2001**, *293*, 2101-2105.

(4) Chandler, D. P.; Schabacker, D. S.; Bavykin, S.; Gavin, I. M. In *Functional Protein Microarrays in Drug Discovery*; Predki, P. F., Ed.; CRC Press LLC: Boca Raton, Florida, USA, 2007; Vol. 8, pp 199-216.

(5) Nagl, S.; Schaeferling, M.; Wolfbeis, O. S. *Microchim. Acta.* **2005**, *151*, 1-21.

(6) Lee, H. J.; Wark, A. W.; Corn, R. M. *Langmuir* **2006**, *22*, 5241-5250.

(7) Homola, J.; Piliarik, M.; Kvasnička, P. *Proceedings of SPIE* **2007**, *6619*, 1-6.

(8) Iordanski, A. L.; Polschuck, A. J.; Zaikov, G. E. *JMS Rev. Macromol. Chem. Phys.* **1983**, *C23*, 33.

(9) Lok, B. K.; Cheng, Y.-L.; Robertson, C. R. *J. Colloid Interf. Sci.* **1983**, *91*, 104.

(10) Wojciechowski, P.; ten Hove, P.; Brash, J. L. *J. Colloid Interf. Sci.* **1986**, *111*, 455.

(11) Cheng, Y.-L.; Darst, S. A.; Robertson, C. R. *J. Colloid Interf. Sci.* **1987**, *118*, 212.

(12) Andrade, J. D.; Hlady, V.; Wei, A.-P.; Ho, C. H. *Clinical Mater.* **1992**, *11*, 67.

(13) Andrade, J. D.; Hlady, V.; Wei, A. P. *Pure & Appl. Chem.* **1992**, *64*, 1777.

(14) Pérez-Luna, V. H.; Horbett, T. A.; Ratner, B. D. *J. Biomed. Mater. Res.* **1994**, *28*, 1111.

(15) Blomberg, E.; Claesson, P. M. In *Proteins at Interfaces II: Fundamentals and Applications*; Horbett, T. A., Brash, J. L., Eds.; American Chemical Society: Washington, DC, 1995, pp 296-310.

(16) Porter, M. D.; Bright, T. B.; Allara, D. L.; Chidsey, C. E. D. *J. Am. Chem. Soc.* **1987**, *109*, 3559-3568.

(17) Morales-Cruz, A. L.; Tremont, R.; Martínez, R.; Romañach, R.; Cabrera, C. R. *Appl. Surf. Sci.* **2005**, *241*, 371-383.

(18) Bain, C. D.; Evall, J.; Whitesides, G. M. *J. Am. Chem. Soc.* **1989**, *111*, 7155-7164.

(19) Stranick, S. J.; Parikh, A. N.; Tao, Y.-T.; Allara, D. L.; Weiss, P. S. *J. Phys. Chem.* **1994**, *98*, 7636-7646.

(20) Ostuni, E.; Chapman, R. G.; Holmlin, R. E.; Takamaya, S.; Whitesides, G. M. *Langmuir* **2001**, *17*, 5605-5620.

(21) Keller, T. A.; Duschl, C.; Kröger, D.; Sévin-Landais, A.-F.; Vogel, H. *Supramolecular Science* **1995**, *2*, 155-160.

(22) Sigal, G. B.; Bamdad, C.; Barberis, A.; Strominger, J.; Whitesides, G. M. *Anal. Chem.* **1996**, *68*, 490-497.

(23) Cheng, F.; Gamble, L. J.; Castner, D. G. *Anal. Chem.* **2008**, *80*, 2564-2573.

(24) Lee, J. K.; Kim, Y.-G.; Chi, Y. S.; Yun, W. S.; Choi, I. S. *J. Phys. Chem. B* **2004**, *108*, 7665-7673.

(25) Nye, J. A.; Groves, J. T. *Langmuir* **2008**, *24*, 4145-4149.

(26) Norde, W.; Gonzalez, F. G.; Haynes, C. A. *Polymers for Advanced Technologies* **1995**, *6*, 518-525.

(27) Huang, Y.-W.; Gupta, V. K. *J. Chem. Phys.* **2004**, *121*, 2264-2271.

(28) Luo, Q.; Andrade, J. D. *J. Colloid Interf. Sci.* **1998**, *200*, 104-113.

(29) Grant, M. L. *J. Phys. Chem. B* **2001**, *105*, 2858-2863.

(30) Roth, C. M.; Neal, B. L.; Lenhoff, A. M. *Biophysical Journal* **1996**, *70*, 977-987.

(31) Shang, H. Ph. D. Dissertaion, University of Alberta, Edmonton, 2008.

(32) Vallières, K.; Chevallier, P.; Sarra-Bournet, C.; Turgeon, S.; Laroche, G. *Langmuir* **2007**, *23*, 9745-9751.

(33) Kindler, B.; University of Heidelberg, 1995.

(34) McKay, D. B.; Steitz, T. A. *Nature* **1981**, *290*, 744-749.

(35) Brayer, G. D.; Yaoguang, L.; Withers, S. G. *Protein Science* **1995**, *4*, 1730-1742.

(36) Aertgeets, K., et al. *Protein Science* **2004**, *13*, 412-421.

(37) Jacobson, R. H.; Zhang, X.-J.; Dubose, R. F.; Matthews, B. W. *Nature* **1994**, *369*, 761-766.

(38) Shumaker-Parry, J. S.; Campbell, C. T. *Anal. Chem.* **2004**, *76*, 907-917.

(39) Voss, N. R.; Gerstein, M. *J Mol. Biol.* **2005**, *34*, 477-492.

CHAPTER III

ELECTROCHEMICALLY GRAFTED ARYL LAYERS FOR USE IN SURFACE PLASMON RESONANCE IMAGING

Introduction

Diazonium cations have been studied for over a century in the field of organic chemistry, being of interest for their ease of synthesis, high reactivity of the diazonium ion, and the ion's strong activating properties towards nucleophilic substitution in both the ortho and para positions.[1-3] Following these early studies, the field of electrochemistry has taken a keen interest in diazonium cations for similar reasons.

It has been shown that the reduction of aromatic diazonium ions in an electrochemical cell coats the working electrode with an aryl film, with the thickness of the layer depending on both the properties of the diazonium chosen as well as the conditions of the electrochemical reduction.[4] The past fifteen years have witnessed efforts to determine the structure and properties of these films, notably the nature of the substrate-film interaction[5-7] and the mechanism of the electrografting. The films possess a high degree of stability, requiring mechanical abrasion for removal. This oft-repeated observation has and continues to lead to speculation that the films are covalently bound to the substrate (carbon, metal, semiconductor) through the carbon of the aromatic ring. The current proposed mechanism, as depicted in Figure 3.01, envisions attachment to occur following the conversion of the diazonium functionality

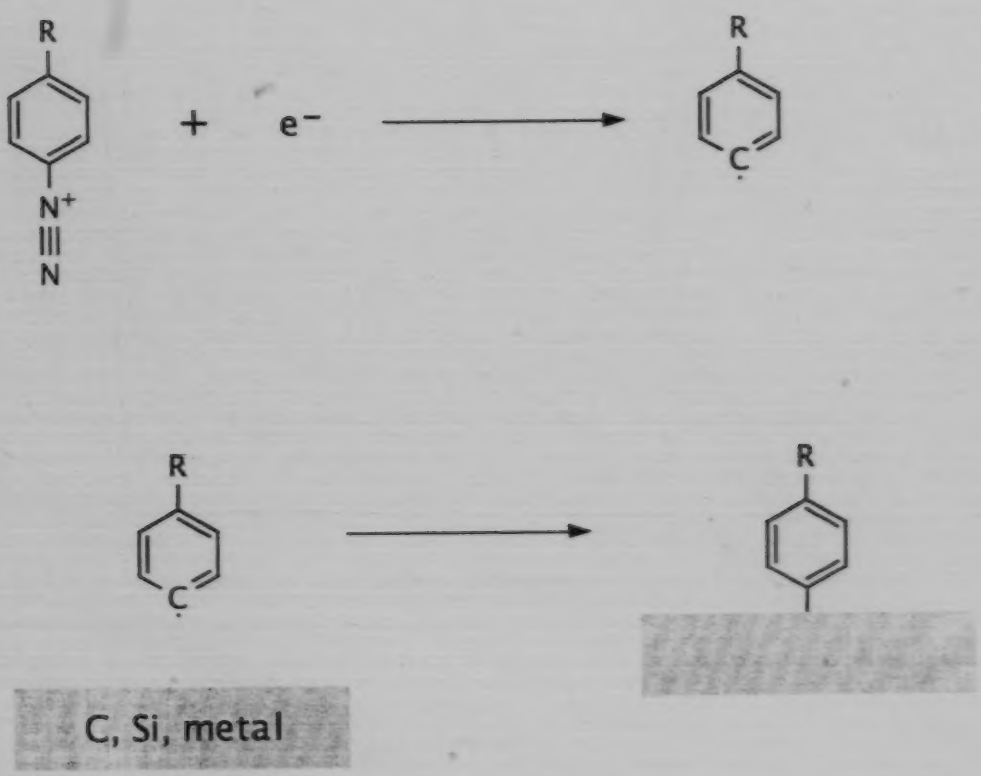

Figure 3.01. Radical formation and attachment to a surface for a diazonium salt.

into nitrogen gas and the generation of an aryl radical.[4] More recently, the possibilities of an azo linkage to the substrate, as well as azo linkages within the branching multilayers, have been raised.[8]

Although much of the initial work on aryl layers derived from diazonium salts was carried out on carbon electrodes, the initial evidence for a carbon-substrate covalent bond resulted from studies on Fe substrates. Boukerma et al. claimed a small carbide shoulder peak at 283.4 eV in the X-ray photoelectron spectrum (XPS) of an iron electrode grafted with a 4-aminobenzoic acid aryl layer as evidence of a C—Fe covalent bond.[9] However, the peak was very close to the detection limit and its existence at a surface sensitive angle (75°) was inferred from peak fitting parameters derived from the small shoulder peak seen at a bulk sensitive 0° take-off angle.

A more convincing demonstration of the existence of an aryl-substrate covalent bond resulted from the time-of-flight secondary ion mass spectrometry (TOF-SIMS) study by Combellas et al. of several diazoniums on glassy carbon.[10] $[Ar_n]^+$, $[Ar_n]^-$ (Ar_n = oligomeric aryl ion C_6H_4 with para substituents, n = 1 – 4), $[CH_2Ar_n]^{+/-}$, $[C_2H_4Ar_n]^{+/-}$, $[CAr_n]^{+/-}$, $[C_2Ar_n]^{+/-}$, and $[OAr_n]^{+/-}$ fragments support the view of a branching oligomeric or polymeric multilayer with covalent attachment to surface carbons and oxides. Interestingly, the authors noted that the fragments assigned to $[CH_2Ar_n]^{+/-}$ and $[C_2H_4Ar_n]^{+/-}$ (from 4-bromophenyl and 4-perfluorohexylphenyl

diazoniums) would have the same masses as $[N{-}Ar_n]^{+/-}$ and $[N{=}N{-}Ar_n]^{+/-}$ at the low mass resolution (m/z ± 1) of their instrument.

The first evidence for the purported azo linkage was the XPS peak at 400 eV for aryl layers on carbon and gold.[8, 11-15] Unfortunately for the studies using 4-nitrophenyl diazonium, the photoelectrons generated in XPS could reduce the nitro functionality and produce this peak. A 1976 study chemically coupled dinitrophenylhydrazine to a glassy carbon electrode and found the ratio of the 400 eV to ~404.5 eV peaks to grow as a function of potential.[16] This adds credence to the proposed reduction of nitro groups as a source for the 400 eV peak. No peak at 400 eV was found on the unmodified GC electrode. However, dinitrophenylhydrazine also produced a 400 eV XPS peak when it was chemically coupled (via surface para-quinones) to both glassy carbon and graphite in the absence of an applied reductive potential. In addition, a study by de Villeneuve et al. found this XPS peak for grafted 4-bromophenyl diazonium on Si(111).[17] At the time the authors attributed the peak to contamination of the sample, but several other studies saw this peak in the spectra of their aryl layers as well as its absence on their unmodified surfaces.[16, 18]

A high resolution TOF-SIMS analysis by Doppelt et al., augmented with Fourier transform infrared attenuated total reflectance (FTIR-ATR) spectroscopy, was conducted in search of evidence of intact azo linkages.[19] Peak fragments from thick aryl layers on both metal (Cu and Fe) and glassy carbon electrodes showed both $[ArN_2]^+$ and $[Ar_2N_2]^+$ (with m/z of ± 0.001

being sufficient to distinguish $[ArN_2]^+$ and $[Ar_2N_2]^+$ from $[CH_2Ar_n]^{+/-}$ and $[C_2H_4Ar_n]^{+/-}$). For grafted 4-iodophenyl (Au), 4-bromophenyl (Cu), and 4-carboxyphenyl (GC) diazoniums, however, no $[Ar_2N_2]^+$ fragments were seen, implying that the nature of the para substituent as well as the substrate may play an important role in determining the locations and the retention of the azo linkages. For the 4-iodophenyl diazonium grafted to gold, FTIR-ATR failed to detect a band in the 1440 to 1465 cm^{-1} range due to the -N=N- stretch, although this band is weak in the IR.[12, 20] A band at 1457 cm^{-1} was observed for the 4-bromophenyl diazonium grafted to copper. Etching of an 80 nm thick grafted layer of benzene diazonium with Cs^+ ions demonstrated a 10-fold increase in the intensity of $[ArN_2]^+$ ions near the surface. The authors interpreted this to mean the rougher outer layers of the film were more sterically favourable towards a higher concentration of azo groups. A proposed mechanism was put forward, with both the conventional pathway of the radical branching of aryl layers as well as a second pathway featuring the reduction of a radical azide cation attached to the polyphenylene layer.

Although the structure of the electrografted layers will be determined by the specific diazonium used as well as the surface of the electrode, defects and edge planes of substrates are thought to be particularly important determinants. Jiang et al. have conducted density functional theory (DFT) calculations of an aryl radical derived from benzene diazonium adsorbing to pristine surfaces of several metals,[21] followed up by a more detailed study of the same species attaching to graphene sheets.[22]

In the latter study, the strongest bonding was found to be on the graphene edges, and the attachment of two aryl groups at para positions of the same six-membered ring of the graphene significantly strengthened this interaction. An earlier study from our research group examining in-situ layer formation of 4-diazo-N, N-diethylaniline fluoroborate (DDEA) on highly oriented pyrolytic graphite (HOPG) in acetonitrile over multiple voltammetric scanning cycles backs up the DFT results.[23] Scanning force microscopy (SFM) images over several applied CV cycles showed nucleation and "mushrooming" along the basal plane and extensive coverage at step edges. It is thought that nucleation sites on the basal plane result from atomic scale defects there, and that the "mushrooms" result from multilayer growth at the nucleation sites. Topographic and lateral force SFM imaging at higher diazonium solution concentrations evidenced a higher number of "mushrooms" after a single voltammetric cycle. Although calculations from IRRAS absorbance and peak areas in cyclic voltammetry in other studies have yielded total surface material close to theoretical monolayer quantities,[7, 24, 25] these are averaging techniques and cannot determine heterogeneity in film structure and thickness.

The investigation of schemes for the chemical modification of surfaces for the immobilization of proteins onto surfaces has become a sizeable area of research. Currently, monolayers derived from alkyl thiols and siloxanes are widely employed.[26, 27] The use of diazonium derived aryl layers for this purpose, however, has been less widely studied. The first

study exploring the immobilization of proteins onto diazonium-derived aryl layers made use of phenylacetic acid diazonium borofluorate. The phenylacetic acid was electrografted to glassy carbon in acetonitrile, followed by the covalent immobilization of glucose oxidase via the carboxylic acid group using carbodiimide coupling chemistry.[28] Corgier et al. created a graphite electrode microarray for the immobilization of human and rabbit IgG using aryl layers.[29] Interestingly, coupling of the 4-carboxymethyaniline, the diazonium precursor, to the IgG occurred prior to transformation of the aniline into the diazonium and electro-attachment to the surface. Several subsequent studies along these lines have taken this approach of coupling the aniline precursor to the protein prior to diazotization and electrografting.[30-32]. This methodology leads to questions regarding the mechanism of the protein attachment, where it is difficult to distinguish physical adsorption of the protein from the covalent attachment desired. For this reason, the work presented here performs the grafting and activation of the aryl layer prior to introducing the protein, allowing attachment to take place under milder and simplified conditions. [33]

All of the previous work shows that functionalized aryl films can be formed on a variety of surfaces, including gold. Building upon the work in Chapter II employing hexahistidine-tagged fusion proteins and the NTA-Ni_2^+-His_6 coordination system on mixed thiol monolayers,[34] we have set out to test and compare the same binding system on electrografted aryl layers. The strong anchoring of the layer, possibly via a carbon-gold covalent bond,

and the ability to control the density of functional groups on the surface via multilayer formation may provide a more stable and flexible interface relative to thiol monolayers. The study herein sets out to explore this protein immobilization method using the well-known NTA-Ni_2^+-His_6 system and surface plasmon resonance imaging. We have also endeavored to determine how manipulation of the electrografting conditions and resultant surface chemistry affects the quality of the sensor array.

Experimental

Materials and Reagents. 4-aminobenzoic acid, sodium nitrite, sulfuric acid, 50 % fluoroboric acid, tetrabutylammonium perfluoroborate [$(C_4H_9)_4NBF_4$], acetonitrile, and ether were used as received from Sigma-Aldrich. (N-5-amino-1-carboxypentyl)imino-diacetic acid (AB-NTA, Dojindo Laboratories), 11-mercapto-1-undecanol ($HSC_{11}OH$, Sigma), and tridecafluoro-1,1,2,2-tetrahydrooctyl-1-dimethylchlorosilane (United Chemical Technologies) were also used as received. 1-ethyl-3-[3-dimethylaminopropyl]carbodiimide hydrochloride (EDC) and *N*-hydroxysuccinamide (NHS) were used as received from Pierce Biotechnology. All aqueous solutions were produced using 18.2 MΩ deionized (DI) water from a Nanopure purification system (Barnstead). All hexahistidine-tagged proteins (His_6, at the C-termini) were obtained via fusion expression from E. coli and were dissolved in a buffer of 50 mM Tris HCl, 100 mM KCl, and 40 mM $NiSO_4 \cdot 6H_2O$ at pH 7.80 unless otherwise noted.

Synthesis of para-benzoic acid diazonium salt. 4-aminobenzoic acid was partially dissolved in 50 % fluoroboric acid at 0°C to form a 225 mM supersaturated solution. A saturated aqueous solution of sodium nitrite at 0°C was then added dropwise in a 3:1 ratio to the 4-aminobenzoic acid, dissolving this acid and causing the resulting solution to become a pale green. The solution was shielded from light and left to react for thirty minutes. Following this, the product was filtered and washed with anhydrous ether. The powdery white solid was then recrystallized in anhydrous acetonitirile at 0°C, filtered, and rotovaped on ice until dry. The product was stored in a dessicator at 4°C and covered from light. FT-IR (cm^{-1}): 1057 (vs), 1222 (m), 1297 (s), 1310 (s), 1388 (m), 1416 (m), 1459 (w),1479 (w), 1582 (w), 1621 (w), 1715 (vs), 1730 (vs), 2307 (s), 2533 (w), 2811 (w), 3114 (m), 3280 (m), 3498 (m), 3574 (m).

Preparation of SPR chips. A sheet of 1.0 mm thick SF-10 glass (Schott Glass) was diced into 1.8 cm X 1.8 cm squares. The squares were cleaned via immersion in boiling Pirhana (3:1 H_2SO_4:H_2O_2) for thirty minutes, thoroughly rinsed with DI water, and dried under a stream of argon. The cleaned squares were placed into a homemade aluminum shadowmask having three groups of connected three spot clusters and a lone central spot for spotting controls. A diagram of the chip is shown in Figure 3.02. The assembly was loaded into a thermal evaporator (Torr International Inc.) and

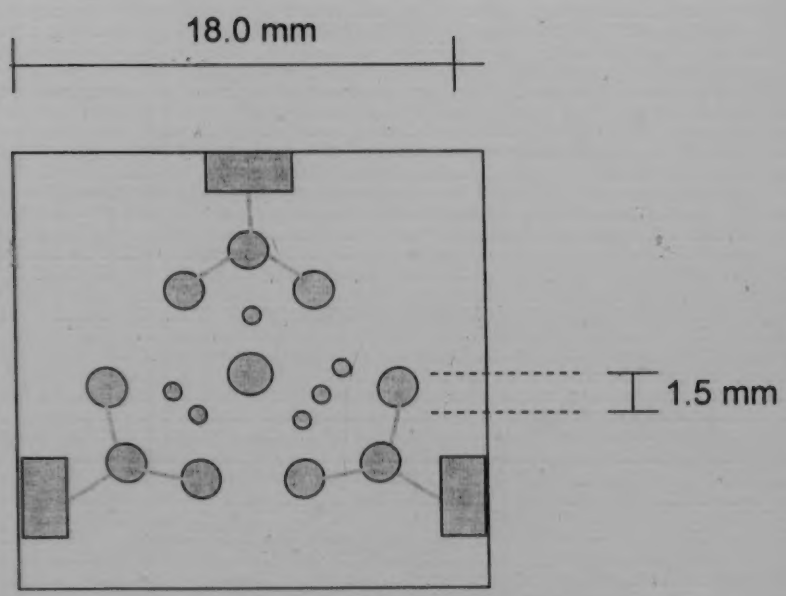

Figure 3.02. SPR chips for the electrochemical grafting of arrays of p-benzoic acid aryl layers. The $HSC_{11}OH$ control is spotted in the centre. The small gold dots are indices to identify the chip's orientation in the SPR flow cell.

the evaporator's chamber was pumped down to 4.0 X 10^{-6} Torr prior to the sequential deposition of 1.0 nm of chromium (adhesive layer, 99.999 % purity relative to other rare earth metals, Electronic Space Products International) and 45.0 nm of gold (99.99 % purity relative to other rare earth metals, Electronic Space Products International). Following deposition, the SPR chips were placed into a dessicator under vacuum containing small open vials of the fluorinated silane and left overnight to react with the exposed glass surfaces. The fluorinated SPR chips were then stored under vacuum prior to the electrochemical grafting of the p-benzoic acid diazonium salt and the surface attachment of $HSC_{11}OH$.

Grafting and modification of the aryl layer. p-Benzoic acid diazonium salt (2.0 mM) and tetrabutylammonium perborofluorate (100 mM) were dissolved in acetonitrile. Immediately prior to the electrochemical grafting of the diazonium salt, the SPR chip was placed into a UV-Ozone Cleaner 144AX (Jelight Company Inc., Irvine, CA) and cleaned for ten minutes to oxidize organic material on the gold spots. The chip was then successively rinsed with DI water and acetonitrile, blown dry with argon, and carefully placed into the diazonium solution, ensuring that only the gold spots, and not the clipped gold pad on the chip's edge, were immersed.

Using $Ag/AgNO_3$ (200 mM in acetonitrile) and platinum gauze as the respective reference and auxillary electrodes, the potential was swept from

+100 to -1000 mV at 10, 50, 200, 400, or 1000 mV/sec (all chips used in SPR control experiments used 200 mV/sec), for two complete cycles under a 100 μA limiting current. This was immediately repeated for the other two groupings of three spots. The chip was then removed and rinsed successively with acetonitrile and DI water. All experiments were performed using fresh solutions of the diazonium salt.

An aqueous EDC/NHS solution (12 mM/30 mM) at pH 7.9 was dispensed onto the gold spots of the grafted chips using a micropipette, and the chip was left for thirty minutes in a sealed petri dish, covered from light, with a wet Kimwipe to allow the surface to be activated. The EDC/NHS droplets were then sucked off using a vacuum line, the chip was rinsed with DI water, and the gold spots were respotted with 4.0 mM aqueous AB-NTA. Figure 3.03 shows the steps of the surface's modification. The Petri dish was resealed with a wet Kimwipe, covered from light, and left overnight prior to SPR analysis.

Surface plasmon resonance imaging of protein attachment. The droplets of AB-NTA solution were sucked off with a vacuum line, followed by a thorough rinse of the chip with DI water. The chip was then immediately placed into a prism flow cell assembly of a GWC SPRimagerII instrument running Digital Optics V^{++} 4.0 imaging software. Buffer was flowed over the chip for two minutes using the instrument's peristaltic pump at a middle setting. All other solutions introduced into the fluid cell in subsequent steps were flowed at this same rate and duration. The angle

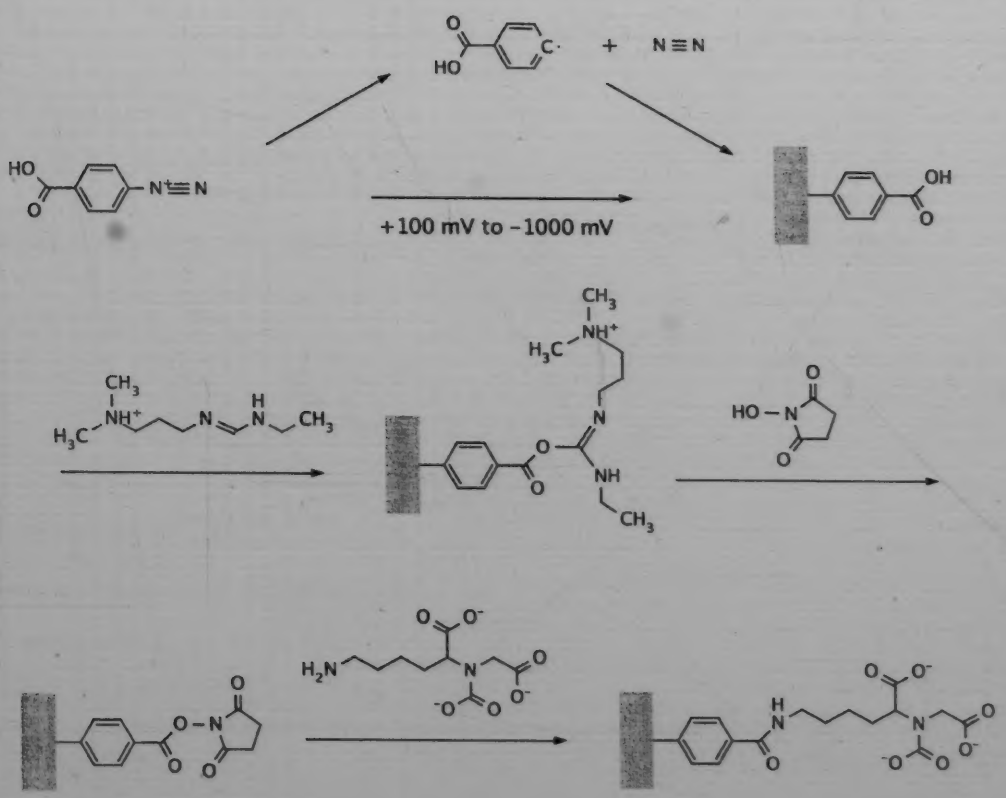

Figure 3.03. Electrochemical grafting of the p-benzoic acid diazonium salt, activation with EDC and NHS, and subsequent modification with AB-NTA.

of incidence of p-polarized light was adjusted until the reflectivity signal at the grafted spots was two-thirds of the minimum on the more linear side of the signal curve. Reference images using both s- and p-polarized light at this angle of incidence were taken immediately prior to the introduction of protein solutions. All gold spots were selected as regions of interest with the software, and the intensity of the reflected light passing through the prism was measured with respect to the protein concentration using a CCD camera.

Protein solutions ranging in concentration from 1.0 nM to 2000 nM were flowed over the chip before turning off the light source and pump for ten minutes to allow protein attachment to occur. Buffer solution was then flowed through, and a reflectivity image was acquired upon stopping the flow. The next highest concentration protein solution was flowed through, and these steps were repeated for all protein concentrations to generate an equilibrium binding curve. The flow cell settled to 22.2 °C ± 0.5 °C after warming up and being shut off during the ten minute long equilibration steps.

FT-IRRAS measurements of grafted aryl layers. The sequential grafting of p-benzoic acid diazonium salt at 200 mV/sec, from +100 to -1000 mV, was repeated on four microscope slides coated with 5.0 nm of chromium and 200.0 nm of gold, using the same solution for all slides (2.0 mM 4-aminobenzoic acid and 100 mM $TBABF_4$ in acetonitrile) over a period of several hours. Following deposition, the slides were rinsed with

acetonitrile, blown dry with argon, and placed into a sample chamber of a Thermo-Mattson Infinity Series FT-IR under nitrogen. After purging the chamber for twenty minutes, an IRRAS spectrum with a resolution of 2 cm^{-1} was acquired. All spectra were acquired at an 80° glancing angle with a liquid nitrogen cooled mercury-cadmium-telluride detector, and used a bare gold slide as a reference. The IRAAS peaks showed no changes in their positions or intensities upon replication of a deposition.

A fresh solution of the diazonium salt was prepared and bubbled witth argon gas for ten minutes. The scan rate in the electrografting was varied between slides, using 5, 20, 50, 200, 400, or 1000 mV/sec. All graftings were performed in rapid succession prior to IRRAS analysis and stored covered from light, under nitrogen.

Results and Discussion

Cyclic voltammetry (CV). Cyclic voltammetry is the most frequently employed technique for the reduction of diazonium salts at electrode surfaces. A typical CV current-voltage curve possesses a single cathodic peak that is attributed to the reduction of the diazonium cation to an aryl radical. A representative voltammogram of 2.0 mM p-benzoic acid diazonium cation (dBA) at a SPR chip electrode is shown in Figure 3.04, showing two cathodic peaks on the negative sweep. No Faradaic current is observed for the reverse wave, suggesting a chemically irreversible electron transfer, consistent with numerous reports in the literature.[23, 24, 33] Despite

a similar multi-peak cyclic voltammogram being previously reported for *N*-(4-diazophenyl)maleimide diazonium salt on a gold electrode,[33] there is no consensus at present on the assignment of the two waves. The authors of the above-cited study observed one sharp reductive peak, as well as a small pre and post-wave adjacent to this peak. These waves were attributed to strong adsorption of both the oxidized and reduced forms of the electroactive species.

The reduction of dBA at the SPR chip electrodes was investigated in some detail by varying the voltammetric sweep rate. Examples of voltammograms at two different sweep rates are shown in Figures 3.04 (50 mV/sec) and 3.05 (400 mV/sec). The peak currents and potentials observed at the different scan rates are listed in Table 3.1. The potential of both peaks observed on our gold film electrodes shift negative with increasing scan rates. This is characteristic of a quasi-reversible electron transfer to the dBA and is consistent with voltammetry for diazonium salts on carbon electrodes.[35]

The nature of the mass transport mechanism of redox species can be assessed by examining the variation of the peak current with sweep rate (ν). The assessment is based on the different functional forms of the peak current with sweep rate for a redox species diffusing to the electrode surface and one that is adsorbed. Briefly, for a diffusion controlled species, $i_p \propto \nu^{1/2}$. The peak current of an electroactive species adsorbed to the electrode surface is directly proportional to ν. To evaluate the mass

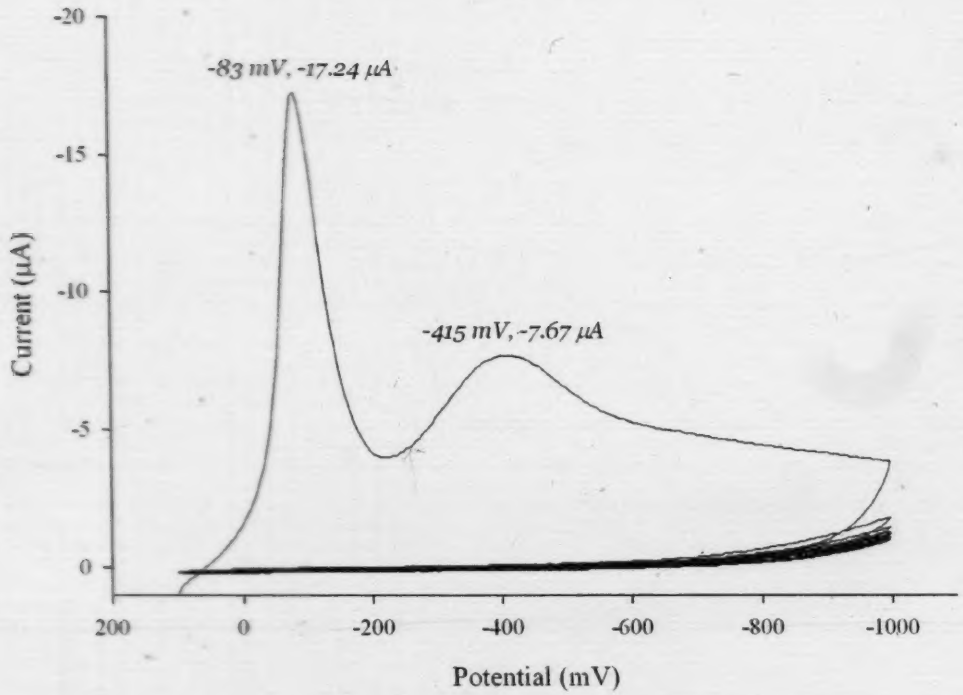

Figure 3.04. Cyclic voltammetry of 2.0 mM dBA (100 mM $TBABF_4$) at an SPR chip electrode. The scan rate was 50 mV/sec. Five consecutive sweeps are shown.

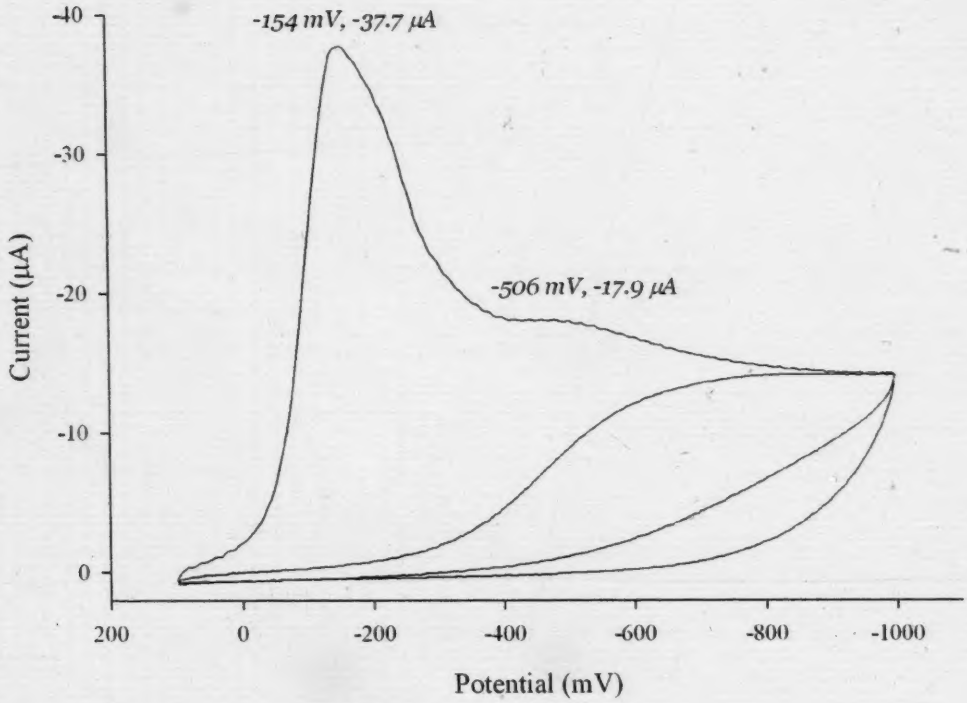

Figure 3.05. Cyclic voltammetry of 2.0 mM dBA (100 mM $TBABF_4$) at an SPR chip electrode. The scan rate was 400 mV/sec SPR chip. Two consecutive sweeps are shown.

Scanning Speed, ν (mV/sec)	Peak #1 Potential (mV)	Current (μA)	Peak #2 Potential (mV)	Current (μA)
10	-48	-3.96	-420	-1.12
50	-83	-17.24	-415	-7.67
200	-88	-32.40	-470	-22.50
400	-154	-37.70	-506	-17.90
1000	-191	-87.90	—	-43.90

Table 3.1. Peaks obtained for the SPR chip electrodes at various scanning speeds in 2.0 mM p-benzoic acid. The potential for peak #2 at 1000 mV/sec. could not be determined.

transport mechanism, $\log(i_p)$ is plotted against $\log(v)$. A slope of 0.5 implies a diffusion controlled redox process and a slope of 1 indicates current due to an adsorbed species.

Figure 3.06 is a plot of $\log(i_p)$ vs $\log(v)$ for the reduction of dBA on a series of SPR chip electrodes. Results are plotted for both peaks observed in Figure 3.04. The lines through the data are the linear least-squares fits. Although there is significant scatter in the data, likely due to variations in electrode area, the slope of each line is ~0.5. This suggests that both peaks observed for the reduction of dBA on our gold film electrodes are diffusion controlled. This contradicts the previous model that attributes one of the peaks to adsorbed diazonium cations. The nature of the two peaks is still uncertain.

Infrared Reflectance Absorption Spectroscopy (IRRAS). Following the electrografting of the aryl layers onto microscope slides at various scan rates, the samples were submitted to IRRAS analysis in order to provide more detailed evidence of variations in the film structure. Validation of a benzoic acid (BA) layer and details on the film structure were provided by IRRAS. Samples for IRRAS are much larger than the SPR chips. Figure 3.07 shows the CV of 2.0 mM dBA on a gold coated microscope slide used for IRRAS experiments. The CV is qualitatively similar to that for the SPR chips (Figure 3.04) and provides evidence that similar films are deposited on both types of electrodes.

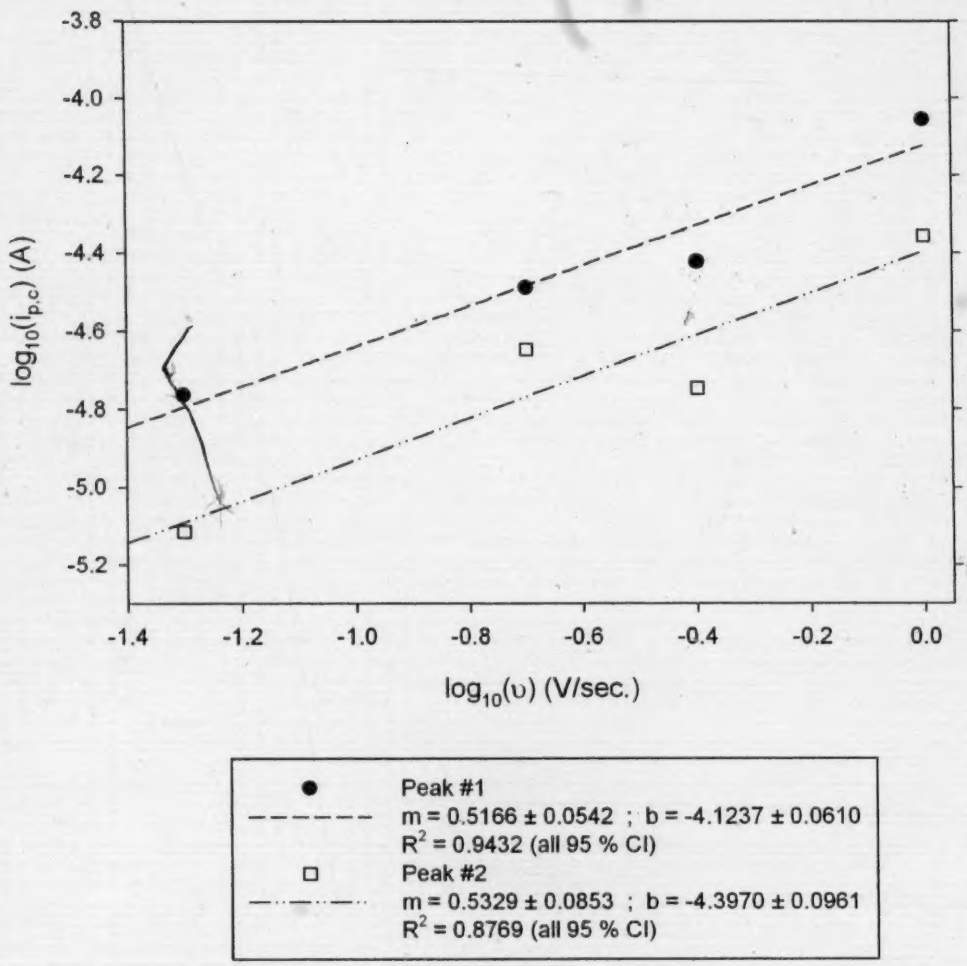

Figure 3.06. Logarithmic plot of peak currents against the scan rate for the SPR chip electrodes. The scan of 10 mV/sec is omitted due to an improper gain setting for that voltammogram. Linear regression of peaks #1 and #2 show slopes of approximately 0.5, predicted from the logarithmic form of the Randles-Sevcik Equation, and characteristic of a diffusion-limited current.

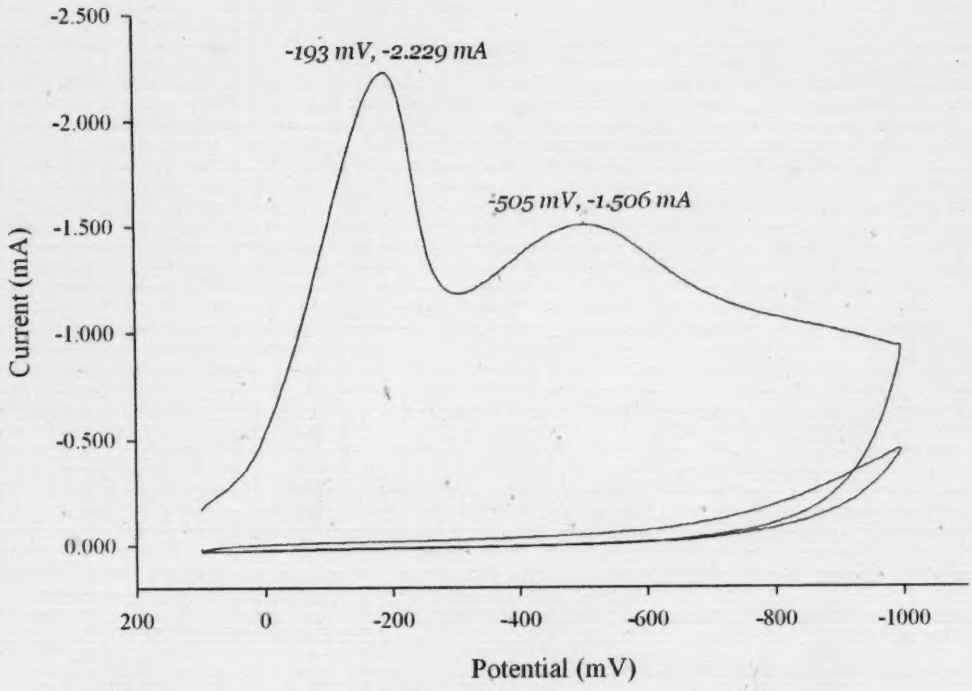

Figure 3.07. Cyclic voltammetry of 2.0 mM dBA (100 mM $TBABF_4$) at an IR slide. The scan rate was 50 mV/sec. Two consecutive sweeps are shown.

Since IRRAS depends on the constructive interference of the electric fields of the substrate and of the p-polarized light from the source, IR active groups of surface species have the greatest absorption when their dipoles are perpendicular to the substrate. As such, changes in absorbance yield information not only on the abundance of these groups at the surface, but also their orientation.

Figure 3.08 shows the IRRAS spectra obtained from the electrografting of the IR samples discussed above. The spectra feature absorbance peaks assigned to the carboxylic acid and phenyl rings on the surface. The presence of these IR peaks confirms the electrografting of the dBA salt to the gold surface, in addition to the CV peaks previously discussed. As an aside, it should be noted that the IR absorbance for an open-chain azo bond (-N=N-) also occurs in a region that overlaps with the aromatic ring stretch (1575-1630 cm^{-1}),[36] although azo groups have a weak IR absorbance that will be swamped by any strong signals in the same region.

Upon closer examination, changes in the carbonyl ($\nu_{C=O}$, 1700 cm^{-1}) stretch can be seen as the scan rate of the electrografting is varied. Figure 3.09 shows a systematic shift of the carbonyl peak to lower wavenumbers as the scan rate is increased. Changes in the absorbance of the carbonyl peak across the range of scan rates are also evident, as displayed in Figure 3.10. The 1700 cm^{-1} carbonyl stretch shows a dramatic drop in absorbance from 5 mV/sec to 200 mV/sec, before leveling off in the rest of the scan rate

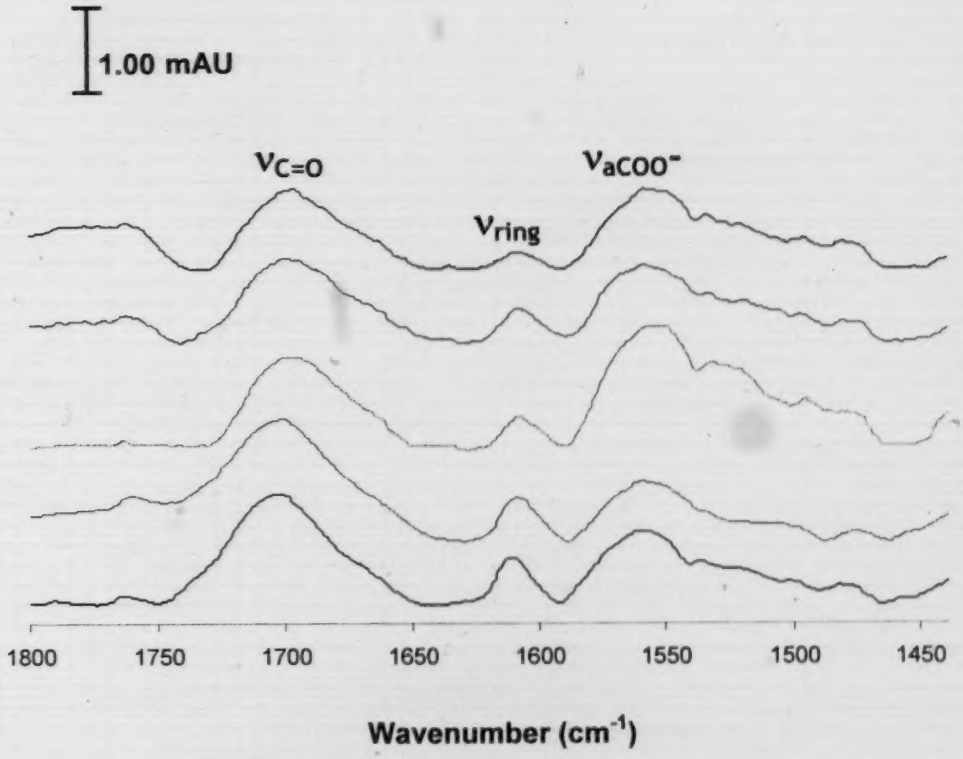

Figure 3.08. IRRAS spectra of the aryl layers grafted at varying scan speeds, stacked upon one another. The labeled peaks, shown above, from left to right: *carbonyl stretch* ($\nu_{C=O}$, 1700 cm^{-1}), *aromatic ring stretches* (ν_{ring}, 1610 cm^{-1}), and *asymmetric carboxylate stretch* (ν_{aCOO^-}, 1556 cm^{-1}).

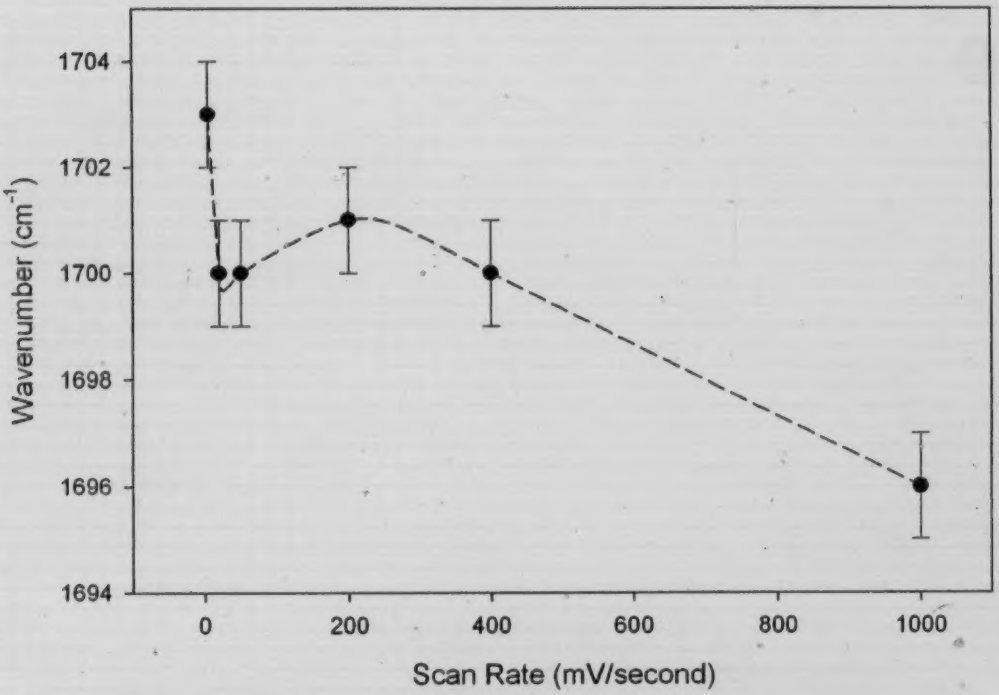

Figure 3.09. Plot of the carbonyl stretch ($\nu_{C=O}$, 1700 cm^{-1}) vs deposition sweep rate for dBA films. Error bars represent the peak resolution. Line connecting the points is a guide for the eye.

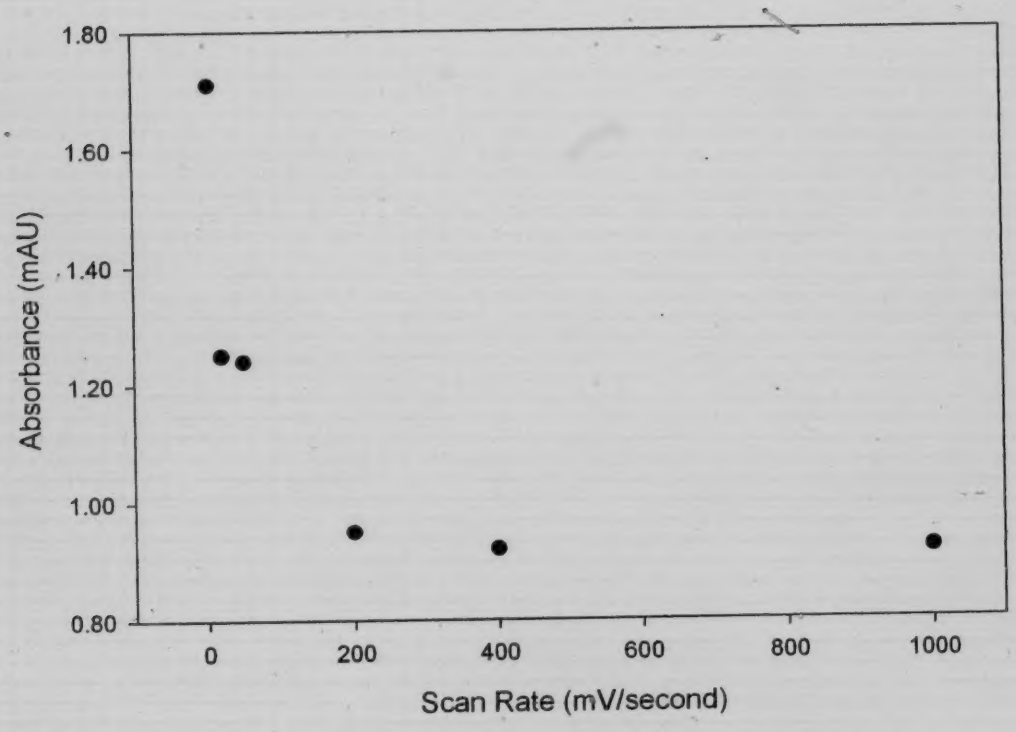

Figure 3.10. Plot of the absorbance of the carbonyl stretch ($\nu_{C=O}$, 1700 cm^{-1}) vs deposition sweep rate for dBA films.

range.

The changes in $\nu_{C=O}$ described above suggest several possibilities. The substantial drop in the carbonyl stretch's absorbance at higher scan rates points to lower coverage of the surface, in agreement with the cyclic voltammograms, while the carbonyl's shift to a lower wavenumber at higher scan rates points to changes in the C=O bond strength, and hence the overall environment. Although cyclic voltammetry indicates the process to be diffusion limited, the diffusion layer will be smaller at higher scan rates, allowing more efficient mass transport per unit time. Ultimately, this means the scan rate of the deposition enables a degree of kinetic control over the attachment of the dBA, and presumably other diazonium salts, to the gold surface. Combined with other adjustable parameters, such as the diazonium salt's concentration, this would potentially enable a very high degree of control over the structure of the aryl layer. This degree of control is not possible with most surface chemistries employed in the generation of biosensing devices.

Figure 3.11 illustrates a possible structure of the aryl layer based on a combination of current evidence from the literature. Several different environments for the carboxylic acid and phenyl ring exist in this hypothetical structure, resulting from both their position relative to the surface and the rest of the oligomeric chain, as well as the resulting combinations of allowed/restricted bond rotations. At this time, insufficient knowledge of the structures of the electrografted aryl layers

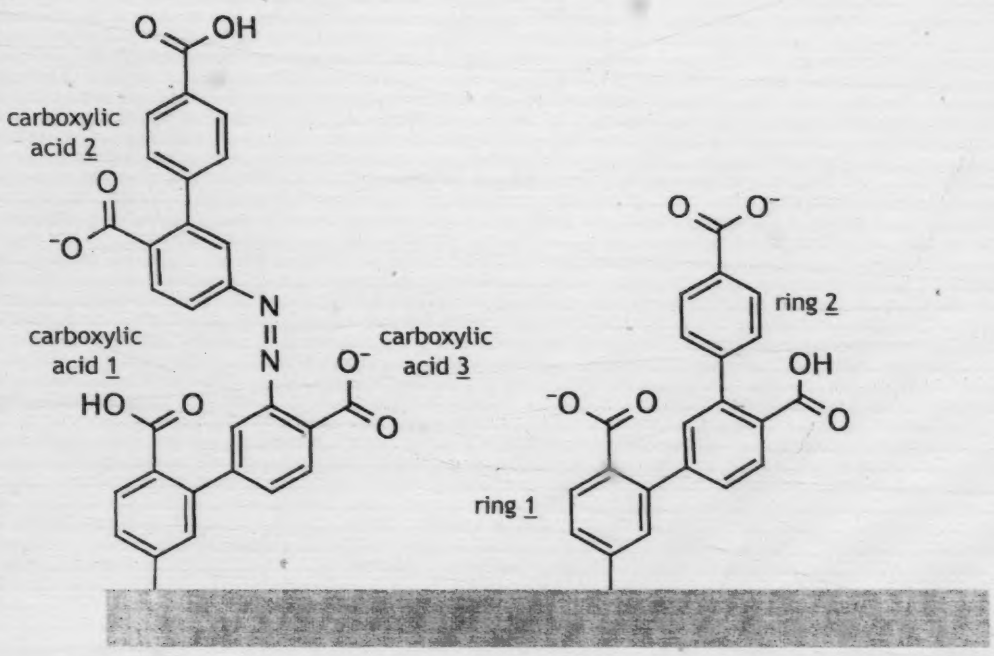

Figure 3.11. Possible structure of the electrografted para-substituted diazonium salt. Several possible environments exist for the carboxylic acid and phenyl groups, due to distance from the surface as well as allowed and restricted bond rotations.

from both this and other diazonium salts rules out going into greater detail on any changes in the structure of this aryl layer.

Surface plasmon resonance imaging. Having shown through cyclic voltammetry and IRRAS analysis that the potential scan rate controls the structure of the dBA aryl layer, we employed surface plasmon resonance (SPR) imaging to examine the effects of this variation on the efficacy of protein attachment, specifically that of His_6-cAMP receptor protein (CRP). First, NTA was conjugated to the dBA layer via the scheme shown in Figure 3.03, and subsequently Ni^{2+}-containing buffer was introduced in order to activate the NTA surface. A representative difference image of an SPR chip electrode showing attachment of CRP to the NTA layer can be seen in Figure 3.12.

The CRP binding curves for NTA conjugated dBA deposited a range of scan speeds are overlaid in Figure 3.13. The signal intensities (Δ%R) for binding to the layers grafted at each of the scan speeds are taken from those seen at 1000 nM of CRP and plotted against the scan speeds employed in Figure 3.14. The changes in reflectivities overlaid above occur well within the linear range of the SPR instrument.[37] There is a sizeable drop in signal intensity between the 50 mV/sec and the 200 mV/sec surfaces, followed by a steady rise in the intensity until a maximum is reached for binding to the 1000 mV/sec surface. This variation in the reflectivities is consistent with similar changes seen in the infrared absorbance of the carbonyl stretch between 50 and 400 mV/sec. This shows that the scan rate

Figure 3.12. Difference image of an SPR chip electrode in the flow cell of the GWC SPRimagerII, in a solution of 2000 nM cAMP receptor protein. The smaller circular gold spots towards the centre are the indices. Clockwise, beginning at the top: 50/50 $HSC_{11}NTA/HSC_{11}OH$ positive control (index •); electrografted p-benzoic acid aryl layers (indices •• and •••, 50 mV/sec for two cycles). The central spot is a negative control of the protein resistant $HSC_{11}OH$ SAM.

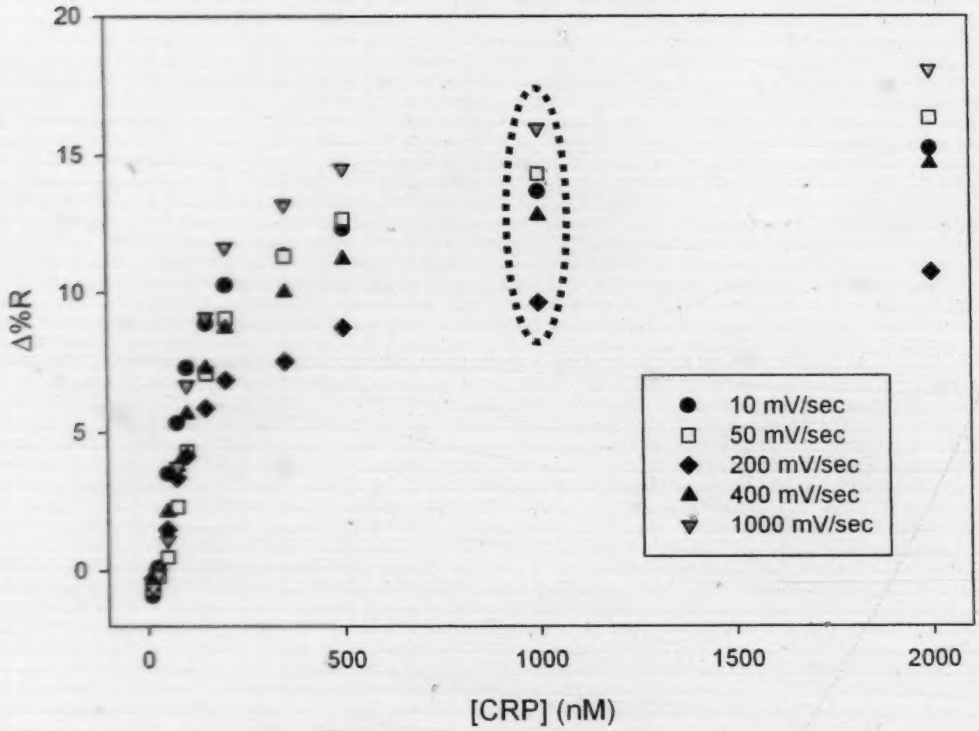

Figure 3.13. Stacked binding curves of cAMP receptor protein on NTA-terminated dBA layers deposited at varying scan rates. The error bars have been omitted for clarity. The NTA groups were activated with Ni^{2+} prior to the introduction of CRP.

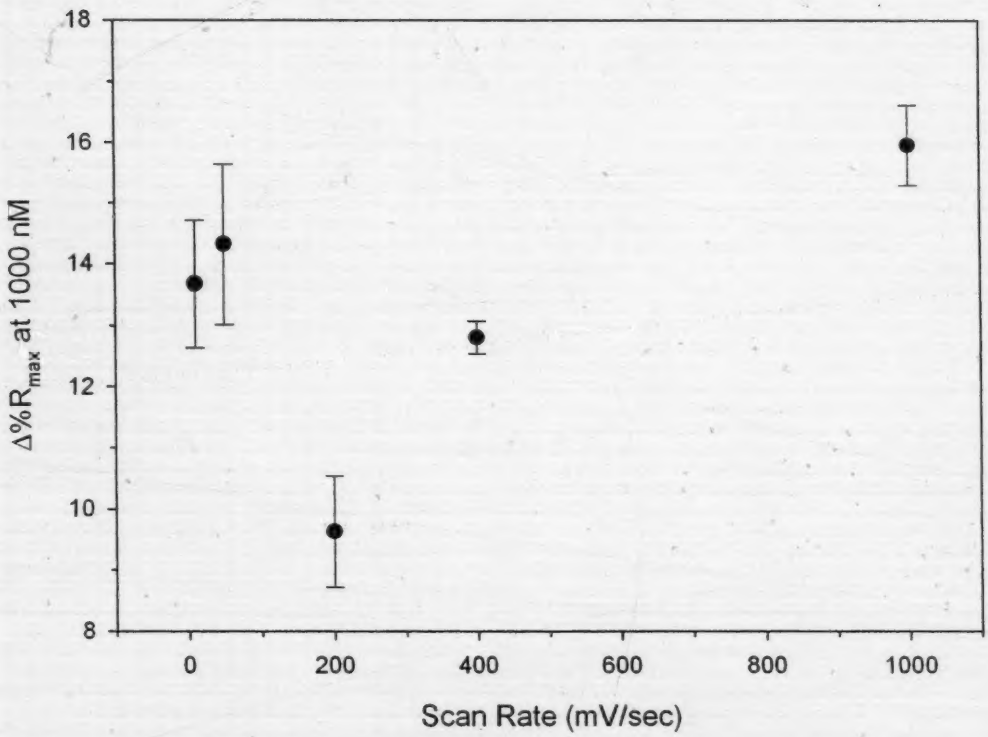

Figure 3.14. Signal intensities from the SPR binding curves of cAMP receptor protein, at 1000 nM, attaching to NTA-conjugated dBA layers deposited over a range of scan rates. The NTA groups were activated with Ni^{2+} prior to the introduction of CRP.

of the deposition, by controlling the structure of the grafted aryl layer, controls the amount of CRP binding to this film, although this relation does not appear to be straightforward.

Several control experiments were performed to confirm that the specific binding via the NTA-Ni^{2+}-His_6 system is a significant component of the factors controlling CRP attachment to the aryl-NTA surface, with signal intensities at a 1000 nM protein concentration plotted in Figure 3.15 employed to quantify the mass of bound protein. All control experiments were performed on aryl layers attached at 200 mV/sec, and each control selectively removed one component of the NTA-Ni^{2+}-His_6 system. At 200 mV/sec, when all components are present for His_6-CRP, Δ%R at 1000 nM = 9.63. In the absence of EDC/NHS coupling of AB-NTA to the carboxylic acid of the aryl layer, a modest increase in intensity is seen. When nickel is removed from the buffer, the intensity shoots up close to 40 Δ%R. Finally, bovine serum albumin (BSA, 60 kDa), a larger protein lacking the hexahistidine tag, gives a similar intensity as CRP in the absence of EDC/NHS coupling (no NTA capture groups). Unsurprisingly, the results of the control experiments demonstrate nonspecific binding to be significant as a component of the His_6-CRP protein attachment on this single component and likely somewhat disordered layer.

Although a *larger* signal intensity in the absence of nickel may seem counterintuitive at first, it must be remembered that this NTA surface is not protein resistant. In the absence of chelation to the NTA functional

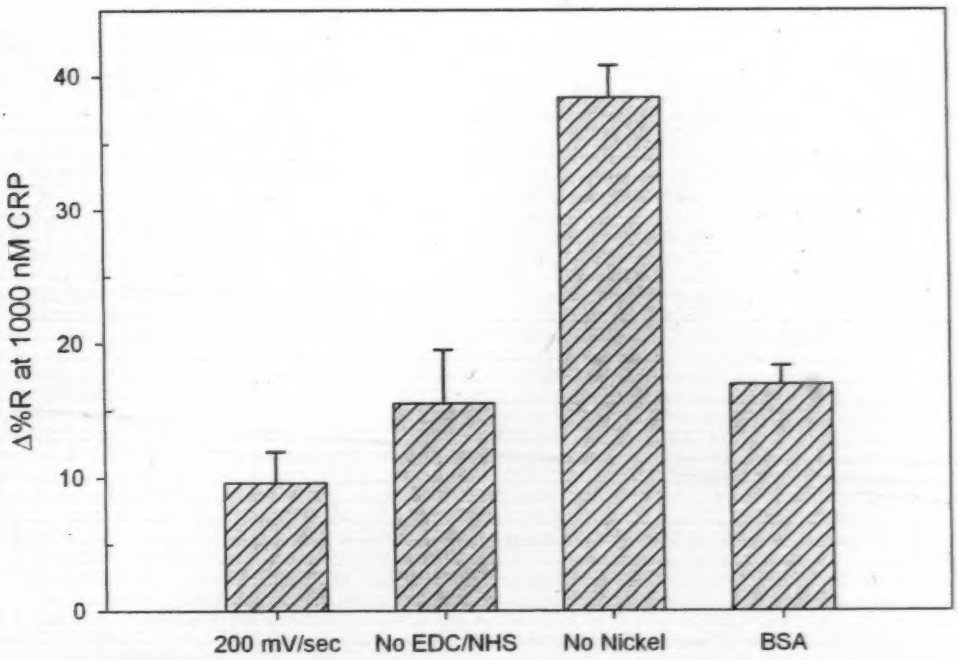

Figure 3.15. Comparison of the signal intensities obtained from the protein binding curves on the four aryl layers grafted at 200 mV/sec. Left to right: cAMP receptor protein (CRP) on the 200 mV/sec sample, CRP on the unactivated surface (no NTA groups), CRP in the absence of nickel sulfate, and bovine serum albumin (60 kDa, no hexahistidine tag).

endgroup, protein adsorption to the surface will be entirely non-specific. Consequently, the protein is no longer constrained by the location of the C-terminal hexahistidine tag, and may adsorb in a variety of orientations. This may change the "packing density" of the CRP on the surface, and in some cases this packing density would increase. A similar argument can be applied to the adsorption of the BSA. Although it is substantially larger than CRP (60 kDa versus 24 kDa), it does not follow that it will adsorb onto the surface in the same manner. In addition, it follows from geometry that a larger protein will not be able to pack as densely on the surface as a smaller protein. In spite of these complications, these control experiments demonstrate the NTA-Ni^{2+}-His_6 system to play an important role in controlling the attachment of the His_6-CRP to the aryl layers. At this time the extent of this control cannot be quantified.

Conclusions

A method for the specific attachment of hexahistidine-tagged proteins employing the electrografting of 4-aminobenzoic acid diazonium salt was developed and tested using surface plasmon resonance imaging. Cyclic voltammetry evidenced a reasonable degree of reproducibility in the electrografting procedure, as seen in reduction peak currents and potentials. IRRAS and SPR analysis showed the potential scan rate of the deposition to be an important factor governing the generation of this sensor assembly, allowing control of the capture film's structure. At present, the

nature of this control is unclear. The absorbance and peak positions in the IRRAS spectra, as well as the signal intensity of the CRP binding curves, suggest a transition in the structure of the aryl layer at scan rates between 50 and 400 mV/sec to be occurring. A larger number of scan rates, with multiple replications, would need to be examined to confirm this. Non-specific adsorption is prevalent, and future work on this sensor surface would require the incorporation of a protein repellant component, perhaps in a mixed layer format.

References

(1) Hantzsch, A. *Berichte der Deutschen Chemischen Gesellschaft* **1897**, *30*, 2334.

(2) Hantzsch, A. *Berichte der Deutschen Chemischen Gesellschaft* **1900**, *33*, 505-522.

(3) Lewis, E. S.; Johnson, M. D. *J. Am. Chem. Soc.* **1959**, *81*, 2070-2072.

(4) Pinson, J.; Podvorica, F. *Chem. Soc. Rev.* **2005**, *34*, 429-439.

(5) Ray, K.; McCreery, R. L. *Anal. Chem.* **1997**, *69*, 4680-4687.

(6) Kariuki, J. K.; McDermott, M. T. *Langmuir* **2001**, *17*, 5947-5951.

(7) Brooksby, P. A.; Downard, A. J. *Langmuir* **2004**, *20*, 5038-5045.

(8) Saby, C.; Ortiz, B.; Champagne, G. Y.; Bélanger, D. *Langmuir* **1997**, *13*, 6805-6813.

(9) Boukerma, K.; Chehimi, M. M.; Pinson, J.; Blomfield, C. *Langmuir* **2003**, *19*, 6333-6335.

(10) Combellas, C.; Kanoufi, F.; Pinson, J.; Podvorica, F. I. *Langmuir* **2005**, *21*, 280-286.

(11) Liu, Y.-C.; McCreery, R. L. *J. Am. Chem. Soc.* **1995**, *117*, 11254-11259.

(12) Nowak, A. M.; McCreery, R. L. *Anal. Chem.* **2004**, *76*, 1089-1097.

(13) Laforgue, A.; Addou, T.; Bélanger, D. *Langmuir* **2005**, *21*, 6855-6865.

(14) Lyskawa, J.; Bélanger, D. *Chem. Mater.* **2006**, *18*, 4755-4763.

(15) Toupin, M.; Bélanger, D. *Langmuir* **2008**, *24*, 1910-1917.

(16) Elliott, C. M.; Murray, R. W. *Anal. Chem.* **1976**, *48*, 1247-1254.

(17) Villeneuve, C. H. d.; Pinson, J.; Bernard, M. C.; Allongue, P. *J. Phys. Chem. B* **1997**, *101*, 2415-2420.

(18) Deinhammer, R. S.; Ho, M.; Anderegg, J. W.; Porter, M. D. *Langmuir* **1994**, *10*, 1306.

(19) Doppelt, P.; Hallais, G.; Pinson, J.; Podvorica, F.; Verneyre, S. *Chem. Mater.* **2007**, *19*, 4570-4575.

(20) Zimmermann, F., et al. *Appl. Spec.* **1993**, *47*, 986-993.

(21) Jiang, D.-e.; Sumpter, B. G.; Dai, S. *J. Am. Chem. Soc.* **2006**, *128*, 6030-6031.

(22) Jiang, D.-e.; Sumpter, B. G.; Dai, S. *J. Phys. Chem. B* **2006**, *110*, 23628-23632.

(23) Kariuki, J. K.; McDermott, M. T. *Langmuir* **1999**, *15*, 6534-6540.

(24) Paulik, M. G.; Brooksby, P. A.; Abell, A. D.; Downard, A. J. *J. Phys. Chem. C* **2007**, *111*, 7808-7815.

(25) Chen, P.; McCreery, R. L. *Anal. Chem.* **1996**, *68*, 3958-3965.

(26) Sandhyarani, N.; Pradeep, T. *Int. Reviews in Physical Chemistry* **2003**, *22*, 221-262.

(27) Rich, R. L.; Myska, D. G. *J. Mol. Recognit.* **2007**, *20*, 300-366.

(28) Bourdillon, C., et al. *J. Electroanal. Chem.* **1992**, *336*, 113-123.

(29) Corgier, B. P.; Marquette, C. A.; Blum, L. J. *J. Am. Chem. Soc.* **2005**, *127*, 18328-18332.

(30) Polsky, R., et al. *Langmuir* **2007**, *23*, 364-366.

(31) Corgier, B. P.; Li, F.; Blum, L. J.; Marquette, C. A. *Langmuir* **2007**, *23*, 8619-8623.

(32) Harper, J. C.; Polsky, R.; Wheeler, D. R.; Dirk, S. M.; Brozik, S. M. *Langmuir* **2007**, *23*, 8285-8287.

(33) Harper, J. C.; Polsky, R.; Wheeler, D. R.; Brozik, S. M. *Langmuir* **2008**, *24*, 2206-2211.

(34) Smith, A. D. E.; Zhang, G.; Shang, H.; Weiner, J.; McDermott, M. T., University of Alberta, Edmonton, 2008.

(35) Allongue, P., et al. *J. Am. Chem. Soc.* **1997**, *119*, 201-207.

(36) Coates, J. In *Encyclopedia of Analytical Chemistry*; Meyers, R. A., Ed.; John Wiley & Sons Ltd: Chichester, 2000, pp 10815-10837.

(37) Shumaker-Parry, J. S.; Campbell, C. T. *Anal. Chem.* **2004**, *76*, 907-917.

CHAPTER IV

CONCLUSIONS AND SUGGESTIONS FOR FUTURE WORK

General Conclusions

The overall goals of this program of research were to investigate the limitations of immobilizing hexahistidine-tagged (His_6) proteins and investigate new surface chemistry to immobilize these proteins. We examined several key factors affecting the immobilization of His_6 proteins to mixed alkyl thiol monolayers of nitrilotriacetic acid (HSC_9NTA) and protein resistant OH functional endgroups ($HSC_{11}OH$). We also developed and characterized a new surface chemistry, based on the electrografting of diazonium-derived aryl layers, for use on the same class of His_6-proteins.

Chapter II ascertained how four His_6-proteins, spanning a range of representative molecular weights, bound to alkyl thiol monolayers of varying composition. To this end, surface plasmon resonance imaging (SPRi) was employed to examine the binding of the His_6-proteins onto a set of three monolayers prepared from solutions containing the following mole percentages: 100 % HSC_9NTA, 50/50 % $HSC_9NTA/HSC_{11}OH$, and 20/80 % $HSC_9NTA/HSC_{11}OH$. Results indicate attachment of the larger proteins (120 and 480 kDa) to be dominated by non-specific adsorption on the 100 % and 50 % HSC_9NTA surfaces. The smaller proteins (24 and 60 kDa) demonstrated competition between coordination at the His_6-tag and non-specific

adsorption. Attachment of all His_6-proteins on the 100 % HSC_9NTA monolayer was shown to be determined largely by close packing.

An alternative surface chemistry, with the potential to produce more robust layers in comparison to thiols, was subsequently explored in Chapter III. Functionalized aryl films produced by the electrochemical reduction of diazonium salts were evaluated as a platform to immobilize His_6-tagged proteins. The scan rate was shown to control the structure of the aryl layer derived from para-benzoic acid diazonium salt (dBA). Peak currents obtained from cyclic voltammetry (CV) increased alongside scanning rates in a manner characteristic of a diffusion-limited process. Currents observed in the second potential scanning cycles at higher sweep rates show evidence of incomplete film formation under those conditions. Infrared reflectance absorbance spectroscopy (IRRAS) of grafted aryl layers and the SPR binding measurements of cAMP receptor protein onto films deposited at varying potential scan rates suggest a transition in the aryl film's structure occurring between 50 and 400 mV/sec. This shows promise as a means of controlling surface chemistries not possible in the case of self-assembled monolayers of thiols.

Suggestions for Future Work

Results from Chapter II suggest it would be fruitful to examine the binding of the smaller proteins to more dilute HSC_9NTA surfaces, at densities on the order of 1 % to 10 % NTA. Since the extent of non-specific

adsorption observed at more concentrated NTA surfaces depends on the size of the His_6-protein, the NTA densities employed would have to be optimized for a standard series of protein masses. This would establish a general protocol for His_6-proteins that would enable maximal performance for biosensing applications; that is, the highest signal without the occurrence of non-specific adsorption.

Chapter III demonstrated diazonium-derived aryl layers to be a viable chemistry for biosensing applications. In its present form, the dBA aryl layer will bind many proteins non-specifically, due to the uniform presentation of carboxylate groups to the solution. One potential solution would be the use of mixed aryl layers, in a parallel fashion to the mixed thiol monolayers. Previous work in our group has shown it is possible to generate partial monolayers of nitroazobenzene (NAB) on gold (111) and subsequently backfill the surface with dodecanethiol.[1] In light of this, it may be possible to generate a mixed layer of NTA terminated dBA and a protein resistant component such as an -OH or PEG terminated alkyl thiolate monolayer. This would allow for a direct comparison with the analogous mixed thiol layers described in Chapter II.

Work is also under way in our laboratory to ascertain the structures of para-benzoic acid films and several other aryl layers. Namely, we are exploring: (1) why this diazonium salt produces two peaks during deposition with cyclic voltamettry, and (2) what grafting conditions, if any, produce intact azo linkages. Surface enhanced Raman spectroscopy (SERS) and

atomic force microscopy (AFM) are being employed to better characterize these films for future applications.[2]

References

(1) Shewchuck, D.; McDermott, M. T. *unpublished results*; University of Alberta: Edmonton, 2007.

(2) Chisholm, R.; McDermott, M. T. *unpublished results*; University of Alberta: Edmonton, 2008.